Analysis of multiple cracking and interfacial debonding of the galvannealed coating layer under applied tensile strain

Sohei Iwamoto

2009

Analysis of multiple cracking and interfacial debonding of the galvannealed coating layer under applied tensile strain

Sohei Iwamoto

Department of Materials Science and Engineering
Kyoto University

2009

Index

Chapter 1

General Introduction

1.1 History of precoated steels for automotive bodies

The hot-dipped GA (galvannealed) steels, consisting of Fe-Zn intermetallic coating layer and substrate steel, are widely used as architectural and car-body materials due to their high corrosion resistance and weldability [1, 2].

Fig. 1.1 shows the secular change of precoated steels used for car bodies. The use of de-icing salt in North America and Canada increased very rapidly from 1950 to 1970. As a result, the corrosion of car bodies was actualized around 1960 in these regions. In the early 1960's American car manufacturers started to apply Zn coated steel sheets for the body parts invisible from-the-outside, such as floor, in order to suppress corrosion.

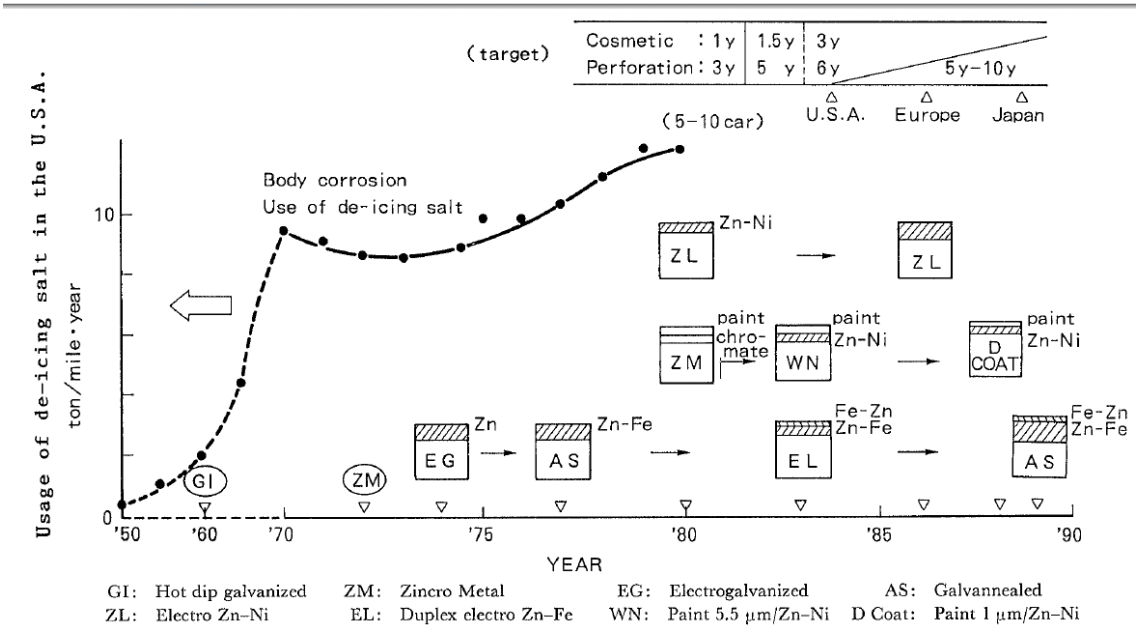

Fig.1.1 History of precoated steel application to automobiles in Japan [3]

Since 1963, Zn plated sheets have been used as visible part panels, such as doors and fenders. In 1972, the application of Zincro Metal (zinc chromated and Zn rich primed sheet) started. In Japan, with the increase of car exports to North America, automobile manufacturers have paid considerable attention to the corrosion problem. Electro-galvanized steel was applied first in 1974 to the body of export cars. In 1977, a steelmaker developed galvannealed sheet with a high performance and started to supply it for body panels. In 1978, the Canadian Government introduced the famous Canadian Code, which is an anticorrosion code establishing minimum levels of corrosion protection to be provided for all vehicles sold in Canada. Japanese car manufacturers were forced to design export vehicles to fulfill the requirements of the Canadian Code, because the United States also applied the corresponding Code [3]. The successful alternative Fe-Zn galvannealed steel was applied to the car body mainly in USA and Japan, in same cases also in Europe. Later on the steel industry has resumed and modified the previous work in the Zn-Mg coating in order to offer the enhanced protection against corrosion. Adding Mg in the HDG process (Zn-Mg) presents two advantages; i) greater protection against corrosion is achieved and ii) less zinc is required. This is very attractive from the economic viewpoint, since, especially in the past few years, the world market price of zinc has risen drastically [4]. It has been found in this connection that Mg levels ranging from 0.3-3% have an especially good influence in terms of enhanced anti-corrosion protection [5]. In Japan, the production of the coating containing about 3% Mg plus 5% Al started recently [6].

1.2 Recent study of the galvannealed steel

The Fe-Zn intermetallic coating is, however, brittle. It is fractured and debonded during the sheet forming process, reducing the coating quality and causing damage to the forming tools [7]. However, the fracture and spalling process are not fully understood.

The various factors affecting on the fracture of the coating, such as composition of substrate [8], preparation of substrate [9, 10], conditions of zinc-bath [11, 12], heating conditions [12-14] and so on, have been reported. Each factor has, however,

been studied independently in a qualitative manner. To reveal the mechanism and to describe the process of the deformation and fracture behavior in a quantitative manner, it is required to develop a comprehensive approach.

Until now, the following general features have been known for the fracture and spalling behavior of the brittle coating layer with a low failure strain on a ductile substrate. (A) The coating layer exhibits multiple transverse cracking under tensile loading [15-21]. (B) When the tensile stress is applied further on samples, the compressive stress perpendicular to the loading axis increases in the coating due to the difference in contraction between the coating (Poisson's ratio 0.2~0.3 for most brittle materials) and the plastically deforming substrate (0.5). The increased compressive stress causes compressive fracture and spalling of the coating when the coating is thin [20].

1.3 Purpose of present work

The purpose of the present work is to describe the fracture and spalling process of the coating and to find the way of the fracture control. The present work consists of the following contents.

In Chapter 2, tensile fracture and spalling-off behavior of the Fe-Zn intermetallic coating of galvannealed steel, together with that of the alumina coating on anodic-oxidized aluminum as a reference were studied based on the fracture morphology observation. The Fe-Zn coating exhibited first multiple-fracture perpendicular to the tensile axis. Then the coating exhibited compressive fracture in the width-direction. The alumina coating on the aluminum substrate exhibited multiple-fracture perpendicular to the tensile stress as similarly as the Fe-Zn intermetallic coating. Then, when the coating was thin, the multiply-cracked layer fractured in compression perpendicularly to the tensile axis, accompanied by buckling and wedging, resulting in spalling as similarly as the galvannealed coating.

In Chapter 3, multiple cracking of the galvannealed coating layer was studied. To estimate the strength of the coating layer and to predict the change of the critical and average crack spacings of the coating layer, finite element analysis was carried out.

From the comparison of the measured crack spacing with the calculated one, the strength of the coating layer was estimated to be around 260 MPa, almost independent from the thickness of the coating layer and the variety of substrate steels. From the calculation results, an empirical equation was proposed, which can be used for rough prediction of the crack spacing as a function of applied strain for any substrate steels and thickness of the coating layer.

In Chapter 4, stress analysis of the buckled- and interfacial debonded-coating layer was carried out. The analytical results of the 3-dimentional finite element models accounted for well the experimentally observed features of the spalling process. Also it was found that the shorter the crack spacing of the coating layer in the tensile direction, the strain at which the interfacial debonding starts is retarded. This result implies that the multiple cracking phenomenon acts to retard the spalling.

In Chapter 5, influences of the high tensile strength steel substrate on the multiple cracking and spalling was studied by the finite element stress analysis. It was revealed that the replacement of the high strength substrate for the low one acts to enhance the multiple cracking and to reduce the interfacial debonding through the enhancement of multiple cracking, if the tensile strength of the coating layer and interfacial bonding strength are retained on the level of those for the low strength steel.

In Chapter 6, influences of the crack spacing in the tensile direction and that in the sample width direction on the interfacial debonding were studied. The calculation results suggested that, in order to supress the interfacial debonding, the crack spacing in the tensile direction should be short to retard the initial debonding, and the crack spacing in the sample width direction should be short, too, to retard the progress of the interfacial debonding.

In Chapter 7, the group-buckling behavior was observed and analyzed. It was observed that the preceding buckling of the coating enhances the buckling of the neighboring coating. Such a behavior was well accounted for by the present analysis.

References

[1] S. Lazik, C. Esling and J. Wegria: *Textures and Microstructures*, **23** (1995), 131.

[2] C. E. Jordan CE, K. M. Goggins and A. R. Marder: *Metall Mater Trans A.*, **25** (1994), 2101.

[3] Y. Miyoshi: *ISIJ Int.*, **31** (1991), 1.

[4] B. Schuhmacher, T. Heller, M. Steinhorst, W. Warnecke: *Proc. Galvatech '07*, Osaka, (2007), 397.

[5] M. Vlot, R. Bleeker, T. Maalman, E. V. Perlstein: Galvanized Steel Sheet Forum 2006, Düsseldorf, (2006).

[6] K. Nagata, S.Masui, R.Yamashita: *Proc. Galvatech '04*, Chicago, (2004), 185.

[7] A. T. Alpas and J. Inagaki: *ISIJ Int.*, **40** (2000), 172.

[8] T. Kiyasu, A. Yasuda, S. Kobayashi, T. Ichida, H. Kubo: *Tetsu-to-Hagane*, **72** (1986), 1005.

[9] N. Fujibayashi, K. Kyouno, C. Katou: *Tetsu-to-Hagane*, **89** (2003), 23

[10] I. Hashimoto, K. Saitou, M. Nomura, T. Yamamoto, H. Takeda: *Tetsu-to-Hagane*, **89** (2003), 31.

[11] T.Nakamori, A. Shibuya: *Tetsu-to-Hagane*, **77** (1991), 955.

[12] M. Urai, M. Arimura, M. Terada, M. Yamaguchi, H. Sakai, S. Nomura: *Tetsu-to-Hagane*, **77** (1991), 971.

[13] T. Nakamori, T. Sakane, C. Sudoh, A. Shibuya: *Tetsu-to-Hagane*, **77** (1991), 963.

[14] M. Sakurai, L. W. Zhang, Y. Tajiri, T. Kondo: *Tetsu-to-Hagane*, **77** (1991), 979.

[15] J. S. Thornton and A. D. Thomas Jr.: *Metall Trans.*, **3** (1972), 637.

[16] A. Kelly A and W. R. Tyson: *J. Mech. Phys. Solids.*, **13** (1965), 329.

[17] S. Ochiai and K. Osamura: *J. Mater. Sci.*, **21** (1986), 2735.

[18] M. S. Hu and A. G. Evans: *Acta Metall.*, **37** (1989), 917.

[19] Y. Leterrier, L. Boogh, J. Andersons and J. A. E. Mason: *J. Polym. Sci., Part B: Polym. Phys.*, **35** (1997), 1449.

[20] S. Ochiai and Y. Murakami: *Metal Sci.*, **41** (1976), 401.

[21] J. Andersons, U. A. Handge, I. M. Sokolov and B. Blumen: *Eur. Phys. J.*, **B17** (2000), 261.

Chapter 2

Fracture and Spalling Behavior of Fe-Zn Intermetallic Coating of Galvannealed Steel Sheet

2.1 Introduction

The hot-dipped galvannealed steels, composed of Fe-Zn intermetallic coating and substrate steel, have high corrosion resistance, weldability and paintability, and therefore widely used as architectural and car-body materials [1, 2]. The coating is, however, brittle. It is fractured and spalled during the sheet forming process, reducing the coating quality and causing damage to the forming tools [3].

The fracture and spalling-off process are, however, not fully understood. In the present work, to reveal the process of the fracture and spalling of the Fe-Zn coating layer on galvannealed steel, tensile test and fracture morphological observation were conducted, laying emphasis on the multiple cracking and compressive fracture-induced spalling behavior of the coating, due to the following reasons.

Until now, the following general features have been known for the fracture and spalling behavior of the brittle coating layer with a low failure strain on a ductile substrate. (A) The coating layer exhibits multiple transverse cracking under tensile loading [4-10]. (B) When the tensile stress is applied further on samples, the compressive stress perpendicular to the loading axis increases in the coating due to the difference in contraction between the coating (Poisson's ratio 0.2~0.3 for most brittle materials) and the plastically deforming substrate (0.5). The increased compressive stress causes compressive fracture and spalling of the coating when the coating is thin [9]. In this way, when tensile strain is applied to samples, tensile and compressive stresses are exerted on the coating in the direction parallel and perpendicular to the loading axis, respectively. The tensile stress is responsible for the transverse multiple cracking of the coating layer. The compressive stress is responsible for the compressive fracture of the coating layer in the sample width direction, followed by powdering and

spalling of the coating.

Concerning the spalling of the Fe-Zn coating layer, which occurs after the progress of the multiple cracking, it has been shown until now that buckling and wedging of the coating take place due to the compressive stress in the width direction of the sheet samples [3, 14] and the coating is spalled through the fracture in the δ_1 layer and at Γ-substrate interface [3, 13, 14]. However, the behavior after the fracture in δ_1 layer and at interface has not been studied in detail.

In the present work, the IF-based galvannealed steels and the anodic-oxidized Al_2O_3 coating on aluminum wires for reference were used for observation of the fracture behavior of the brittle coating. Al_2O_3/Al wires were used because of their ease of making test specimens and the smooth surface of their coating which makes it possible to detect the detailed fracture process.

2.2 Experimental procedure

2.2.1 Samples

The hot-dipped Fe-Zn intermetallic coated IF steels, supplied as the common research samples for the research group on structure and property of the coating on GA (galvannealed) steels, organized in The Iron and Steel Institute of Japan, were used for experiments. The chemical composition of the IF steel as the substrate is C:0.002, Si:0.008, Mn:0.1, P:0.01, Al:0.024, Ti:0.051 (mass%). The overall thickness of the coating was 10μm. The coating consisted of a series of Fe-Zn intermetallic compounds, as schematically shown in Fig.2.1: (i) Γ intact to the steel substrate, (ii) Γ_1, which nucleates at the Γ-δ_1 interface in the form of columns, penetrating into δ_1 [3], (iii) thick δ_1 in the middle, occupying around 70-80 % in volume of the coating, and then (iv) ζ layer at the surface (covered by very thin zinc η layer [3]), In the present paper, the layers consisting of (i) Γ, (ii) Γ_1+δ_1, (iii) δ_1 and (iv) ζ are noted as Γ, Γ_1, δ_1 and ζ layers for convenience.

The monofilamentary Al_2O_3-coated aluminum composite wires were prepared by the anodic oxidation of electro-polished 1100 aluminum wires with a

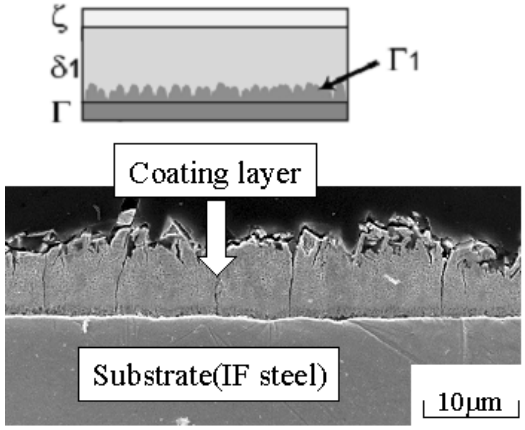

Fig.2. 1 Structure of the galvannealed coating.

nominal diameter of 800μm in the electrolyte of 20 mass% sulphuric acid solution. The anodizing conditions were 20V at 0◦C. The thickness of the Al_2O_3 coating layer was varied from zero to 56μm by controlling the anodic-oxidation time.

2.2.2 Tensile test

Tensile test was carried out at room temperature at a crosshead speed of $8.3x10^{-6}$ m/s for a gage length 50mm using the GA steel samples with a length 100mm, width 10mm and thickness 0.8mm.

Tensile test for Al_2O_3/Al wires was also carried out at room temperature at a crosshead speed of $8.3x10^{-6}$ m/s for a gage length 25mm. The strain was measured by the non-contact laser extensometer (Shimadzu DVE-200).

2.2.3 SEM observation and EPMA analysis

The samples were strained to the prescribed strains and then unloaded. The

fracture morphology of the coating was observed with the SEM (scanning electron microscope (Joel, JSM-5410LS)).

As shown later, the compressive fracture of the coating took place two times in the width direction of the samples, which caused the coating fracture parallel to the surface of the substrate (mode II type fracture) at different layer and interface. As a result, different layer was exposed after the first and second compressive fractures. The exposed layer after the first and second compressive fracture-induced spalling was studied with an EPMA (Electron-Probe Micro Analyzer**,** Hitachi X-650).

2.3 Results and discussion

2.3.1 Fracture behavior of Al_2O_3 coating layer on aluminum wires

The Al_2O_3 coating layer exhibited multiple cracking as well as the GA coating layer. When the Al_2O_3 coatings were thin ($t < 30\mu m$), the coatings exhibited compressive fracture in the circumferential direction after multiple cracking as shown in Fig.2.2 (a), (b) and (c). When the Al_2O_3 coatings were thick ($t > 30\mu m$), the coatings exhibited interfacial debonding as shown in Fig.2.2 (d). In the specimens with thin Al_2O_3 coatings, buckling and wedging patterns were observed as shown in Fig.2.2 (b) and (c), respectively. The risen parts of the coating were broken into flakes and the contact parts between the fracture-ends of the coating were crushed into powders. These fracture behaviors in the sample width direction have been observed also for the GA coating layer [3, 13, 14]. It is noted that the buckling and wedging caused by the compression stress under the applied tensile strain are the common phenomenon for the brittle coating layer on the ductile substrates.

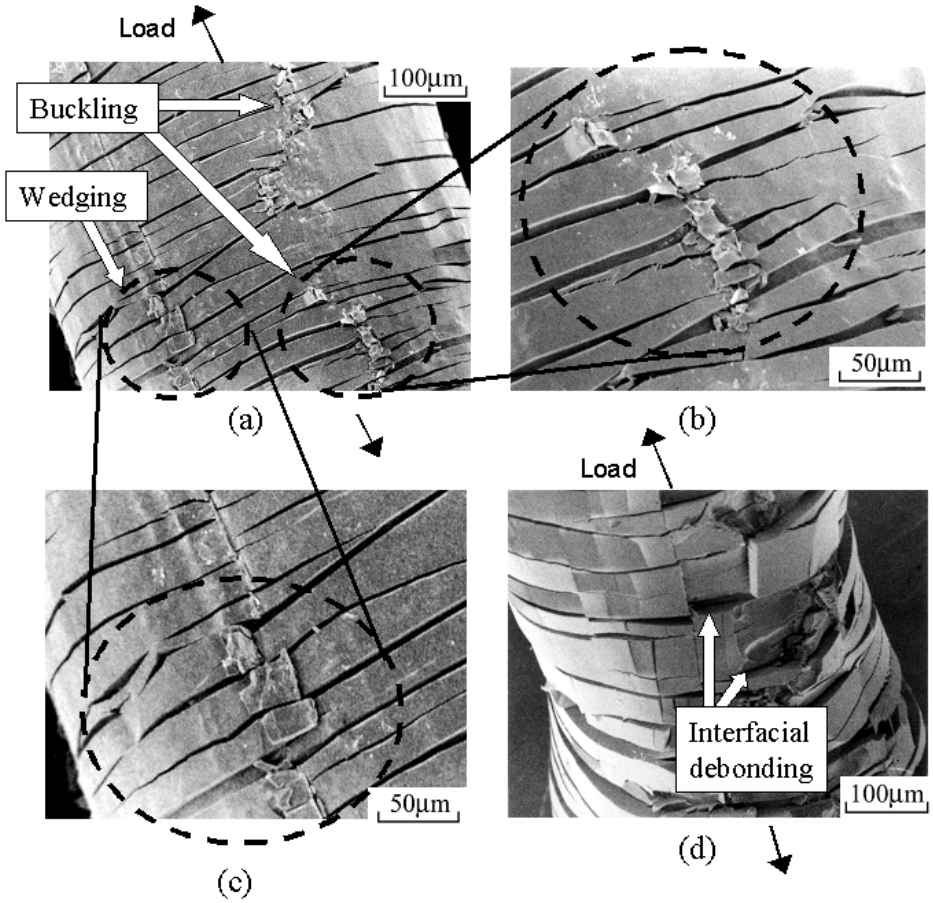

Fig.2.2 Fracture morphology of the Al_2O_3-coated aluminum wire, showing (a, b and c) compressive fracture of the multiply cracked Al_2O_3 layer in the circumferential direction, which takes place when the Al_2O_3 layer is thin (8.0μm in this example) and (b) interfacial debonding, which takes place when the layer is thick (34μm).

2.3.2 Multiple cracking of Fe-Zn coating layer

Figure 2.3 shows the progress of multiple fracture of the galvannealed coating with applied tensile strain. Evidently, the number of cracks increases with increasing tensile strain.

The multiple cracking process of the coating layer is as follows. The stress

of the coating is zero at the cracked part and it increases with distance, reaching maximum at the middle, then decreases symmetrically and becomes again zero at the another cracked part. When the maximum stress $\sigma_{x, max}$ exerted on the coating layer is higher than the strength of the coating layer $\sigma_{c, UTS}$, the long coating layer is cracked again. In this way, the cracking occurs continually until $\sigma_{x, max}$ becomes lower than $\sigma_{c, UTS}$. With increasing applied tensile stress, the stress in the coating layer increases because of the work-hardening of the substrate. As a result, the cracking occurs again until $\sigma_{x, max}$ becomes lower than $\sigma_{c, UTS}$. In this way, the coating layer exhibits multiple cracking.

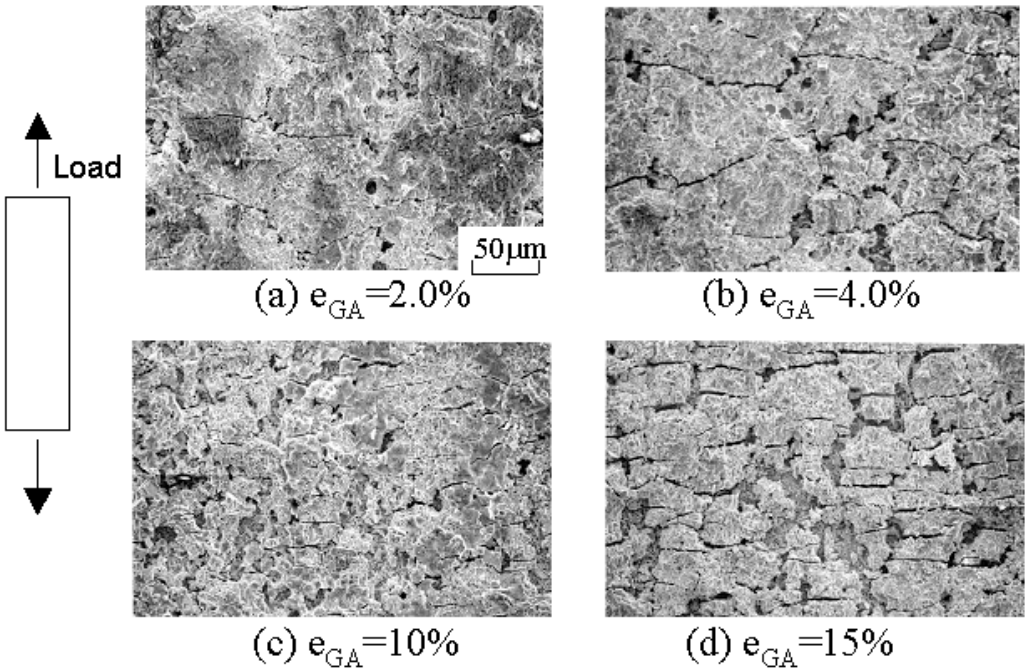

Fig.2.3 Progress of multiple fracture of the galvannealed coating, e_{GA} = (a) 2.0, (b) 4.0, (c) 10 and (d) 15 %.

2.3.3 Compressive fracture and spalling of Fe-Zn coating layer

After the progress of transverse multiple cracking of the coating by the tensile stress, the compressive fracture of the multiply cracked coating occurred two times in the width direction of the samples. At each time, different layers were fractured and spalled.

The spalling of the coating occurred mostly at high applied-strains near the necking strain of the substrate. In order to detect the influence of the deformation amount on the behavior, the samples were pulled in tension beyond the necking strain of the substrate, and the less deformed region apart from the necking and the more deformed region in the necking were observed for comparison. Figures 2.4 and 2.5 show the fracture morphology in the necked region and in the regions apart from the necked region, respectively. Figure 2.6 shows the example of appearance of the strained GA steel with partially and fully spalled coating. Table.2.1 shows the results obtained by EPMA. From Figs.2.4, 2.5 and 2.6, the following features are read.

(1) As shown in Figs.2.4 and 2.5, the amount of the remaining coating became small in the necked region (Fig.2.4) in comparison with that in the region apart from the necked portion (Fig.2.5). Namely the spalling of the coating progressed more in the more deformed region.

(2) The spalling off of the coating occurred not only at the flaked and powdered portions but also for some areas (Figs.2.5 and 2.6). The fracture surface of such areas was nearly flat and parallel to the substrate surface. This indicates that mode II type fracture occurred in such areas.

(3) The appearance of the exposed fracture surface after spalling (the region indicated by "thin $\delta_1+\Gamma_1+\Gamma$ or $\Gamma_1+\Gamma$ layer" in Fig.2.5 and the regions A and C in Fig.2.6) was different from the original surface of the coating indicated by "overall $\zeta+\delta_1+\Gamma_1+\Gamma$ layer" in Fig.2.5 and Fig.2.6 (b). It was also different from the appearance of the exposed substrate steel (the region indicated by "substrate steel" in Fig.2.4 and the region B in Fig.2.6 (b)). These observation results suggest that the spalling of overall coating did not occur at once and a part of the coating remained after the spalling of the upper part.

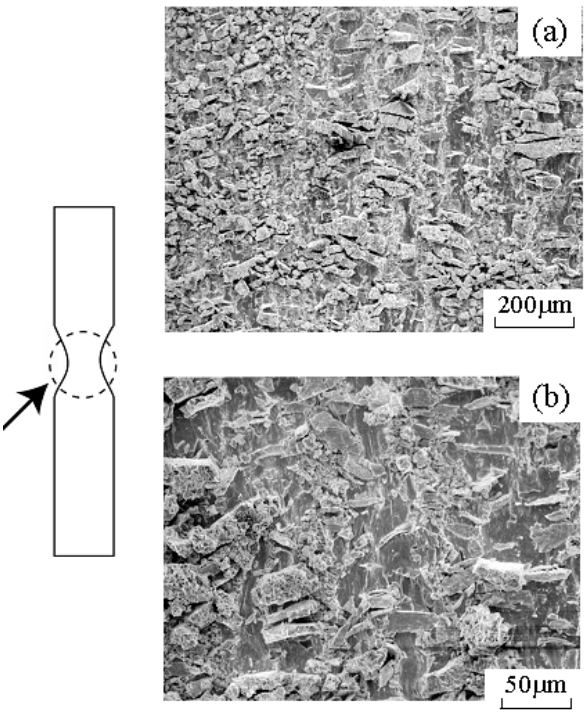

Fig.2.4 Appearance of the galvannealed coating in the necked region of the GA steel.

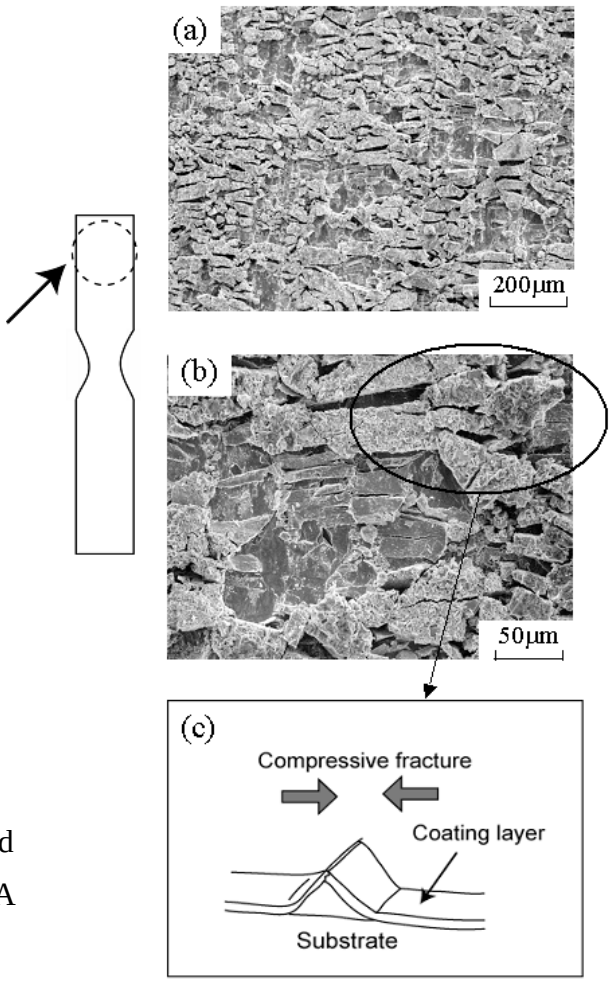

Fig.2.5 Appearance of the galvannealed coating apart from the necked region of the GA steel.

(4) The exposed phases were analyzed with EPMA to know where the mode II type fracture occurred. Typical result is presented in Fig.2.6. The Fe content (at%) of δ_1, Γ_1 and Γ phases has been reported to be 8.5~13.0, 18.5~23.5 and 24.0~31.0 at%, respectively [15]. By comparing these values with the measured ones and referring the structure of the coating shown in Fig.2.1, the fractured layers and interface at A, B and C in Fig.2.6 were determined as follows.

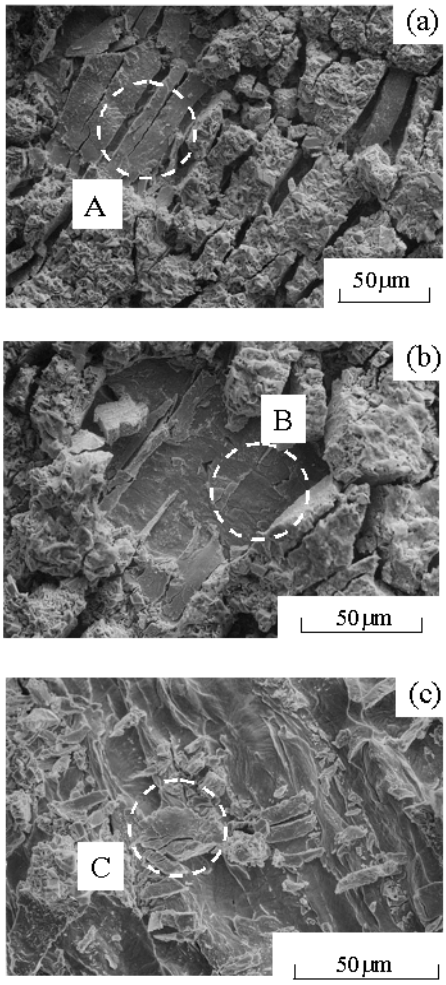

Fig.2.6 SEM image of the side surface of the strained GA steel with partially and fully spalling coating. The dotted circles (A, B and C) indicate the regions whose chemical composition was analyzed with EPMA.

Table 2.1 Results of EPMA analysis and identified exposed layers for the regions A, B and C indicated in Fig.2.6.

Analyzed area	Chemical composition (at%)		Exposed layer
	Zn	Fe	
A	88.03	11.97	δ_1
B	2.98	97.02	Substrate
C	80.13	19.87	Γ_1

At A, the chemical composition of the exposed region corresponded to δ_1 phase. The mode II type fracture in δ_1 and fracture at ζ-δ_1 interface could be mentioned as the candidates to account for the exposure of the δ_1. Between these candidates, only the former could account for the thin thickness of the remaining layer (A in Fig.2.6). Actually, the fracture in the δ_1 has been observed also in the other samples [3, 14], while no report of fracture of the ζ-δ_1 interface was found in the literature survey. Consequently, it was judged that, at A, due to the mode II type fracture in the δ_1, the thin layer of δ_1+Γ_1+Γ remained after the spalling of the thick ζ+δ_1 layer. It has been reported that the defects such as voids and micro cracks forming during fabrication exist in the as supplied condition [3, 14]. It is inferred that such defects act as the initiation sites for the mode II fracture in the δ_1 under the compressive stress.

At C, the chemical composition of the exposed region corresponded to Γ_1. Until now, the fracture at the Γ_1-Γ interface has been reported [3]. In such a case, the exposed layer shall be Γ with higher Fe content than Γ_1, which could not account for the present result. The Γ_1 coexists with δ_1 [3] (Fig.2.1). Therefore, some average composition of Γ_1 and δ_1 is expected if Γ_1 layer containing δ_1 is fractured. From this viewpoint, the analyzed Fe content seems to be high. However, as the layer that remained after the mode II type fracture was thin (C in Fig.2.6 (c)), the influence of underlying Γ with higher Fe content was considered to be contained in the analyzed result. Namely the composition at C was considered to correspond to some average composition of δ_1, Γ_1 and Γ. Accordingly, it was concluded that, at C, the mode II type fracture occurred in Γ_1 layer and the Γ_1+Γ layer remained after the spalling of the thick ζ+δ_1+Γ_1 layer.

At B, the substrate was exposed. The coating was totally spalled off at B. This means that the fracture at the Γ-substrate interface occurred. In the experiment, the fracture of the Γ-substrate interface was, however, observed only in the extensively deformed region (Fig.2.4) but not just after the first compressive fracture, as indicated in Figs.2.5 and 2.6 (a) for relatively less deformed region.

(5) In the region apart from the necking (Fig.2.5), the compressive fracture of the thick ζ+δ_1 or ζ+δ_1+Γ_1 layer, shown with a solid circle, was observed. The exposed fracture surface after such a compressive fracture-induced spalling of the coating is

found in the center. The exposed fracture surface of the thin δ_1+Γ_1+Γ or Γ_1+Γ layer had multiple cracks with narrower crack spacing than that of the overall coating. This is attributed to the increase in stress transfer efficiency; the thinner the coating, the higher becomes the transferred stress [6].

(6) The amount of the coating in the regions in the necking (Fig.2.4) was small in comparison with that in the region apart from the necking (Fig.2.5). This result means that the thin layer that remained in the less deformed region came to be spalled off by further deformation.

The result stated in (6) indicates that, while the thin layer remains after first compressive fracture of the coating, it is spalled off in the later stage. Namely the mechanism to cause spalling of the remaining layer takes place when the sample is deformed more. The observation of the fracture surface of the region near the necking revealed that the remaining layer was fractured also by the compressive stress in the width direction of the samples. An example is presented in Fig.2.7 where the buckling fracture of the remaining Γ_1+Γ layer occurred, accompanied by the powdering. In this case, the Γ-substrate interface is debonded under further deformation, resulting in spalling of the Γ_1+Γ layer.

In this way, the spalling mechanism of the coating was characterized by the two times compressive fracture process of the coating, accompanied by the mode II type fracture in the δ_1 and Γ_1 layers in the first compressive fracture and by that at the Γ–substrate interface in the second one. The fracture and spalling process of the coating layer is summarized as shown in Fig.2.8.

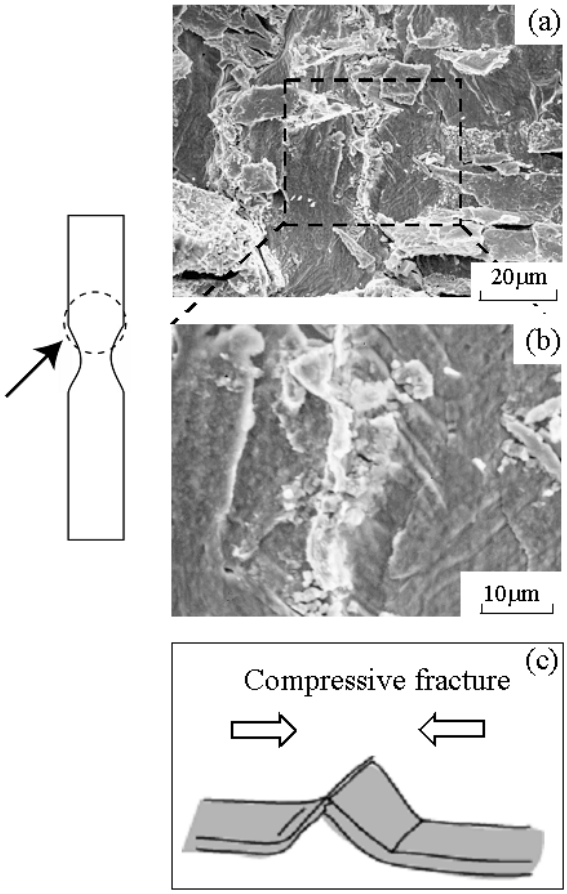

Fig.2.7 Compressive fracture of the thin layer that remained after spalling off of the upper layer due to the mode II-type fracture in the Γ_1 layer near the $\Gamma_1 - \Gamma$ interface.

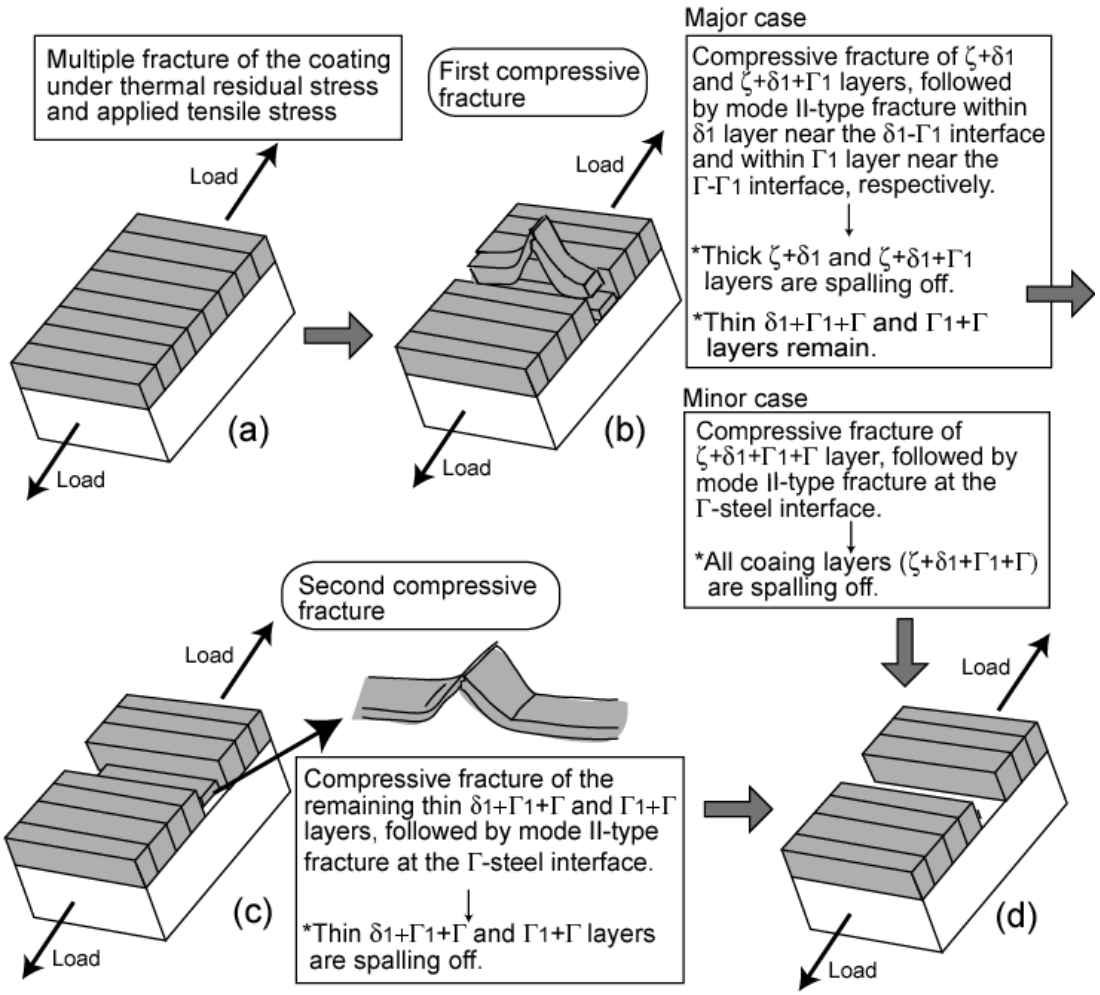

Fig.2.8 Schematic representation of the fracture and spalling-off process of the galvannealed coating.

2.4 Conclusions

(1) The coating showed multiple cracking in the as-supplied condition. When tensile strain was applied, the multiple cracking progressed more.

(2) After the progress of the multiple cracking, the coating was fractured two times compressively in the width direction of the sheet samples. In the first compressive fracture process, buckling, wedging and wearing of coating occurred, causing flaking and powdering of the coating and mode II type fracture in the δ_1 and Γ_1 layers. Thus the upper thick $\zeta+\delta_1$ and $\zeta+\delta_1+\Gamma_1$ layers were spalled off, and, the $\delta_1+\Gamma_1+\Gamma$ and $\Gamma_1+\Gamma$ layers remained on the substrate. Then, in the second compressive fracture process, the layers that remained after the first compressive fracture were fractured also compressively under further increased applied strain due to the increased compressive stress in the width direction. The second compressive fracture caused the mode II type fracture of the Γ-substrate interface and spalling of the remaining layers.

(3) When the Al_2O_3 coatings were thin ($t < 30\mu m$), the coatings exhibited compressive fracture in the circumferential direction. When the Al_2O_3 coatings were thick ($t > 30\mu m$), the coatings exhibited interfacial debonding. In the specimens with thin Al_2O_3 coatings, buckling and wedging patterns were observed.

ACKNOWLEDGEMENT

The authors wish to express their gratitude to JFE 21st Century Foundation, Tokyo, and The Iron and Steel Institute of Japan and for the support of this work.

References

[1] S. Lazik, C. Esling and J. Wegria: *Textures and Microstructures*, **23** (1995), 131.

[2] C. E. Jordan CE, K. M. Goggins and A. R. Marder: *Metall Mater Trans A.*, **25** (1994), 2101.

[3] A. T. Alpas and J. Inagaki: *ISIJ Int.*, **40** (2000), 172.

[4] J. S. Thornton and A. D. Thomas Jr.: *Metall Trans.*, **3** (1972), 637.

[5] A. Kelly A and W. R. Tyson: *J. Mech. Phys. Solids.*, **13** (1965), 329.

[6] S. Ochiai and K. Osamura: *J. Mater. Sci.*, **21** (1986), 2735.

[7] M. S. Hu and A. G. Evans: *Acta Metall.*, **37** (1989), 917.

[8] Y. Leterrier, L. Boogh, J. Andersons and J.-A. E. Mason: *J. Polym. Sci., Part B: Polym. Phys.*, **35** (1997), 1449.

[9] S. Ochiai and Y. Murakami: *Metal Sci.*, **41** (1976), 401.

[10] J. Andersons, U. A. Handge, I. M. Sokolov and B. Blumen: *Eur. Phys. J.*, **B17** (2000), 261.

[11] J. Foct: *Scripta Metall.*, **28** (1993), 127.

[12] A. Iost and J. Foct: *J. Meter. Sci. Lett.*, **12** (1993), 1340.

[13] M. Sakurai, J. Inagaki and T. Alpas: *CAMP-ISIJ*, **12** (1999), 550.

[14] E. Tzimas and G. Papadrimitriou: *Surf. Coat. Technol.*, **145** (2001), 176.

[15] K. Yamato: The 138th and 139th Nishiyama Memorial Lecture, The Iron and Steel Instutite of Japan, (1985), 15.

Chapter 3

Stress Analysis and Prediction of Multiple Cracking of Coating Layer of Galvannealed Steel under Applied Tensile Strain

3.1 Introduction

The hot-dipped GA (galvannealed) steels, consisting of Fe-Zn intermetallic coating layer and substrate steel, are widely used as architectural and car-body materials due to their high corrosion resistance and weldability [1, 2]. As these materials are composed of brittle coating layer with low failure strain and ductile substrate with far higher failure strain, the coating layer exhibits multiple cracking perpendicular to the tensile direction [3-8].

In our former work [9], residual stress analysis of the galvannealed coating layer was carried out. It was found that the residual stress is reduced from 720MPa to around 130MPa by the multiple cracking and the strength of the coating layer is 260-270MPa.

The aim of the present work is to predict the change of the critical and average crack spacing of the coating layer with applied tensile strain. For this aim, the fracture behavior of the coating layer was observed using two kinds of the specimens with different substrate and different thickness of the coating layer. Then the results were analyzed with the finite element method.

3.2 Experimental procedure

3.2.1 Samples and tensile test

The used samples were the hot-dipped Fe-Zn intermetallic compound-coated IF

(Interstitial Free) and SPCC (Steel Plate Cold Commercial) steels. The chemical compositions of the substrate IF and SPCC steels are C:0.002, Si:0.008, Mn:0.1, P:0.01, Al:0.024, Ti:0.051 and C:0.04, Si:0.005, Mn:0.18, P:0.013, Al:0.014 (mass%), respectively. Hereafter, the IF and SPCC steel-based samples are noted as sample I and sample S, respectively. The steel plates were prepared by the heat-treatment at 773K for 80s of the hot-dipped galvanized steel. The coating layer was composed of thin ζ phase layer covered by very thin zinc η phase resulting from solidification, followed by thick δ_1 phase occupying approximately 80% in volume of the coating layer and then a thin Γ_1 phase layer in contact to the substrate steel. The overall thickness of the coating layer was 10 and 5 μm for the IF and SPCC steels, respectively.

Tensile test was carried out at room temperature at a crosshead speed of 8.3×10^{-6} m/s for a gage length 50mm using the specimens with a length 100mm, width 10mm and thickness 0.8mm. The crack spacings of the coating layer at 4, 10, 15 and 20% applied strain were measured with the scanning electron microscope (SEM). The strain of the specimens was measured with the non-contact laser extensometer (Shimadzu DVE-200).

3.2.2 Finite element analysis

The morphology of the specimen with multiply cracked Fe-Zn intermetallic compound coating layer is schematically shown in Fig.3.1 (a) where L is the crack spacing and T is the thickness of the coating layer. In the finite element analysis to calculate the stress distribution, a plane-strain model was used, in which the region ABFE was taken up as the representation. The longitudinal distance y was taken from the center plane: y = 0 at AB, y = 400μm at CD and y= 400μm +T at EF. The horizontal distance x was defined to be zero at the broken end, L/2 at the middle, and L at the another broken end, as shown in Fig.3.1.

An example of the finite element mesh of the plane-symmetric model and the boundary conditions employed in the present analysis are shown in Fig.3.1 (b). The displacements of the cross-sections ACE and AB were taken to be zero. Common compulsory tensile displacement was given for the cross-section BDF in the x-direction.

For analysis of the stress distribution, the crack spacing L = 10, 20, 30, 40 and

80μm and the thickness of the coating layer T = 2, 5, 10 and 15μm were used. As mentioned above, the present specimens were heated for formation of the intermetallic compounds at 773K and cooled down to room temperature. Therefore the temperature change ΔT = -475K was input. The stress of the coating layer in the x-direction, σ_x, was calculated for the applied tensile strain = 10, 20 and 30%.

The analysis was carried out with the commercial finite element code MARC/Mentat2001. The Young's modulus, shear modulus, Poisson's ratio and coefficient of linear expansion of the steel substrate were taken to be 210GPa [10], 81GPa, 0.30 [10] and 2.2×10^{-5}/K [11, 12] respectively [13] and those of the coating layer to be 140GPa [10], 54GPa, 0.30 [10] and 1.1×10^{-5}/K [11, 12] respectively from the reported value for δ_1 phase. The shear modulus is given by,

$$G = \frac{E}{2(1+\nu)} \tag{1}$$

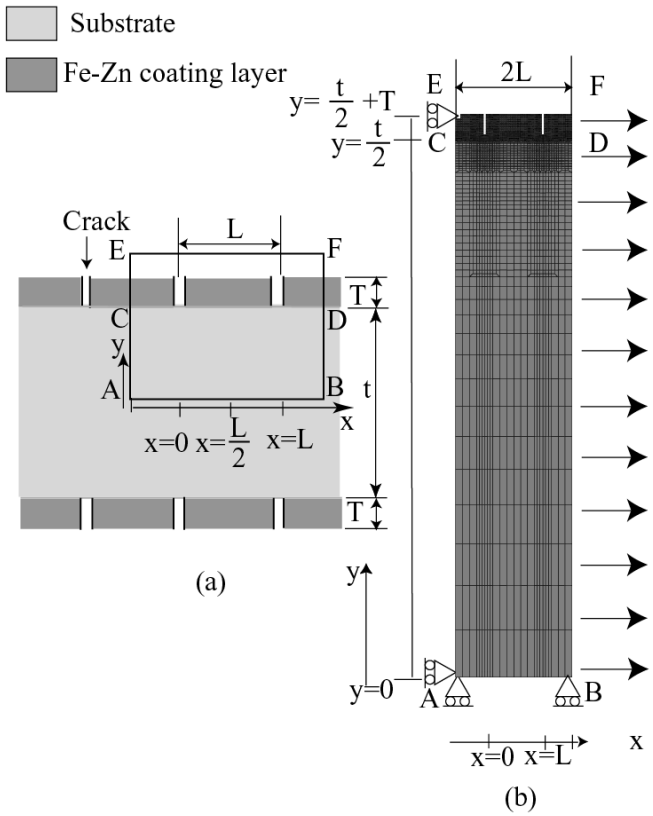

Fig.3.1 FEM-mesh and boundary condition of the GA steel for stress analysis.

It has been known that the coating layer has a multilayered structure composed mainly of the ζ, δ_1, Γ_1 and Γ phases and δ_1 phase is the thickest under the usual fabrication route [10, 13]. In the present samples, the volume fraction of the δ_1 phase was estimated to be 70-80% from the composition image of the polished cross-sectional surface. Concerning the elastic constants (E, ν and G), no data have been reported for the ζ, Γ_1 and Γ phases. Only the values for the δ_1 phase [10] have been experimentally studied and therefore only they are available. Due to these reasons, the elastic constants of the δ_1 phase, which occupies 70-80% of the coating layer and therefore practically governs the behavior of the coating layer, were used as an approximation.

The yielding condition for the steel substrate was given by the von Mises criterion.

$$Y = \bar{\sigma} = \left[\frac{1}{2} \left\{ (\sigma_1 - \sigma_2)^2 + (\sigma_2 - \sigma_3)^2 + (\sigma_3 - \sigma_1)^2 \right\} \right]^{\frac{1}{2}} \quad (2)$$

From the measured nominal stress- nominal strain curves, the true stress (σ) - true plastic strain (ε) curves of the substrate materials in the form of the Ludwik equation (3) were expressed by,

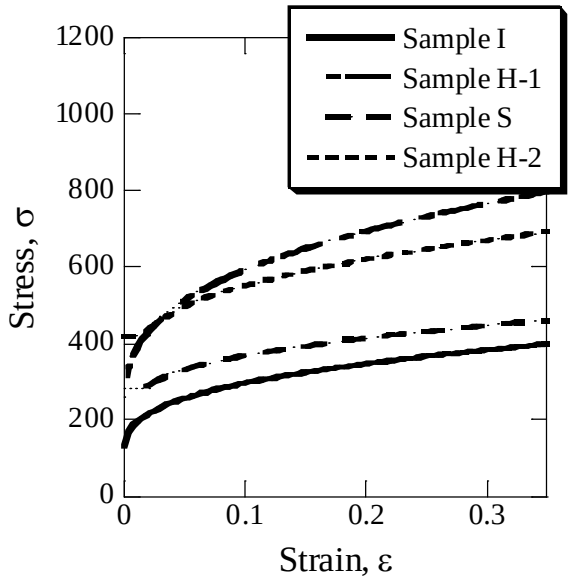

Fig3.2 True stress – true strain curves of Samples I, H-1, S and H-2.

$$\sigma = \sigma_y + k\varepsilon^n \quad (3)$$

$$\sigma = 130 + 400\varepsilon^{0.38} \quad (\varepsilon_y \le \varepsilon) \quad \text{(Sample I)} \quad (4)$$

$$\sigma = 280 + 320(\varepsilon - 0.02)^{0.51} \quad (0.02 \le \varepsilon) \quad \text{(Sample S)} \quad (5)$$

To investigate the influence of the species of the steel substrate, imaginary high strength steels with two times yield stress and ultimate strength in comparison with that of IF steel (Sample H-1), and with 1.5 times yield stress and ultimate strength in comparison with that of SPCC steel (Sample H-2) were taken up. Figure 3.2 shows the true stress - true plastic strain curves of Samples I, H-1, S and H-2.

3.3 Results and discussion

3.3.1 Tensile test

The thermally induced average crack spacings of the coating layer at 0% strain were 22 and 55 μm for Samples I and S, respectively. The Fe-Zn intermetallic coating layer exhibited multiple cracking when tensile stress was applied externally. The measured average crack spacing with applied strain is presented in Table 3.1. Evidently, the crack spacing decreased with increasing strain.

Table 3.1 Measured average crack spacing of Samples I and S.

	Average crack spacing (μm)	
Strain (%)	Sample I	Sample S
4	44.0	21.5
10	37.4	16.7
15	28.9	15.5
20	26.5	14.3
33		10.5

3.3.2 Finite element analysis

First, the tensile stress at the nominal strain = 10, 20 and 30% of the coating layer were calculated for L = 10, 20, 30, 40 and 80μm and for T = 10μm (Sample I) and 5μm (Sample S). In the following parts, the tensile stress σ_x in the x-direction, averaged along the y-direction, of the coating layer, is used.

Figure 3.3 shows the variations of the calculated tensile stress σ_x in the x-direction of the coating layer with distance from the crack x for L=0 to 80μm at an applied nominal strain of 10% (Sample S). Evidently, the σ_x is highest ($\sigma_{x,\,max}$) at the middle point x = L/2. It is noted that the exerted stress on the coating layer increases with increasing crack spacing. As the cracking occurs when σ_x exceeds the strength of the coating layer $\sigma_{c,\,UTS}$, the longer segment tends to be cracked more.

When the cracking of the coating layer occurred at x = L/2, the relation between the critical length of the coating layer L_c (= the necessary length for the coating layer to be cracked) and the average crack spacing L_{ave} is given by [8],

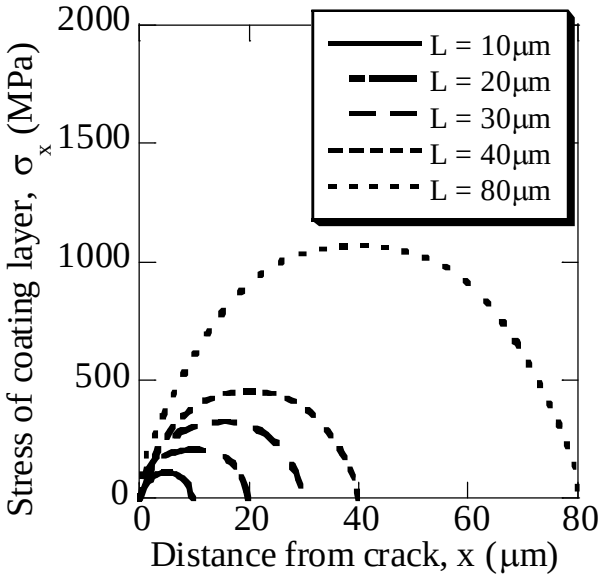

Fig.3.3 Distribution of tensile stress σ_x of the coating layer at the nominal strain e = 10%, for the crack spacing L = 10, 20, 30, 40 and 80μm. (Sample S, coating layer thickness T = 5μm)

$$L_c = \frac{4}{3} L_{ave} \tag{6}$$

Substituting the measured L_{ave} value into Eq.(6), we had the critical length of the coating layer L_c. Figure 3.4 shows the relation between the maximum tensile stress $\sigma_{x,max}$ multiplied by the coating layer thickness T and crack spacing L at the applied strain = 10% (Sample S). The calculation results showed that the thinner and the longer the coating layer, the higher becomes $\sigma_{x,\,max}$. The $\sigma_{x,\,max}$ T is nearly proportional to L.

In description of the exerted stress on fiber in the composite material, the Kelly – Tyson equation derived empirically is well – known. This equation was applied to the present coating model. When L is smaller than L_c, the following equation is obtained,

$$\frac{L}{T} = \frac{2\sigma_{x,\,max}}{\tau_i} \tag{7}$$

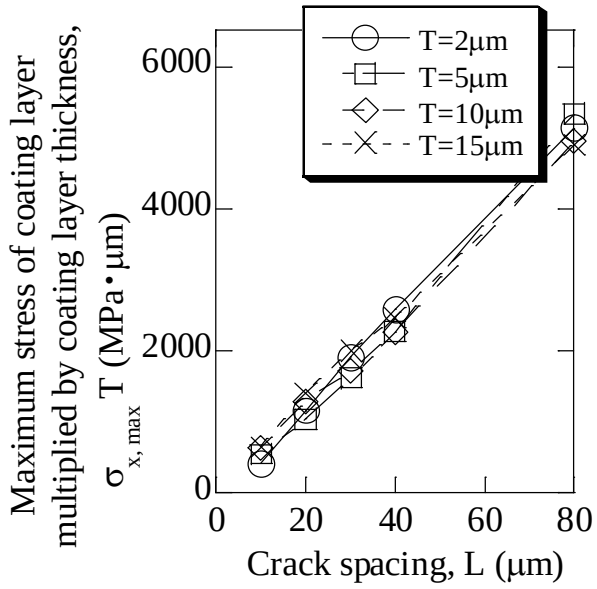

Fig.3.4 Relation between the maximum tensile stress $\sigma_{x,\,max}$ of the coating layer multiplied by the coating layer thickness T and crack spacing L, at the nominal strain e = 10%, for the coating layer thickness T = 2, 5, 10 and 15μm. (Sample S)

where τ_i is the average share stress in the substrate /coating interface. As the τ_i is almost independent of the thickness of the coating layer T and crack spacing L when $L \leq L_c$ [9], $\sigma_{x,\,max}$ is proportional to L/T. This relation is coincidental to the result of the present numerical analysis.

For the saving of gasoline, it is planned to use galvannealed high strength steels for the car body materials. However, the influence of the high strength steel substrate on the fracture behavior of the coating layer has not been revealed yet. To reveal the influences of the substrate material on the multiple cracking, the measured samples (I and S) and the imaginary high strength steel samples (H-1 and H-2) were taken up for calculation.

Figure 3.5 shows the relation between the $\sigma_{x,\,max}\,T/\sigma_s$ and applied strain for a given crack spacing L = 40 μm, where σ_s is the tensile stress of the substrate at the corresponding strain. Figure 3.5 suggests that the $\sigma_{x,\,max}\,T$ is proportional to σ_s at any strain, to a first approximation.

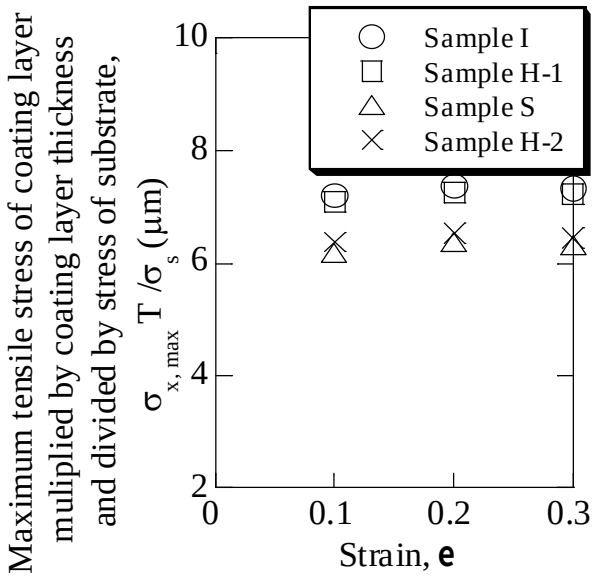

Fig.3.5 Relation between $\sigma_{x,\,max}\,T/\sigma_c$ (the maximum tensile stress of coating layer multiplied by the coating layer thickness and divided by the stress of substrate) to the nominal strain e. (Coating layer thickness T = 10μm for Samples I and H-1, and T = 5μm for Samples S and H-2. Crack spacing L = 40μm.)

For wide variety of L, T, and strain, similar calculation was carried out. The result indicated that $\sigma_{x\,max}$ T is nearly proportional to L and σ_s, namely $\sigma_{x\,max}/\sigma_s$ is nearly proportional to L/T at any strain as shown in Fig.3.6. These results suggest that the following equation is hold as a first approximation.

$$\frac{\sigma_{x,\,max}}{\sigma_s} = C\frac{L}{T} \qquad C=\text{const.} \qquad (8)$$

From the slope in Fig.3.6, the constant C was estimated to be around 0.18 commonly to all substrates, despite the difference in mechanical properties (yield stress, tensile strength, and strain hardening coefficient) among the substrates.

The linear relation of $\sigma_{x,\,max}$ to σ_s is explained as follows. The coating layer exhibits multiple cracking and therefore the stress is released at the crack. Tensile stress in the coating layer is transferred from the substrate through the coating / substrate interface by the interfacial shear stress τ_i. When the Kelly-Tyson equation (7) is substituted into Eq.(8), the relation of σ_s to τ_i is derived as Eq.(9).

$$\tau_i = 2C\sigma_s \qquad C=\text{const.} \qquad (9)$$

The τ_i is proportional to σ_s. As a result, $\sigma_{x,\,max}$ is proportional to σ_s.

Noting the strength of the coating layer $\sigma_{c,\,UTS}$, and substituting $\sigma_{x,\,max} = \sigma_{c,\,UTS}$ and $L = L_c$ into Eq.(8), we have the critical length of the coating layer L_c and the average crack spacing L_{ave},

$$L_c = \frac{T}{C}\left(\frac{\sigma_{c,\,UTS}}{\sigma_s}\right) \qquad (10)$$

$$L_{ave} = \frac{3T}{4C}\left(\frac{\sigma_{c,\,UTS}}{\sigma_s}\right) \qquad (11)$$

Substituting the parameters C = 0.18, T = 10μm (Samples I and H-1) and 5μm (Sample S and H-2), and σ_s as a function of strain, the variation of L_{ave} as a function of strain can be calculated if the strength of the coating layer $\sigma_{c,\,UTS}$ is known. In the present work, as the $\sigma_{c,\,UTS}$-value was unknown, various values of $\sigma_{c,\,UTS}$ were input into Eq.(11) and the fit value of $\sigma_{c,\,UTS}$ to the measured variation of critical length were sought.

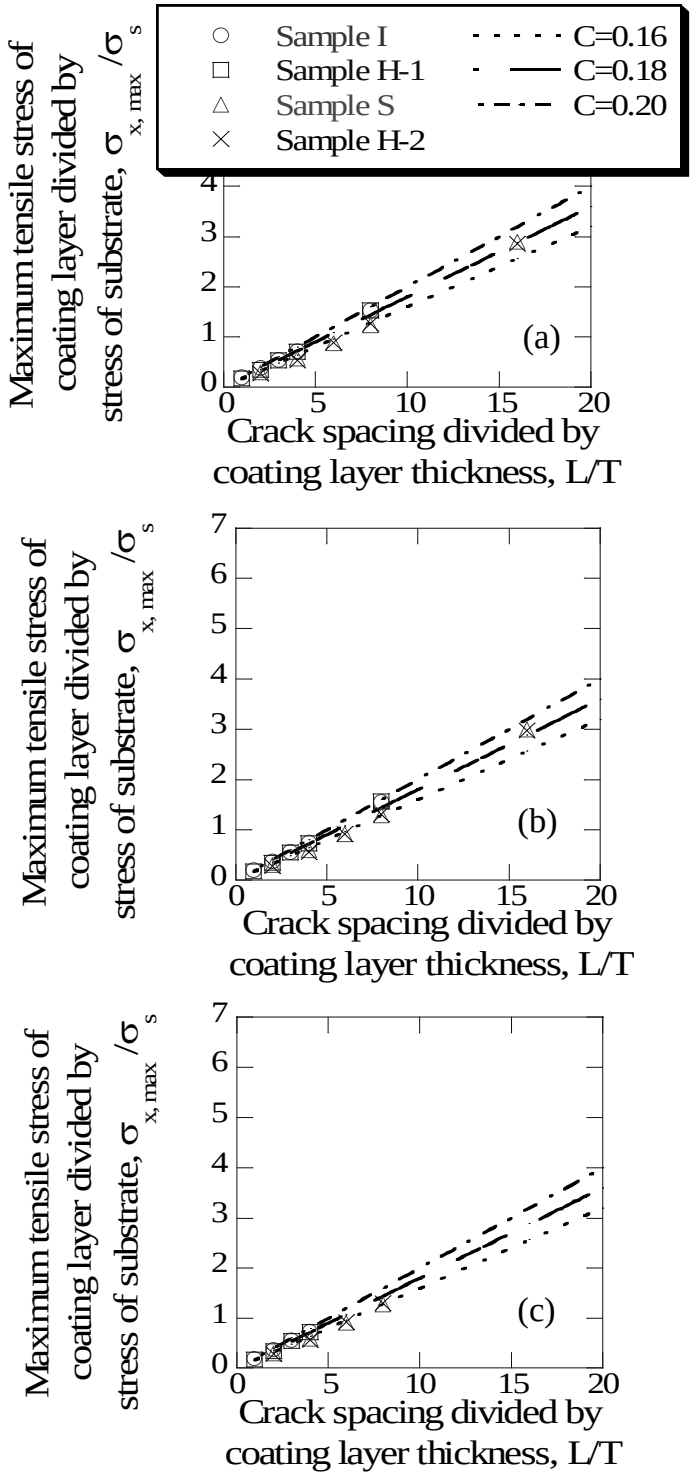

Fig.3.6 Relation between $\sigma_{x,\,max}$ / σ_c (the maximum tensile stress of coating layer divided by the stress of substrate) to L/T (crack spacing divided by coating layer thickness) for applied nominal strain e = (a) 10%, (b) 20% and (c) 30%.

Figures 3.7 and 3.8 show the change of L_{ave} with nominal strain e for Samples I and S, respectively. The L_{ave} –values were calculated using $\sigma_{c,\ UTS}$ = 230, 260 and 290MPa and compared with the measured values (Table 3.1). It was found that $\sigma_{c,\ UTS}$ = 260MPa could describe the experimental result for both IF and SPCC substrate specimens. This value is nearly equal to the value estimated from the analysis of the thermally induced multiple cracking during cooling of the sample [9].

The constant C and the average strength of the coating layer $\sigma_{c,\ UTS}$ were almost independent of the species of the substrate steel. It is noted that, if the values of C and $\sigma_{c,\ UTS}$ estimated to be around 0.18 and 260MPa, respectively, are common for any substrate steel, we can predict the L_{ave} as a function of applied strain by substituting T and σ_s into Eq.(11) for any substrate steels. As an example, the change of L_{ave} with applied strain calculated with $\sigma_{c,\ UTS}$ = 260MPa, under the condition of T = 10μm, for Samples I, S, H-1 and H-2, is presented in Fig.3.9. The higher the stress of the substrate, the shorter the L_{ave} becomes. This result indicates that the stress is transferred more efficiently to the coating layer and therefore the multiple cracking progresses more for high strength steel substrate.

As shown in Fig.3.10, the changes of L_{ave} with applied strain e for various substrate steels with different strength and for various coating layer thickness T can easily be calculated. This approach is rough but is very simple, being convenient for prediction in practice.

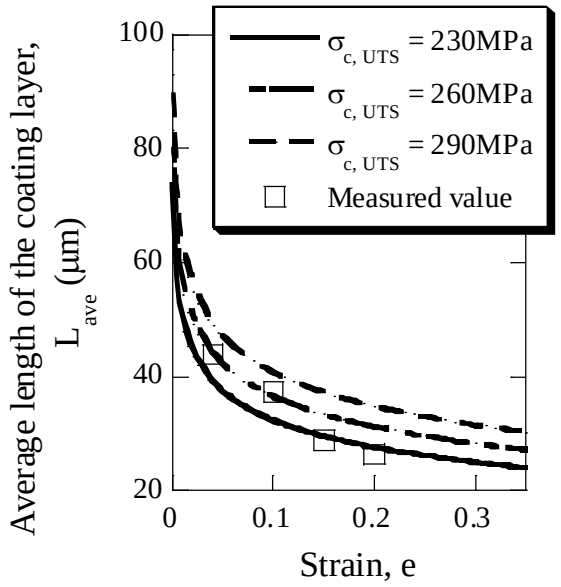

Fig.3.7 Change of the average length of the coating layer L_{ave} with nominal strain e, for the strength of coating layer $\sigma_{c, UTS}$ = 230, 260 and 290MPa. (Sample I, coating layer thickness T = 10μm)

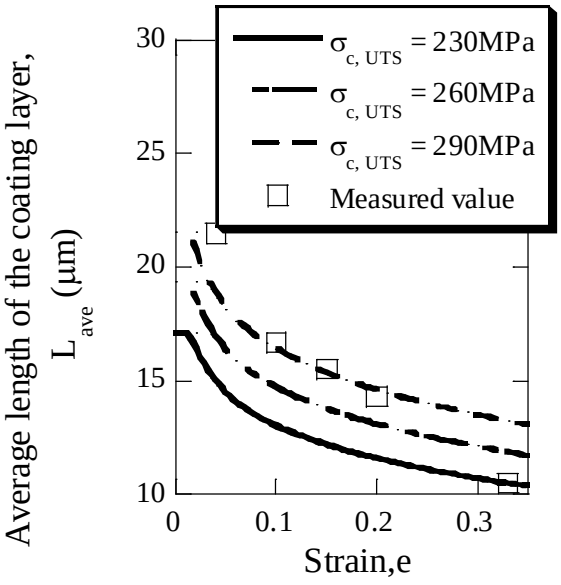

Fig.3.8 Change of the average length of the coating layer L_{ave} with nominal strain e, for the strength of coating layer $\sigma_{c, UTS}$ = 230, 260 and 290MPa. (Sample S, coating layer thickness T = 5μm)

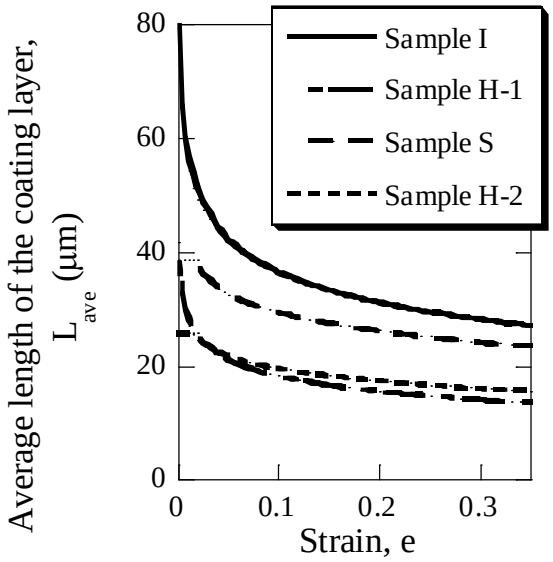

Fig.3.9 Change of the average length of the coating layer L_{ave} with nominal strain e, for. Samples I, H-1, S and H-2. (strength of coating layer $\sigma_{c,\,UTS}$ = 260MPa, coating layer thickness T = 10μm)

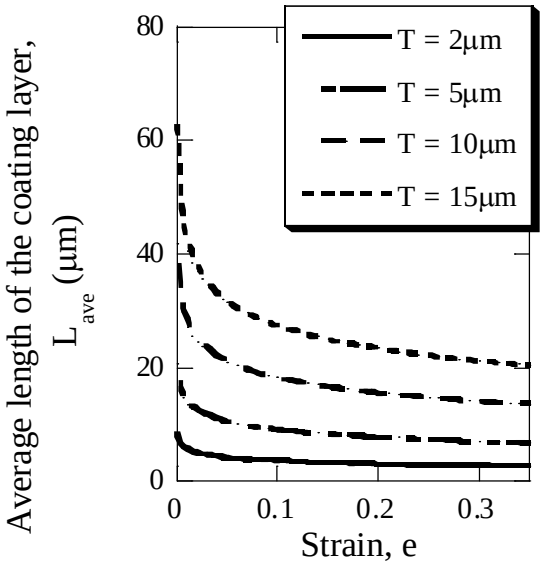

Fig.3.10 Change of the average length of the coating layer L_{ave} with nominal strain e, for the coating layer thickness T = 2, 5, 10 and 15μm. (Sample H-1, strength of coating layer $\sigma_{c,\,UTS}$ = 260MPa)

3.4 Conclusions

The fracture behavior of the Fe-Zn intermetallic compound coating layer on ductile steel substrate sheets was studied. The main results are summarized as follows.

(1) Based on the finite element analysis and Kelly – Tyson equation, the following equation was derived,

$$\frac{\sigma_{x,\,max}}{\sigma_s} = C\frac{L}{T} \qquad C \approx 0.18$$

(2)Application of equation in (1) to the experimental results revealed that the average strength of coating layer $\sigma_{c,\,UTS}$ on IF and SPCC substrate steels was around 260MPa.

(3) The critical length of the coating layer L_c and the average crack spacing of the coating layer L_{ave} at the strain were expressed as,

$$L_c = \frac{T}{C}\left(\frac{\sigma_{c,\,UTS}}{\sigma_s}\right) \quad , \quad L_{ave} = \frac{3T}{4C}\left(\frac{\sigma_{c,\,UTS}}{\sigma_s}\right)$$

With these equations, as the $\sigma_{c,\,UTS}$-value is now known (260MPa), the changes of the critical length and average crack spacing of the coating layer with applied strain could be predicted to a first approximation for any species of the substrate steel and for any coating layer thickness only by substituting the flow stress at the corresponding strain of the substrate.

ACKNOWLEDGEMENT

The authors wish to express their gratitude to JFE 21st Century Foundation, Tokyo, and The Iron and Steel Institute of Japan and for the support of this work.

References

[1] C. E. Jordan CE, K. M. Goggins and A. R. Marder: *Metall. Mater. Trans. A*, **25A** (1994), 2101.

[2] S. Lazik, C. Esling and J. Wegria: *Textures Microstruct.*, **23** (1995), 131.

[3] A. Kelly A and W. R. Tyson: J. Mech. *Phys. Solids*, **13** (1965) 329.

[4] S. Ochiai and K. Osamura: *J. Mater. Sci.*, **21** (1986), 2735.

[5] M. S. Hu and A. G. Evans: *Acta Metall.*, **37** (1989), 917.

[6] Y. Leterrier, L. Boogh, J. Andersons and J. A. E. Mason: *J. Polym. Sci. B. Polym. Phys.*, **35** (1997), 1449.

[7] S. Ochiai and Y. Murakami: *Met. Sci.*, **41** (1976), 401.

[8] J. Andersons, U. A. Handge, I. M. Sokolov and B. Blumen: *Eur. Phys. J.*, **B17** (2000), 261.

[9] S. Ochiai, S. Iwamoto, T. Tomida, T. Nakamura, H. Okuda M. Tanaka and H. Hojo: *Tetsu-to-Hagane*, **91** (2005), 327.

[10] G. Reumont, J. B. Vogt, A. Iost and J. Foct: *Surf. Coat. Technol.*, **139** (2001), 265.

[11] J. Foct: *Scr. Metall. Mater.*, **28** (1993), 127.

[12] A. Iost and J. Foct: *J. Mater. Sci.*, **12** (1993), 1340.

[13]E. Tzimas and G. Papadrimitriou: *Surf. Coat. Technol.*, **145** (2001), 176.

Chapter 4

Analysis of Buckling and Interfacial Debonding of Galvannealed Coating Layer on Steel Substrates under Applied Tensile Strain

4.1 Introduction

The hot-dipped GA (galvannealed) steels, consisting of Fe-Zn intermetallic coating layer and substrate steel, are widely used as architectural and car-body materials due to their high corrosion resistance and weldability [1, 2]. As these materials are composed of brittle coating layer with low failure strain and ductile substrate with far higher failure strain, the coating layer exhibits multiple cracking perpendicular to the tensile direction [3-8], followed by spalling, when tensile stress is applied externally. The spalling of the coating layer is caused by the compressive fracture such as buckling and wedging in the sample width direction [7], followed by interfacial debonding. When the tensile stress is applied up to high level, such a compressive stress increases in the coating due to the difference in contraction between the coating (Poisson's ratio 0.2~0.3 for most brittle materials) and the plastically deforming substrate (0.5). Accordingly, the amount of the spalled coating layer increases with increasing applied strain.

However, the spalling process and its relation to the preceding multiple cracking have not been clarified in detail. In the present work, to detect the features of the spalling process and the relation between multiple cracking and spalling of the Fe-Zn coating layer on steel sheet, tensile test and fracture morphology observation were conducted. Then, in order to reproduce the spalling process in the computer and to clarify the relation of the spalling behavior to crack spacing, numerical analysis was carried out based on the finite element analysis for three cases with different crack spacing of the coating layer in the tensile direction.

4.2 Experimental procedure

4.2.1 Fracture morphology observation of the coating layer

The used samples were the hot-dipped Fe-Zn intermetallic compound-coated IF (Interstitial Free) steels. These samples were supplied as the common samples for the research group on structure and property of the coating on GA (galvannealed) steels, organized in The Iron and Steel Institute of Japan. The overall thickness of the coating layer was 10 μm.

The results of tensile test of the sample have been presented [14] in our former work. In the present work, compressive fracture and spalling behavior of the coating layer of the tensile-tested samples were carefully observed with the scanning electron microscope to reveal the events that take place in the spalling process.

4.2.2 Finite element analysis

3-dimentional models for analysis of interfacial debonding of the coating layer were prepared as follows. The morphology of the specimen with multiple- cracked Fe-Zn intermetallic compound coating layer is schematically shown in Fig.4.1 (a) where L is the crack spacing in the tensile direction, W is the crack spacing in the width direction and T is the thickness of the coating layer. An example of the finite element mesh of the model employed in the present analysis is shown in Fig.4.1 (b). As indicated in Fig.4.1 (a), the longitudinal distance x was taken to be zero at the middle, and to be L/2 at the broken end. The distance across-the-width y was taken to be zero at the broken end, to be W/2 at the middle, and to be W at the other broken end. The vertical distance z was taken to be zero at the middle of substrate in the thickness direction. As the thickness of the substrate was 800μm, the distance z of the coating layer / substrate interface was taken to be 400μm, and the distance z was taken to be 400 μm +T (= 10μm in the present sample) at the surface of the coating layer. For this analysis, the crack spacing in the x-direction L = 20, 40 and 60μm, and that in the y-direction W = 80μm were used, where W = 80μm corresponds to the thermally

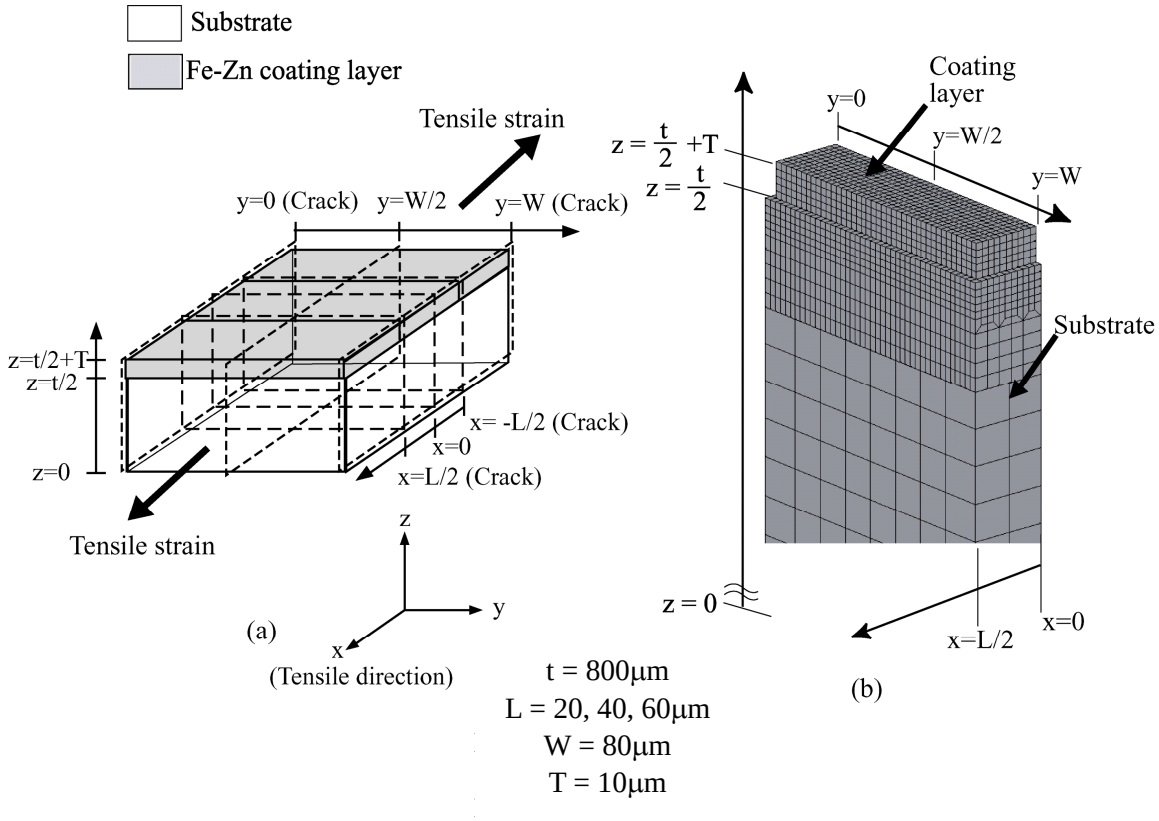

Fig.4.1 FEM-mesh of the GA steel for stress analysis.

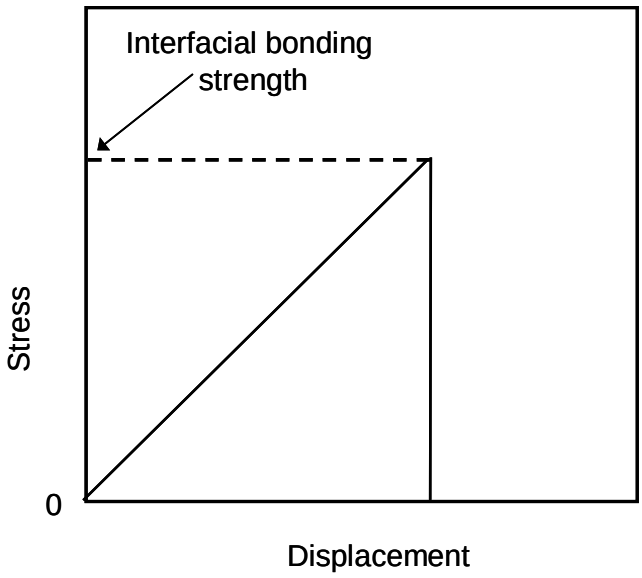

Fig.4.2 Schematic representation of the stress-displacement diagram of the interfacial connector spring employed in the present analysis.

induced critical crack spacing in the coating layer [14, 16], and L = 40μm corresponds to the critical length at which buckling behavior of the coating layer were observed. The present specimens had been heated at 773K for formation of the intermetallic compounds and cooled down to room temperature. Therefore the temperature change ΔT = -475K was input in order to incorporate the residual stress. In the calculation, the tensile strain was applied from 0 to 30% in the x-direction, similarly to the practical tensile test.

To describe the interfacial debonding of the brittle material with finite element method, spring elements were commonly used. As will be mentioned later in Sec.4.3.1, the coating layer exhibits buckling before interfacial debonding. Thus tensile stress at the coating layer / substrate interface plays a dominant role for debonding. In the present work, we used spring elements which are fractured at certain stress and don't work after their fracture as schematically shown in Fig.4.2. The critical stress to cause the fracture of the spring elements was regarded as the interfacial bonding strength. It was taken to be 100MPa, which could account for the experimental result fairly well.

The analysis was carried out with the commercial finite element code MARC/Mentat2003. The Young's modulus, shear modulus, Poisson's ratio and coefficient of linear expansion of the steel substrate were taken to be 210GPa [15], 81GPa, 0.30 [15] and 2.2×10^{-5}/K [9, 10] respectively [12]. Those of the coating layer were taken to be 140GPa [15], 54GPa, 0.30 [15] and 1.1×10^{-5}/K [9, 10] respectively from the reported value for δ_1 Phase, due to the following reasons [16]. It has been known that the coating layer has multilayered structure composed mainly of the ζ, δ_1, Γ_1 and Γ phases and δ_1 phase is the thickest under the usual fabrication route [9, 12, 13]. In the present samples, the volume fraction of the δ_1 phase was estimated to be 70-80% from the composition image of the polished cross-sectional surface. Concerning the elastic constants (E, ν and G), no data have been reported for the ζ, Γ_1 and Γ phases. Only the values for the δ_1 phase [15] have been experimentally studied and available. Due to these reasons, the elastic constants of the δ_1 phase, which occupies 70-80% of the coating layer and therefore practically governs the behavior of the coating layer, were used as an approximation.

The true stress (σ) - true plastic strain (ε_p) curve of the present steel substrate has been measured in our former work [14, 16], which is expressed by,

$$\sigma=130+400\varepsilon_p^{0.38} \quad (1)$$

The yielding condition for the steel substrate was given by the von Mises criterion.

4.3 Results and discussion

4.3.1 Results of tensile test

The Fe-Zn intermetallic coating layer exhibited multiple cracking when tensile stress was applied externally. It is noted that the coating layer shows buckling behavior under high applied strain, as shown later in Sec.4.3.2. As a result, the tensile side is cracked. In the present work, in order to describe the influence of buckling-induced crack on spalling behavior, we carry the stress analysis for two models (type-A model without such a crack and type-B with such a crack). The measured value of the average crack spacing L_{ave} is shown in Fig.4.3. In our recent research, the tensile strength of the coating layer $\sigma_{c,\,UTS}$ for this sample was estimated to be 260MPa [14]. It has been revealed that the tensile stress in the coating layer is proportional to the crack spacing and therefore the crack spacing is proportional to the tensile strength of the coating layer [14, 16]. Thus if the strength is low (130MPa for instance as shown in Fig.4.3), the crack spacing of the coating layer becomes short. On the contrary, if the strength is high (390MPa), it becomes long. In this way, when the strength of the coating layer is different, the crack spacing becomes different. In the present work, the influence of the crack spacing on the spalling behavior will be described in Sec.4.3.3.

The SEM images of the spalling behavior of the coating layer are shown in Fig.4.4, from which the following features of the spalling were found. (i) The coating layer is bent as indicated by (A). (ii) The top of the tensile side of the bent coating layer is cracked as indicated by (B). (iii) The coating layer is spalled from the substrate steel as indicated by (C). These results imply the following spalling process, as schematically shown in Fig. 4.5. The coating layer exhibits multiple cracking both under thermally induced residual stress and externally applied stress as indicated by Fig.4.5 (a) and (b). With increasing tensile strain, the compressive stress in the width direction increases in

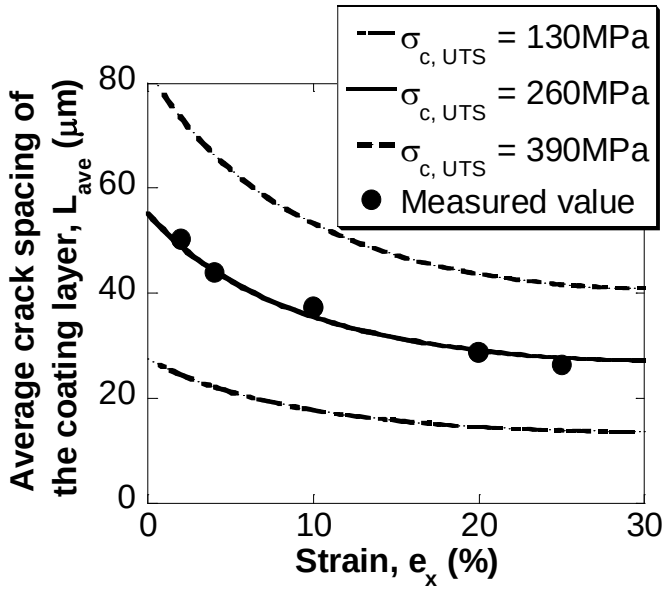

Fig.4.3 Measured average crack spacing Lave in the coating layer with applied nominal strain [14], together with the predicted changes of Lave for weak ($\sigma_{c,\,UTS}$ = 130MPa) and strong (390MPa) coating layer.

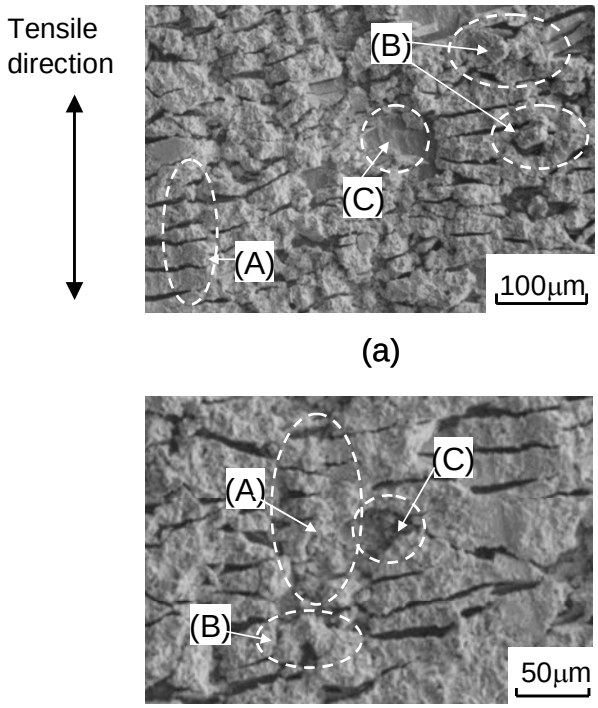

Fig.4.4 SEM images of the fractured specimen.

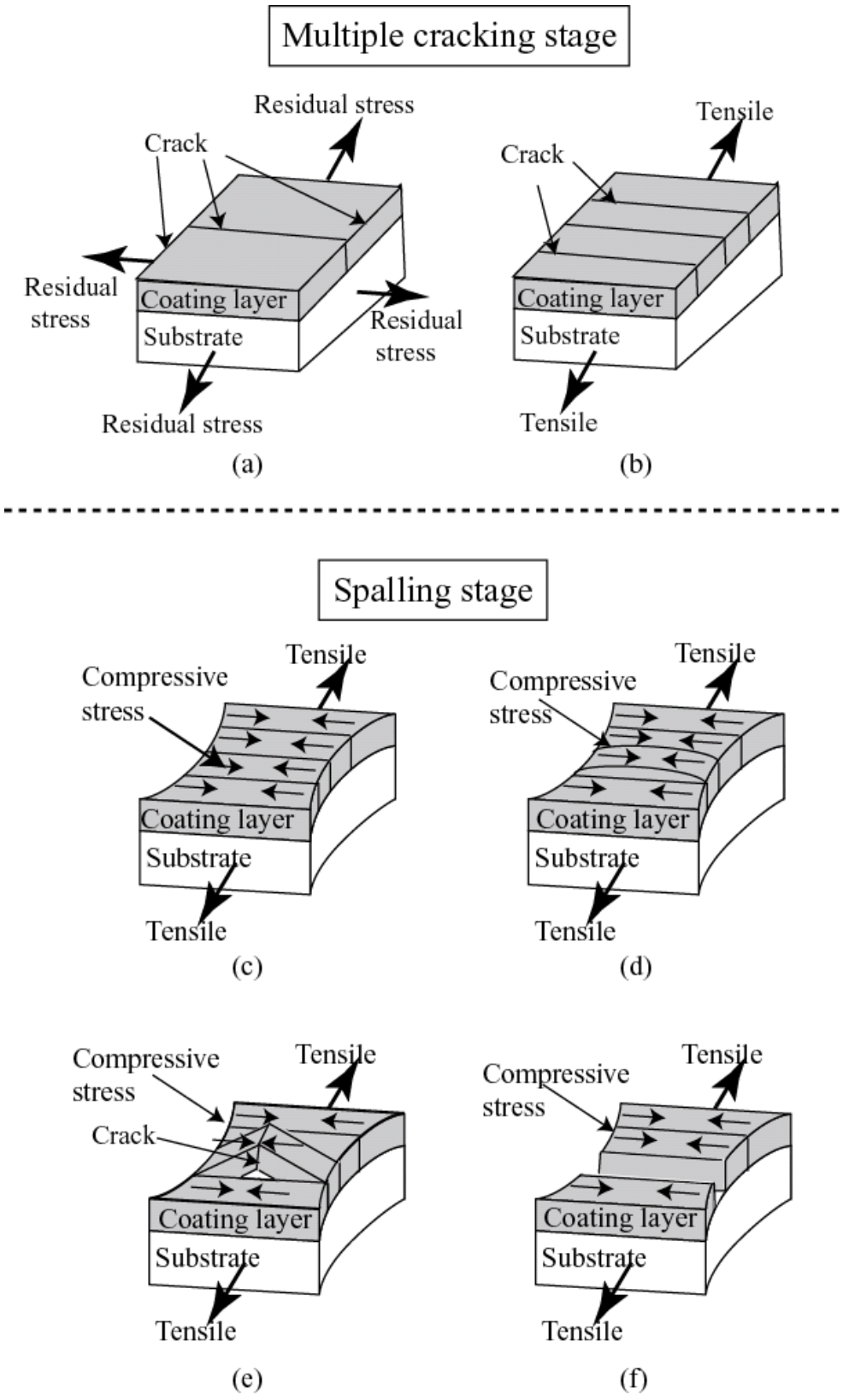

Fig.4.5 Schematic representation of the spalling process of the coating layer.

the coating layer as indicated by Fig. 4.5 (c). Then the coating layer is bent (Fig.4.5 (d)) according to which, the upper side is cracked due to the tensile stress. Such a crack enhances the buckling of the coating layer (Fig.4.5 (e)). In the progress of the buckling, tensile stress is exerted at the interface, due to which interfacial debonding occurs. Finally the debonded coating layer is spalled (Fig.4.5 (f)).

4.3.2 Spalling process calculated by the finite element method

The finite element analysis was carried out for three cases. Each case has different crack spacing of the coating layer in the tensile direction, L= 20 (corresponding to the coating layer strength 130MPa), 40 (260MPa) and 60μm (390MPa). As the calculation results using these three models had the common feature in the spalling process of the coating layer, the result for L = 40μm is representatively taken up in this part.

Figure 4.6 shows the calculation results of the spalling process for type-A model. The stress distribution of the coating layer in the width direction (= y-direction) is shown in color. The yellow and blue colors refer to tensile and compressive stresses, respectively.

The change of stress distribution in the width direction was characterized as follows. (i) At zero applied tensile strain e_x = 0%, only the thermal residual tensile stress is found. (Fig.4.6 (a)). The tensile stress of the coating layer is maximum at the middle (y = W/2). On the contrary, the stress approached zero at the broken end of coating layer (y = 0, W). (ii) When tensile strain was applied (e_x = 5%, Fig.4.6 (b)), tensile stress in the width (y) direction was changed to compressive stress especially near the interface. The compressive stress increased with increasing applied tensile strain. As mentioned above, the compressive stress in the width direction took place due to the difference in contraction between the coating and the plastically deforming substrate. (iii) When the applied tensile strain was raised further (e_x = 10%, Fig.4.6 (c) and e_x = 15%, Fig.4.6 (d)), the compressive stress of the coating layer in the width direction increased only slightly due to the bending deformation.

In the bending deformation of the coating layer, high tensile stress is exerted on

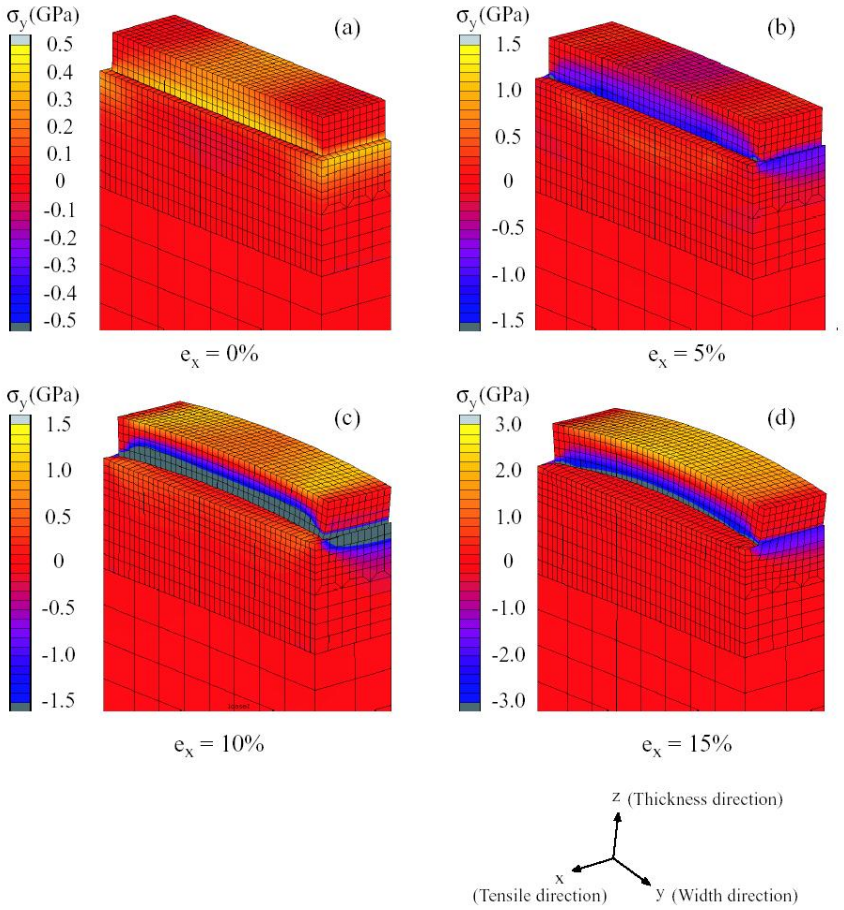

Fig.4.6 Calculation results of the debonding behavior and stress in the width direction. (type-A model, L = 40μm)

the upper side of the coating layer. The tensile stress in the width direction is highest in the middle and the upper side (y=W/2, z=400μm+T) of the coating layer. At 10 to 15% applied tensile strain, the maximum tensile stress becomes 0.8GPa and 2.4GPa, respectively, which are far higher than the fracture strength of the coating layer (around 260MPa, (Fig.4.3)). These results suggest that the coating layer exhibits flex crack at the middle (y=W/2), as (B) in Fig.4.4. To analyze the influence of the flex crack on the spalling behavior of the coating layer, the new crack-induced models at y=W/2 (type-B model) were analyzed. The result is presented in Fig.4.7.

In the low tensile strain range (e_x = 0 to 5%), the calculation results were not so different between type-A model and type-B model. At e_x = 15%, the induced-crack at

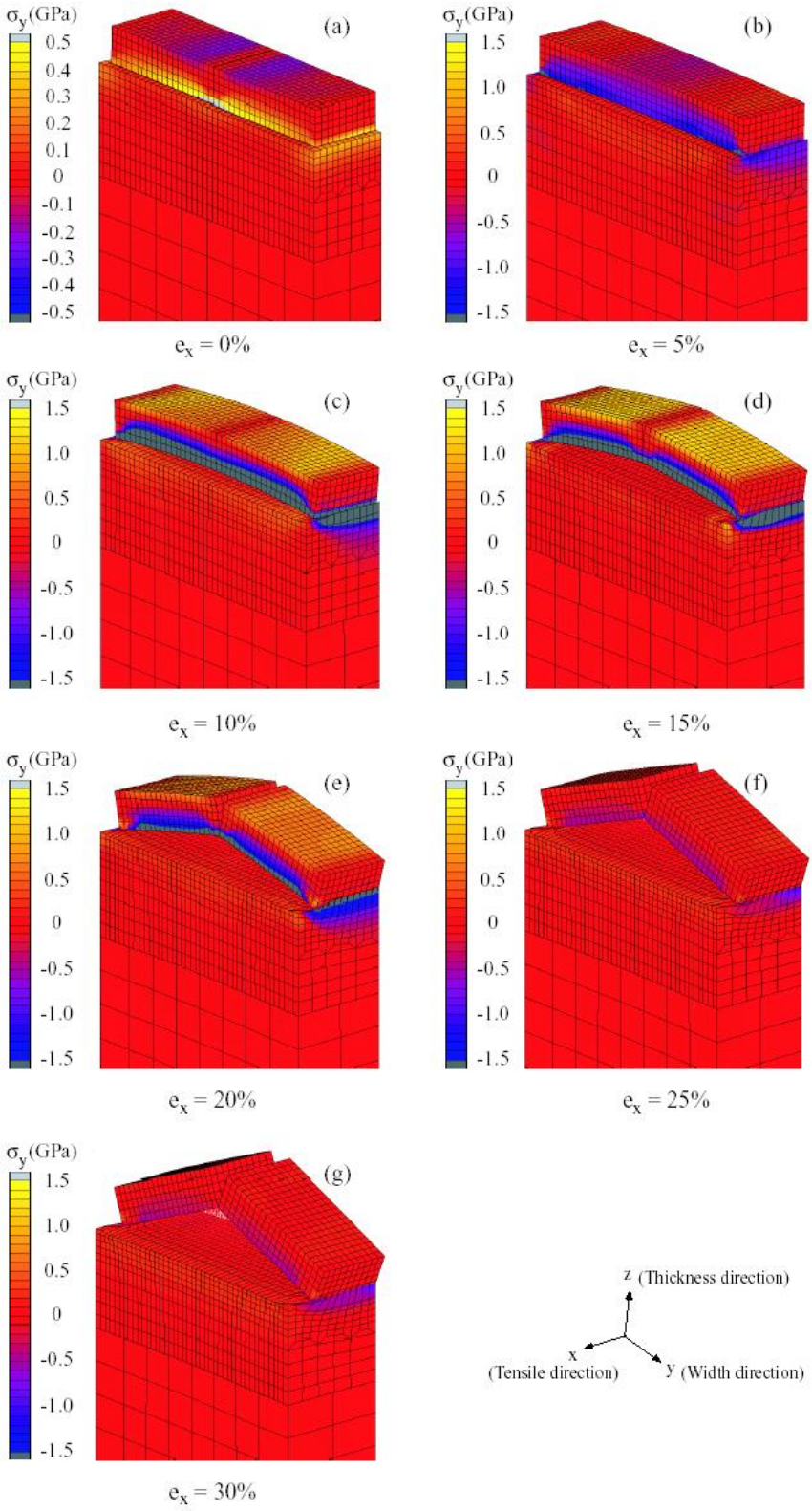

Fig.4.7 Calculation results of the debonding behavior and stress in the width direction. (type-B model, L = 40μm)

y = W/2 was opened, and the coating layer of the type-B model exhibited interfacial debonding more than that of type-A ones as will be shown in detail in Sec.4.3.3. On the other hand, the bending stress of the coating layer in the width direction decreased due to the flex crack opening. In the higher strain range (e_x > 20%), the interfacial debonding was enhanced with increasing tensile strain.

4.3.3 Influence of crack spacing on the spalling behavior of the coating layer

The debonding distance of coating from substrate was maximum at y = W/2 for any x and for all calculation results using both type-A and type-B models. Hereafter, the maximum debonding distance at y = W/2 is noted as d_{max}. To estimate the influence of the crack spacing of the coating layer in the tensile direction on the interfacial debonding, the maximum debonding distance d_{max} at x = L/2 was calculated for L= 20, 40 and 60μm.

Figure 4.8 shows the change of d_{max} with applied tensile strain e_x for L= 20, 40 and 60μm. The shorter the crack spacing of the coating layer in the tensile direction, the smaller became the debonding distance. The applied strain at which the interfacial debonding started also became higher for shorter crack spacing in the tensile direction. These results revealed that, the interfacial debonding of the coating layer could be retarded by enhancing the multiple cracking in the tensile direction. This implies that the progress of the multiple cracking phenomenon acts to retard the spalling.

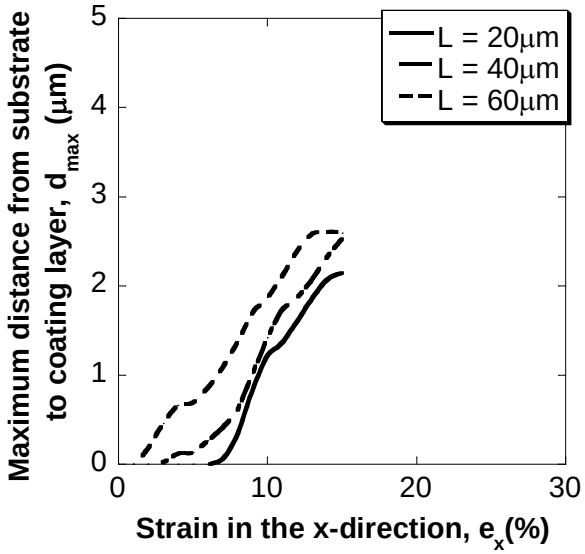

(a) type-A model

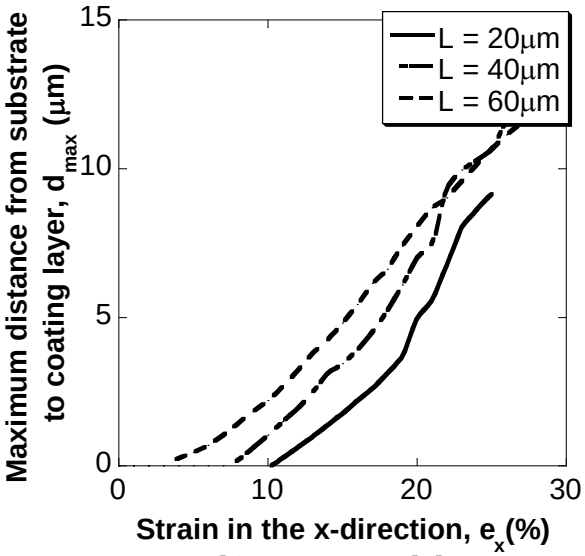

(b) type-B model

Fig.4.8 Change of maximum distance from substrate steel to the debonded coating layer with applied nominal strain for the crack spacing L = 20, 40, and 60μm.

4.4 Conclusions

(1) The observation of the specimens revealed that (i) the galvannealed coating layer on steel substrate exhibited interfacial debonding under applied tensile strain,

following the multiple cracking of the coating layer, (ii) in the debonding process, the coating layer is first bent by the compressive stress in the width direction, then the tensile side of the bent coating layer is cracked, and finally the coating layer is spalled from the substrate steel due to the buckling induced interfacial debonding.

(2) The analytical results of the 3-dimentional finite element models revealed the following features for the interfacial debonding. (a) At zero tensile strain, the stress of the coating layer in the width direction is tensile due to the residual strain arising from the mismatch of the coefficient of thermal expansion between the coating layer and substrate. (b) With increasing applied tensile strain, the compressive strain is exerted in the width direction due to the larger plastic deformation of the substrate. Also, due to the same reason, the coating layer is bent and the tensile stress is generated at the coating layer / substrate interface. (c) Then the stress on the tensile side of the bent coating layer becomes high enough to cause tensile fracture of the coating layer. Accordingly, the coating layer exhibited flex crack, and then interfacial debonding is enhanced more with increasing tensile strain, due to the enhanced interfacial tensile stress. These analytical results accounted for well the experimentally observed features of spalling process.

(3) The shorter the crack spacing of the coating layer in the tensile direction, the strain at which the interfacial debonding starts is retarded. This result implies that the multiple cracking phenomenon acts to retard the spalling and also, if the fracture strength of the coating is made low, the buckling-induced spalling at a given applied strain can be minimized.

ACKNOWLEDGEMENT

The authors wish to express their gratitude to Japan Society for the Promotion of Science for Young Scientists and to The Iron and Steel Institute of Japan for the support of the present work.

References

[1] C. E. Jordan CE, K. M. Goggins and A. R. Marder: *Metall. Mater. Trans. A,* **25** (1994), 2101.

[2] S. Lazik, C. Esling and J. Wegria: *Textures and Microstructures,* **23** (1995), 131.

[3] A. Kelly A and W. R. Tyson: *J. Mech. Phys. Solids,* **13** (1965), 329.

[4] S. Ochiai and K. Osamura: *J. Mater. Sci.*, **21** (1986), 2735.

[5] M. S. Hu and A. G. Evans: *Acta Metall.*, **37** (1989). 917.

[6] Y. Leterrier, L. Boogh, J. Andersons and J. A. E. Mason: *J. Polym. Sci., Part B: Polym. Phys.*, **35** (1997), 1449.

[7] S. Ochiai and Y. Murakami: *Metal Sci.*, **41** (1976), 401.

[8] J. Andersons, U. A. Handge, I. M. Sokolov and B. Blumen: *Eur. Phys. J.*, **B17** (2000), 261.

[9] J. Foct: *Scripta. Metall.*, **28** (1993), 127.

[10] A. Iost and J. Foct: J. *Mat. Sci.*, **12** (1993), 1340.

[11] M. Sakurai, J. Inagaki and T. Alpas: *CAMP-ISIJ*, **12** (1999), 550.

[12] E. Tzimas and G. Papadrimitriou: *Surf. Coat. Technol.*, **145** (2001), 176.

[13] A. T. Alpas and J. Inagaki: *ISIJ Int.*, **40** (2000), 172.

[14] S. Iwamoto, S. Ochiai, T. Nakamura and H. Okuda: *Tetsu-to-Hagane*, **91** (2005), 335.

[15] G. Reumont, J. B. Vogt, A. Iost and J. Foct: *Surf. Coat. Tech.*, **139** (2001), 265.

[16] S. Ochiai, S, Iwamoto, T. Tomida, T. Nakamura, H. Okuda, M. Tanaka and H. Hojo: *Metall. Mater. Trans. A*, **36A** (2005), 1807.

Chapter 5

Finite Element Analysis of the Interfacial Debonding of the Galvannealed Coating Layer with High Tensile Strength Steel Substrates

5.1 Introduction

The hot-dipped GA (galvannealed) steels, consisting of Fe-Zn intermetallic coating layer and substrate steel, are widely used as architectural and car-body materials due to their high corrosion resistance and weldability [1, 2]. As these materials are composed of brittle coating layer with low failure strain and ductile substrate with far higher failure strain, the coating layer exhibits multiple cracking perpendicular to the tensile direction [3-8], followed by spalling, when tensile stress is applied externally. The spalling of the coating layer is caused by the compressive stress in the sample width direction [7], followed by interfacial debonding. The SEM image and schematic representation of the buckling behavior of the coating layer are shown in Fig. 5.1.

Until now, relatively low strength steels with high formability such as interstitial free steels have been used as car body materials. In recent years, the high strength steel is counted on the car application to reduce the car weight which critically affects on the fuel economy. However, the influences of the high tensile strength steel substrate on multiple cracking- and spalling- behaviors have not been revealed yet.

In our recent works, the tensile strength of the coating layer, which is one of the major controlling factors for the multiple cracking, was estimated to be 260MPa commonly for IF (interstitial free steel) and SPCC (steel plate cold commercial, JIS) steel substrate samples [9, 10]. Also, it was revealed that the crack spacing affects largely the subsequent spalling behavior of the coating layer [11].

In the present work, we assumed that the tensile strength of the coating layer and the interfacial bonding strength are common for low and high strength samples.

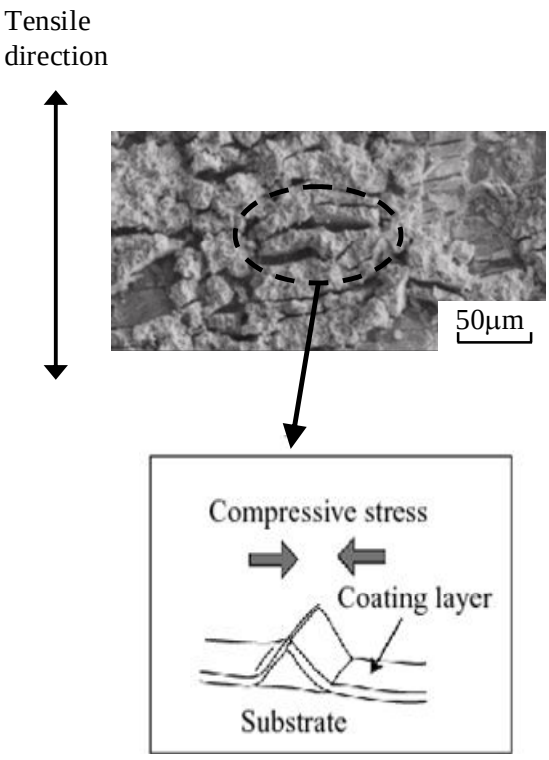

Fig.5.1 SEM image and schematic representation of the buckling behavior of the coating layer.

Under such an assumption, we carried a numerical analysis using a finite element method to predict the multiple cracking- and debonding- behaviors for high strength substrate samples. It will be shown in this paper that the higher the tensile strength of the substrate, the shorter becomes the crack spacing of the coating layer and the less interfacial debonding takes place in high strength substrate steels due to the short crack spacing, as long as the coating layer- and interfacial bonding- strengths of high strength substrate samples are the same as those of low strength ones.

5.2 Experimental procedure

5.2.1 Samples and input values for calculation

The present study aims to reveal the influences of the substrate material on the multiple cracking and spalling. For this aim, the IF steel was taken up as an example of low strength steel for calculation. As an example of high strength steel, an imaginary high strength steel with two times yield stress and ultimate strength in comparison with that of IF steel was taken up. Hereafter, the IF and imaginary steel-based samples are noted as sample I and sample H, respectively.

The Young's modulus, shear modulus, Poisson's ratio and coefficient of thermal expansion of the steel substrate were taken to be 210GPa [12], 81GPa, 0.30 [12] and $2.2\text{x}10^{-5}$ /K [13, 14] respectively [15], commonly for I and H samples. Those of the coating layer were taken to be 140GPa [12], 54GPa, 0.30 [12] and $1.1\text{x}10^{-5}$ /K [13, 14] respectively, approximated as a single layer consisting of δ_1 Phase ($FeZn_7$), as similarly as in our preceding works [9-11]. Based on the measured stress-strain curve in our preceding works [9, 10], the true stress (σ) - true plastic strain (ε_p) curve of the sample I was given by,

$$\sigma=130+400\varepsilon_p^{0.38} \tag{1}$$

The true stress (σ) - true plastic strain (ε_p) curve of the sample H was given by,

$$\sigma=260+800\varepsilon_p^{0.38} \tag{2}$$

The yielding condition for the steel substrate was given by the von Mises criterion. The stress analysis was carried out under the plane-strain condition.

5.2.2 Finite element analysis of the multiple cracking

The morphology of the specimen with multiply-cracked Fe-Zn intermetallic compound coating layer is schematically shown in Fig.5.2 (a) where L is the crack spacing and T is the thickness of the coating layer. In the finite element analysis to calculate the stress distribution, the region ABFE was taken up as the representation. The longitudinal distance y was taken from the center plane: y = 0 at AB, y = 400μm at CD and y= 400μm +T (= 10μm in the present sample) at EF. The horizontal distance x was defined to be zero, at the broken end, L/2 at the middle, and L at the another broken end as shown in Fig.5.2.

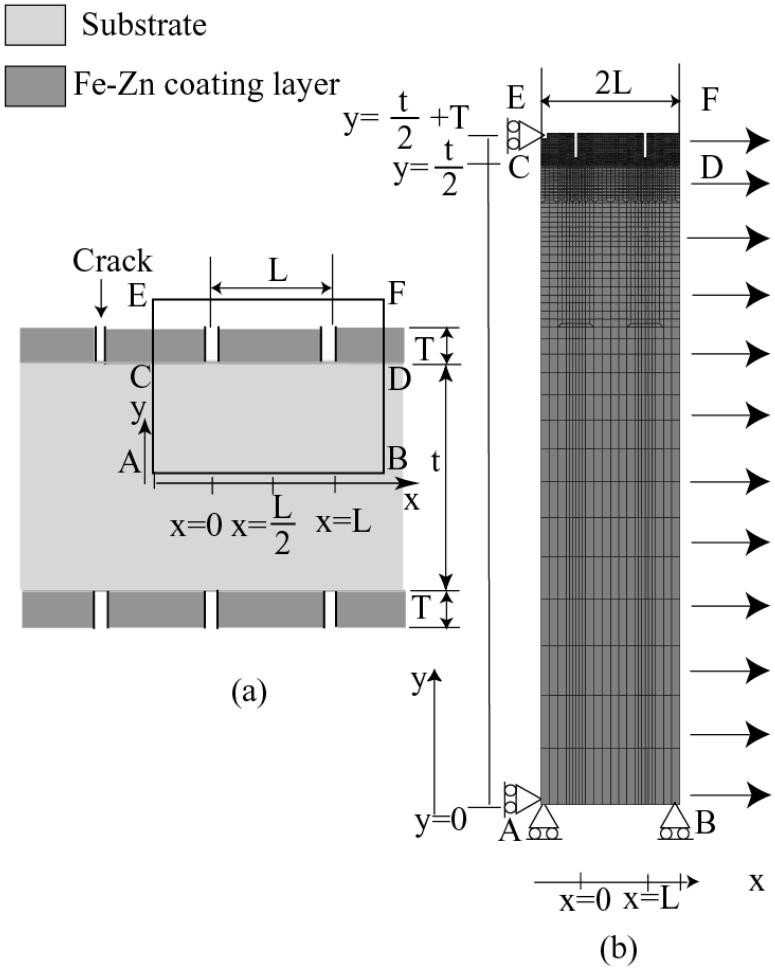

Fig.5.2 FEM-mesh and boundary condition for the multiple cracking analysis.

An example of the finite element mesh of the plane-symmetric model and the boundary conditions employed in the present analysis are shown in Fig.5.2 (b). The displacements of the cross-sections ACE and AB were taken to be zero. Common compulsory tensile displacement was given for the cross-section BDF in the x-direction.

For analysis of the stress distribution, the crack spacing L = 10, 20, 40 and 80μm were used. As mentioned above, the present samples were heated for formation of the intermetallic compounds at 773 K and cooled down to room temperature. Therefore the temperature change ΔT = -475 K was input. The stress of the coating layer in the x-direction, σ_x, was calculated for the applied tensile strain = 10, 20 and 30%.

5.2.3 Finite element analysis of the interfacial debonding

3-dimentional models for analysis of the interfacial debonding of the coating layer were prepared as follows. The morphology of the specimen with multiply cracked Fe-Zn intermetallic compound coating layer is schematically shown in Fig.5.3 (a) where L is the crack spacing in the tensile direction, W is the crack spacing in the width direction and T is the thickness of the coating layer. An example of the finite element mesh of the model employed in the present analysis is shown in Fig.5.3 (b). As indicated in Fig.5.3 (a), the longitudinal distance x was taken to be zero at the middle, and to be L/2 at the broken end. The distance across-the-width y was taken to be zero at the broken end, to be W/2 at the middle, and to be W at the other broken end. The vertical distance z was taken to be zero at the middle of substrate in the thickness direction. As the thickness of the substrate t was 800μm, the distance z of the coating layer / substrate interface was taken to be 400μm (=t/2), and the distance z was taken to be 400 μm +T (= 10μm in the present sample) at the surface of the coating layer. For the analysis of the real sample, the crack spacing in the x-direction L = 40μm, and that in the y-direction W = 80μm were used, where W = 80μm corresponds to the thermally induced critical crack spacing in the coating layer [9, 10], and L = 40μm corresponds to the critical length at which buckling behavior of the coating layer were observed, as shown later in Fig.5.7. The transverse isotropy of the elasto-plastic deformation and the multiple cracking behavior of the IF steel-based samples (sample I) were observed

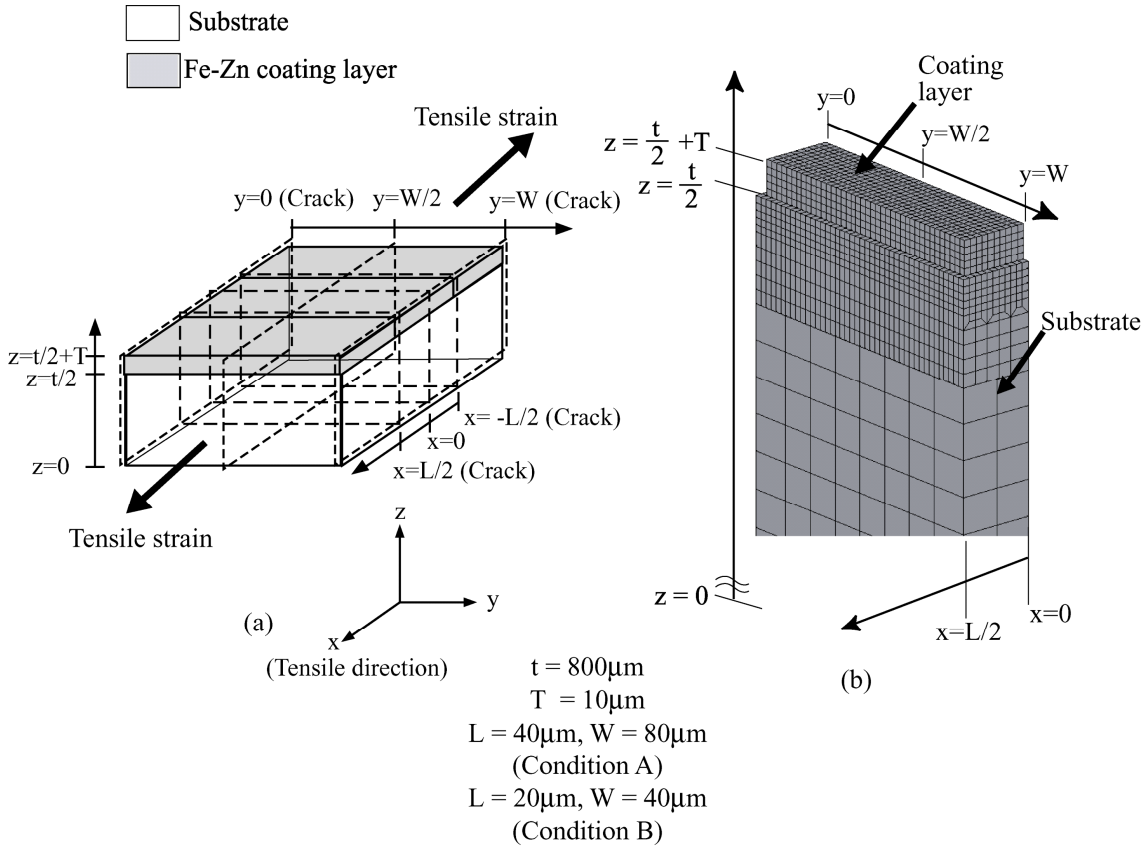

Fig.5.3 FEM-mesh of the GA steel for the interfacial debonding analysis.

experimentally [18], in our former work. For that of the imaginary sample, L = 40μm and W = 80μm were given for one model, and L = 20μm and W = 40μm were given for the other model which corresponded to the result of the multiple cracking analysis as will be mentioned later in Sec. 5.3.1. The present specimens had been heated at 773K for formation of the intermetallic compounds and cooled down to room temperature. Therefore the temperature change ΔT = -475K was input in order to incorporate the residual stress. In the calculation, the tensile strain was applied from 0 to 30% in the x-direction, similarly to the practical tensile test.

To describe the interfacial debonding of the brittle material with finite element method, spring elements were commonly used. As shown by our former work, the coating layer exhibits buckling before interfacial debonding. Thus tensile stress at the

coating layer / substrate interface plays a dominant role for debonding. In the present work, we used spring elements which are fractured at certain stress and don't work after their fracture. The critical stress to cause the fracture of the spring elements was regarded as the interfacial bonding strength. It was taken to be 100MPa, which could account for the experimental result fairly well.

5.3 Results and discussion

5.3.1 Finite element analysis of the multiple cracking

The finite element analysis was carried out for both samples I and H. To describe the change of the crack spacing with applied tensile strain, first, the tensile stress distribution in the coating layer was calculated for the crack spacing L = 10, 20, 40 and 80μm at the applied tensile strains 10, 20 and 30% for both samples, as shown below.

The calculation results showed that the exerted stress on the coating layer increases with increasing applied tensile strain both for samples I and H. Figure 5.4 shows the variations of the calculated tensile stress σ_x in the x-direction of the coating layer with distance x from the crack at the applied nominal strain of 20% as an example. It is noted that the exerted stress on the coating layer of high strength steel sample is higher than that of real sample.

As shown in Fig.5.4, the σ_x is highest ($\sigma_{x,\,max}$) at the middle point x = L/2, and the longer the crack spacing L, the higher becomes $\sigma_{x,\,max}$. The cracking tends to occur at L/2 with highest $\sigma_{x,\,max}$. When the coating layer is cracked at x = L/2, the relation between the critical length of the coating layer L_c (= the necessary length for the coating layer to be cracked) and the average crack spacing L_{ave} is given by [17],

$$L_c = 4/3L_{ave} \tag{3}$$

Figure 5.5 shows the relation between the calculated maximum tensile stress $\sigma_{x,\,max}$ and crack spacing L for sample I and sample H. The maximum tensile stress is

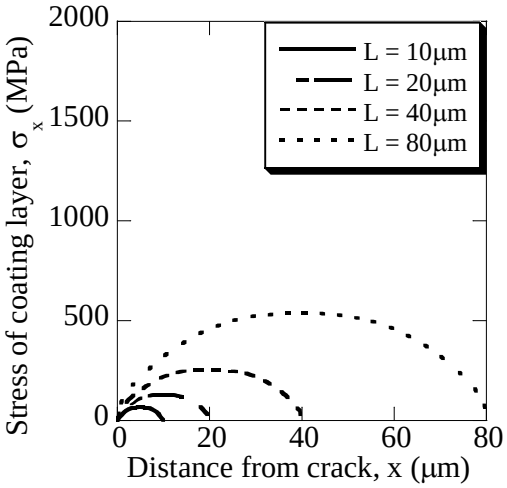

(a)

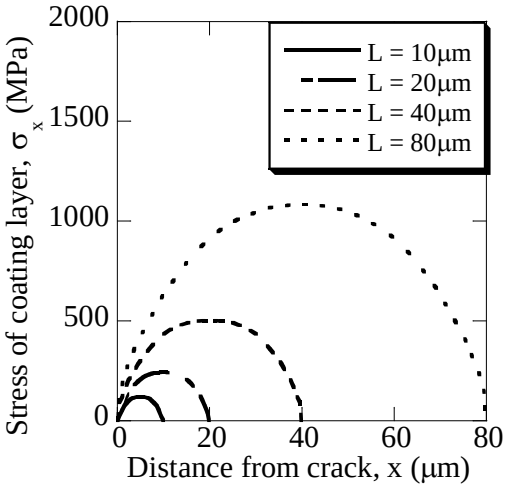

(b)

Fig.5.4 Distribution of tensile stress σ_x of the coating layer at the nominal strain e = 20%, for sample I (a) and sample H (b).

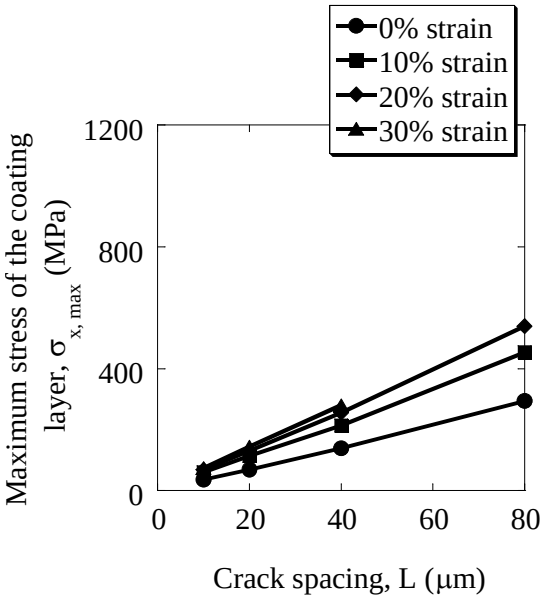

(a)

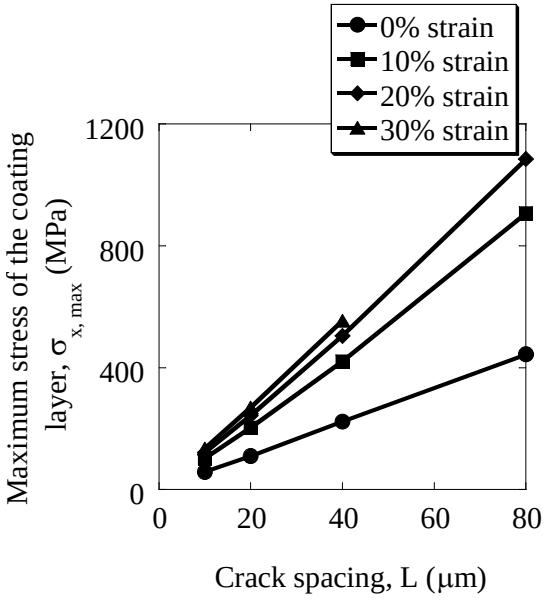

(b)

Fig.5.5 The relation between the maximum tensile stress $\sigma_{x,\ max}$ and crack spacing L for sample I (a) and sample H (b).

proportional to crack spacing at each applied strain. The slope of the linear relation between $\sigma_{x,\ max}$ and L in Fig.5.5 corresponds to the stress transfer efficiency to the coating layer per unit length, $\sigma_{x,\ max}/L$ [9-11]. The values of $\sigma_{x,\ max}/L$ at e=0, 10, 20 and 30%, estimated from Fig.5.5, are presented in Fig.5.6.

The relation of $\sigma_{x,\ max}/L$ to applied strain e in the applied strain range up to 30% was approximated with the following cubic function for sample I and sample H, respectively.

$$\sigma_{x,\ max}/L = 3.63+25.5e-61e^2+47e^3 \quad \text{(Sample I)} \quad (4)$$

$$\sigma_{x,\ max}/L = 5.55+77.9e-250e^2+270e^3 \quad \text{(Sample H)} \quad (5)$$

The strength of the coating layer $\sigma_{c,\ UTS}$ has been estimated to be around 260MPa [9, 10] in our former work for IF- and SPCC substrate samples. The critical crack spacing L_c was calculated by setting $L = L_c$ and $\sigma_{x,\ max}$ = 260MPa and e into Eqs. (4) and (5) for sample I and sample H, respectively. Figure 5.7 shows the calculated change of the critical crack spacing of the coating layer L_c with nominal strain for $\sigma_{c,\ UTS}$=260±30MPa. For reference, the measured L_c-e relation sample I, which is well described by $\sigma_{c,\ UTS}$=260±30MPa, is presented in Fig.5.7. For the same coating layer strength ($\sigma_{c,\ UTS}$ = 260MPa), the change of crack spacing with applied nominal strain is estimated for sample H, as shown in Fig.5.7.

As shown in Fig.5.7, the critical length of the coating layer of sample H is almost a half as long as that of sample I. As has been shown in our preceding works [9-11], the critical crack spacing values of sample I at 0% (= the thermally induced critical crack spacing) and at or higher than 20% (= the strain at which interfacial debonding occurs) were about 80μm and 40μm, respectively. In contrast, those of sample H at the former and latter strains were about 40μm and 20μm, respectively.

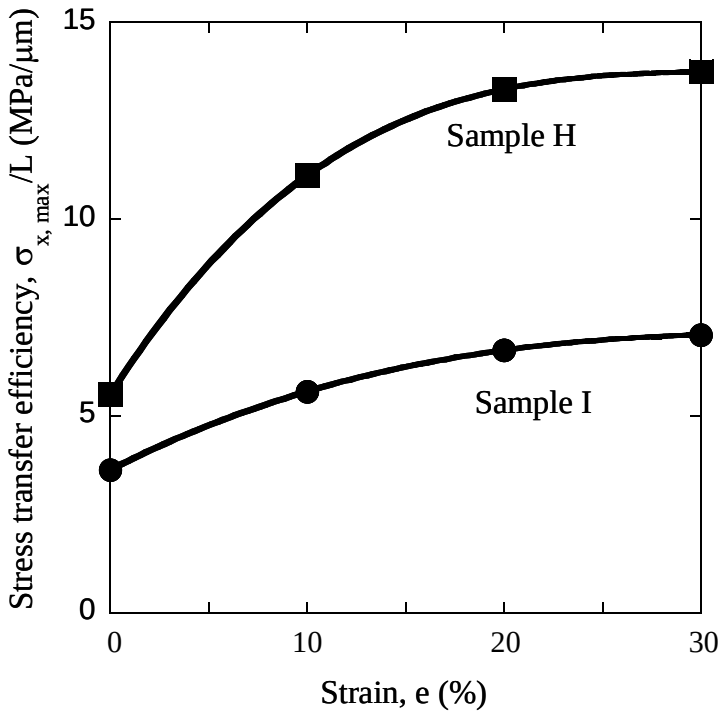

Fig.5.6 Change of stress transfer efficiency $\sigma_{x,\,max}$ /L with applied strain e for sample I and sample H.

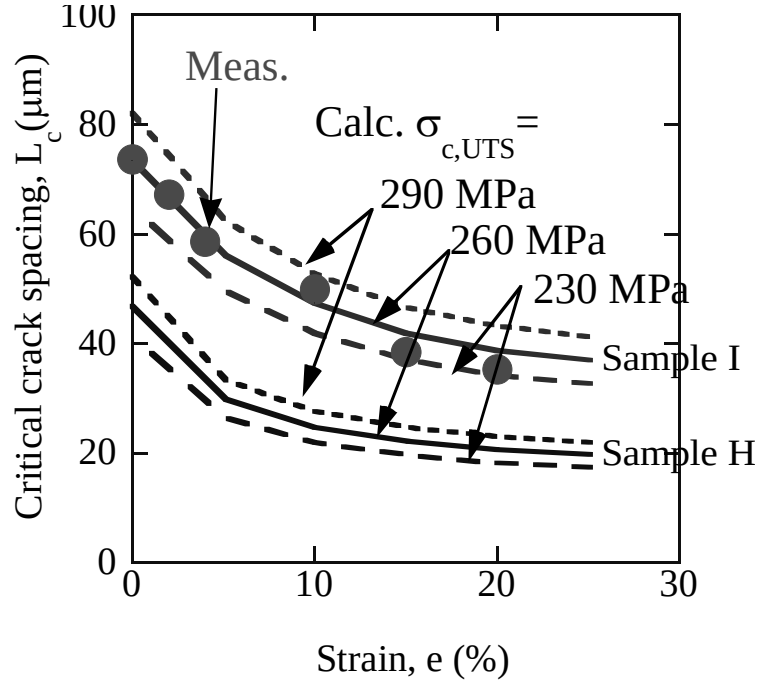

Fig.5.7 Change of the crack spacing of the coating layer with nominal strain for $\sigma_{c,\,UTS}$ =260±30MPa together with the experimental result for the sample I.

5.3.2 Finite element analysis of the interfacial debonding

From the results of the multiple cracking analysis, the crack spacing values (L in the tensile direction and W in the width direction in Fig.5.3) for calculation of the interfacial debonding behavior were given as follows. In both samples I and H, the tensile strain was applied in one direction. Before the application of tensile strain, the crack spacings in the coating layer were 80 and 40μm for the samples I and H, respectively, as stated in Sec. 5.3.1. The experimentally measured applied strain at which the spalling of the coating layer occurred in sample I was around 20% or slightly higher than 20%. At these strain, the crack spacing values in the coating layer were 40 and 20μm for the samples I and H, respectively, as stated also in Sec. 5.3.1. Based on these results, the crack spacing values in the tensile direction L and that in the width direction W (Fig.5.3) were given by 40 and 80μm, respectively, for calculation of the debonding behavior of the sample I. The geometrical condition of L=40μm and W=80μm for calculation of interfacial debonding behavior is hereafter noted as the condition A for simplicity.

Due to the same reason, the values of L and W (Fig.5.3) at which interfacial debonding takes place in the sample H are given by 20 and 40μm, respectively. The geometrical condition of L=20μm and W=40μm for calculation of interfacial debonding behavior is hereafter noted as the condition B for simplicity.

In the calculation in this work, the conditions A and B were used for analysis of interfacial debonding in the samples I and H, respectively. In addition, for reference, the condition A was used also for the analysis of the sample H, with which the influence of substrate material on the debonding behavior under the same geometrical condition was revealed as shown below.

Figure 5.8 shows the variations of the distribution of the interfacial debonding distance from substrate to coating layer. The x-, y-and z-axes in Fig.5.8 show the coordinates indicated in the coating layer (Fig.5.3). The distribution of the interfacial debonding distance from the substrate to coating layer in the z-direction is shown with color. The debonding distance from substrate to coating layer was maximum at x = L/2 and y = W/2 for all calculation results. Figure 5.9 shows the change of the maximum debonding distance d_{max} with applied tensile strain e for sample I (condition A) and

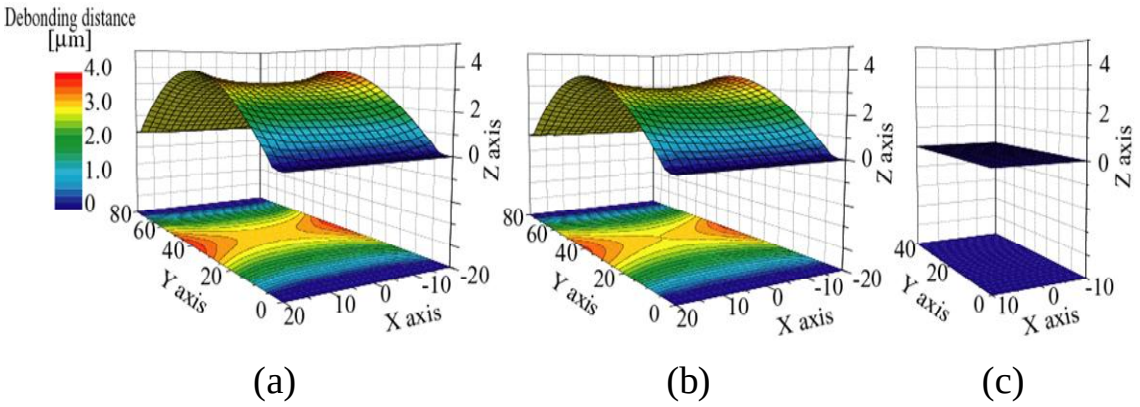

Fig.5.8 Calculated distributions of the interfacial debonding distance from substrate to coating layer at 20% tensile strain in the x-direction in (a) sample I (condition A), (b) sample H (condition A) and (c) sample H (condition B).

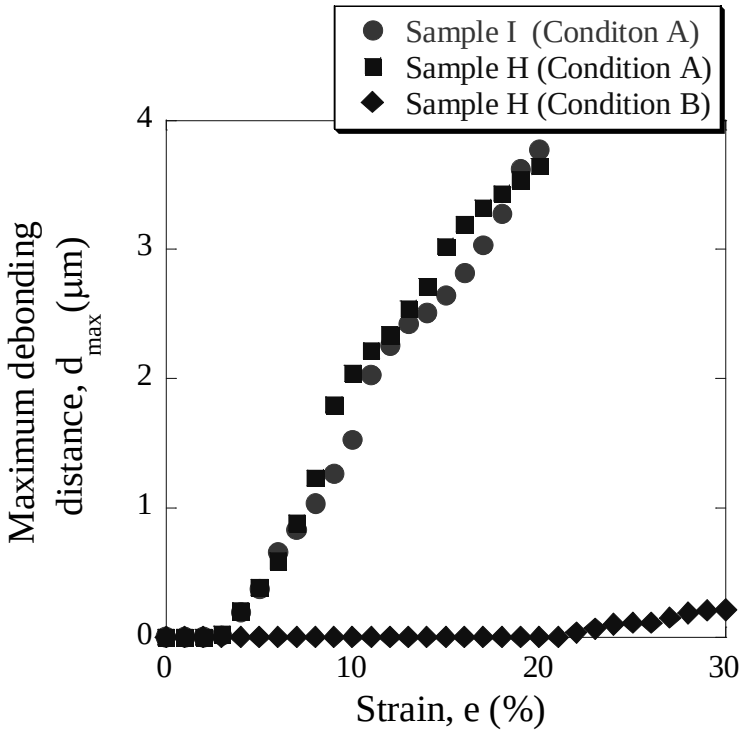

Fig.5.9 Calculated change of the maximum debonding distance d_{max} with applied tensile strain e for the sample I (condition A) and H (conditions A and B).

sample H (condition A and B).

As shown in Fig.5.8 and Fig.5.9, the debonding distances of samples I and H are not so much different under the condition A (L=40μm and W=80μm). It revealed that the strengthening of the substrate itself does not give a big influence on the debonding behavior. On the other hand, the debonding distance in the sample H under the condition B (L=20μm and W=40μm), which refers to the actual behavior due to the preceding progress of the multiple cracking of the coating layer, is definitely short in comparison with that of samples I and H under the condition A. This result evidently shows that the replacement of the high strength substrate for the low one acts to reduce the interfacial debonding through the enhancement of multiple cracking, if the tensile strength of the coating layer and interfacial bonding strength that have been actually obtained for the low strength steel (IF and SPCC) substrates, are retained for the high strength substrate.

5.4 Conclusions

The influences of the high tensile strength steel substrate on the multiple cracking and spalling was studied by the finite element stress analysis. It was revealed that the replacement of the high strength substrate for the low one acts to enhance the multiple cracking and to reduce the interfacial debonding through the enhancement of multiple cracking, if the tensile strength of the coating layer and interfacial bonding strength are retained on the level of those for the low strength steel (IF and SPCC).

ACKNOWLEDGEMENT

The authors wish to express their gratitude to Japan Society for the Promotion of Science for Young Scientists and to The Iron and Steel Institute of Japan for the support of the present work.

REFERENCES

[1] C. E. Jordan CE, K. M. Goggins and A. R. Marder: *Metall. Mater. Trans. A*, **25** (1994), 2101.

[2] S. Lazik, C. Esling and J. Wegria: *Textures and Microstructures*, **23** (1995), 131.

[3] A. Kelly A and W. R. Tyson: *J. Mech. Phys. Solids.*, **13** (1965), 329.

[4] S. Ochiai and K. Osamura: *J. Mater. Sci.*, **21** (1986), 2735.

[5] M. S. Hu and A. G. Evans: *Acta Metall.*, **37** (1989), 917.

[6] Y. Leterrier, L. Boogh, J. Andersons and J. A. E. Mason: *J. Polym. Sci., Part B: Polym. Phys.*, **35** (1997), 1449.

[7] S. Ochiai and Y. Murakami: *Metal Sci.*, **41** (1976), 401.

[8] J. Andersons, U. A. Handge, I. M. Sokolov and B. Blumen: *Eur. Phys. J.*, **B17** (2000), 261.

[9] S. Ochiai, S, Iwamoto, T. Tomida, T. Nakamura, H. Okuda, M. Tanaka and H. Hojo: *Metall. Mater. Trans. A*, **36A** (2005), 1807.

[10] S. Iwamoto, S. Ochiai, T. Nakamura and H. Okuda: *Tetsu-to-Hagane*, **91** (2005), 335.

[11] S. Iwamoto, S. Ochiai, H. Okuda and T. Inoue: *ISIJ Int.*, **47** (2007), 930.

[12]G. Reumont, J. B. Vogt, A. Iost and J. Foct: *Surf. Coat. Tech.*, **139** (2001), 265.

[13] J. Foct: *Scripta. Metall..*, **28** (1993), 127.

[14] A. Iost and J. Foct: *J. Mat. Sci.*, **12** (1993), 1340.

[15] E. Tzimas and G. Papadrimitriou: *Surf. Coat. Technol.*, **145** (2001), 176.

[16] A. T. Alpas and J. Inagaki: *ISIJ Int.*, **40** (2000), 172.

[17] T. Osawa, A. Nakayama, M. Miwa and A. Hasegawa: *J. Appl. Polymer Sci.*, **22** (1978), 3203.

[18] T. Nakamura, S. Ochiai, S. Iwamoto, and H. Okuda: *Tetsu-to-Hagane*, **91** (2005), 342.

Chapter 6

Influence of the Crack Spacing in the Coating Layer on the Progress of Interfacial Debonding in Galvannealed Steel Pullled in Tension

6.1 Introduction

The hot-dipped GA (galvannealed) steels, consisting of Fe-Zn intermetallic coating layer and substrate steel, are widely used as architectural and car-body materials due to their high corrosion resistance and weldability [1, 2]. As these materials are composed of brittle coating layer with low failure strain and ductile substrate with far higher failure strain, the coating layer exhibits multiple cracking perpendicular to the tensile direction [3-12], followed by spalling, when tensile stress is applied externally. The spalling of the coating layer is caused by the compressive fracture such as buckling and wedging in the sample width direction [7, 13, 14], followed by interfacial debonding.

Figure 6.1 shows the SEM image of the multiple cracking of the GA coating layer in the sample used in this work under applied tensile strain. As shown in Fig.6.1, the coating layer was cracked not only perpendicular to the tensile direction but also parallel to the tensile direction. Cracks induced perpendicularly to the tensile direction were caused by the multiple cracking, as mentioned above. On the other hand, the cracks induced parallel to the tensile direction (namely the cracks in the sample width direction) were caused by the thermally induced residual stress [13-16, 19-21]. However, the influences of the crack spacing in the tensile direction and that in the sample width direction have not been clarified until now, despite the importance to clarify the spalling behavior. In our recent study, concerning the fracture of GA coating layer with high tensile strength steel substrates, it was newly suggested that the interfacial debonding could be reduced through the enhancement of multiple cracking [22]. In the present

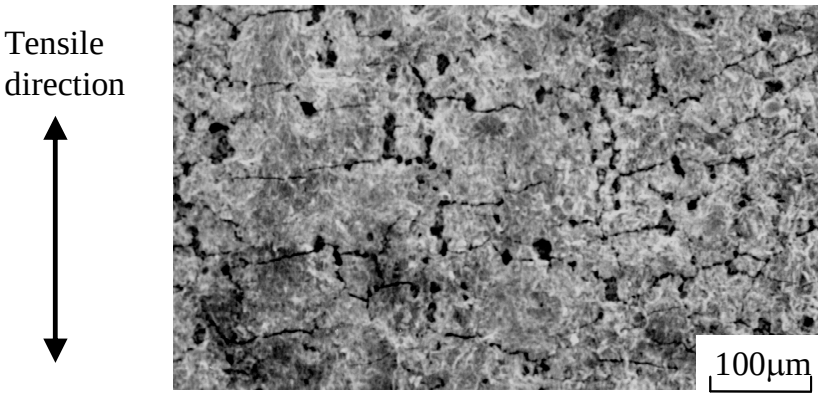

Fig.6.1 SEM image of the multiple cracking of the coating layer.

work, it was attempted to reveal the influences of the crack spacing in both tensile and sample width directions on the spalling behavior of the coating layer with the finite element stress analysis.

6.2 Finite element analysis

3-dimentional models for analysis of interfacial debonding of the coating layer were prepared as follows. The morphology of the specimen with multiple cracked Fe-Zn intermetallic compound coating layer is schematically shown in Fig.6.2 (a) where L is the crack spacing in the tensile direction, W is the crack spacing in the width direction and T is the thickness of the coating layer. The finite element mesh is dependent on the value of L and W. An example of the finite element mesh of the model employed in the present analysis is shown in Fig.6.2 (b). As indicated in Fig.6.2 (a), the longitudinal distance x was taken to be zero at the middle, and to be L/2 at the crack. The distance y in the sample width direction was taken to be zero at the crack, to be W/2 at the middle, and to be W at another crack. The vertical distance z was taken to be zero at the middle of substrate in the thickness direction. As the thickness of the substrate t was 800μm, the distance z of the coating layer / substrate interface was taken to be 400μm (= t/2), and the distance z at the surface of the coating layer was taken to

be 400μm +T (= 10μm in the present sample).

In the present analysis, the crack spacing L in the x-direction (tensile direction) was taken to be 40μm, and that W in the y-direction (sample width direction) to be 80 μm, where L = 40μm corresponds to the critical length at which buckling behavior of the coating layer were observed and W = 80μm corresponds to the thermally induced critical crack spacing in the coating layer [10, 12, 16]. In addition, to detect the influence of the crack spacing in each direction on the interfacial debonding separately, the crack spacing L and W were varied as (L/μm, W/μm) = (20, 80), (40, 80), (60, 80) and (40, 40), (40, 60), (40, 80), respectively.

The present specimens had been heated at 773K for formation of the intermetallic compounds and cooled down to room temperature. Therefore the temperature change ΔT = -475K was input in order to incorporate the residual stress. In the calculation, the tensile strain was applied from 0 to 15% in the x-direction.

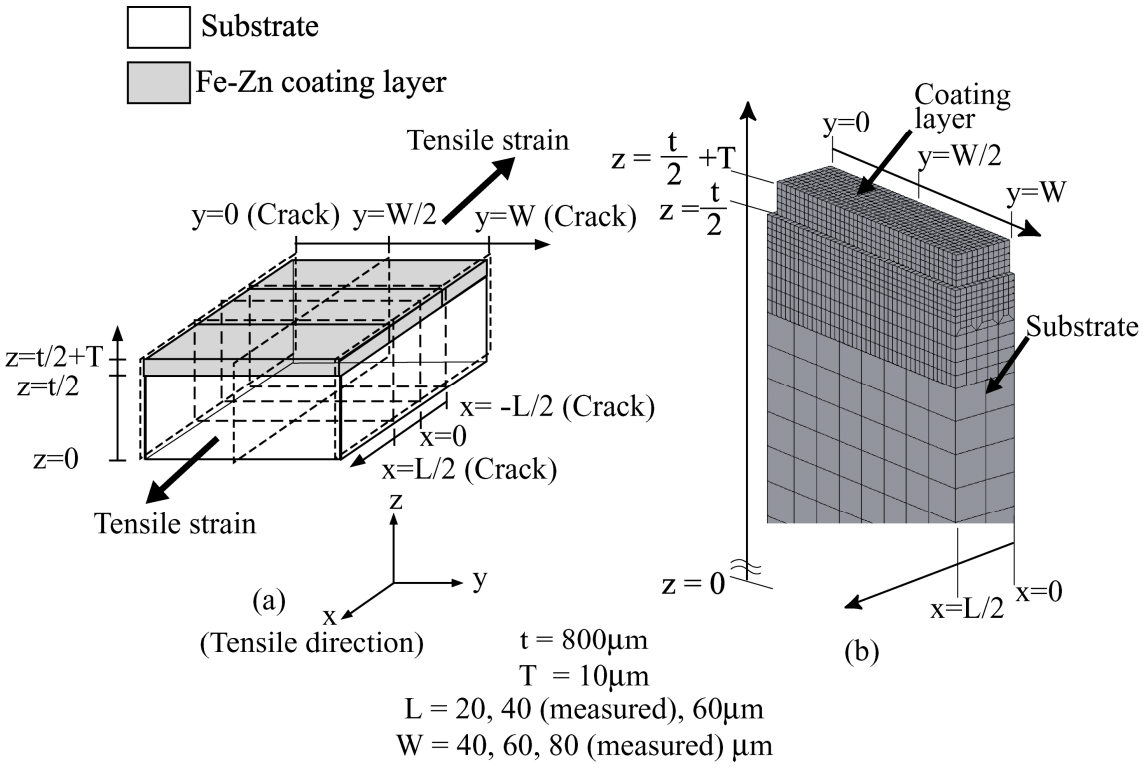

Fig.6.2 FEM-mesh of the GA steel for the interfacial debonding analysis.

To describe the interfacial debonding of the brittle material with the finite element method, the spring elements have commonly been used. In the present work, we also used the spring elements which are fractured at certain stress and don't work after their fracture. The critical stress to cause the fracture of the spring elements was regarded as the interfacial bonding strength. In the present analysis, it was taken to be 100MPa as in our preceding work [17, 22].

The analysis was carried out with the commercial finite element code MARC/Mentat2003. The Young's modulus, shear modulus, Poisson's ratio and coefficient of thermal expansion of the steel substrate were taken to be 210GPa [18], 81GPa, 0.30 [18] and $2.2\text{x}10^{-5}$/K [19, 20], respectively [21]. Those of the coating layer were taken to be 140GPa [18], 54GPa, 0.30 [18] and $1.1\text{x}10^{-5}$/K [19, 20], respectively, as similarly as in our preceding works [15-17, 22, 23].

The true stress (σ) - true plastic strain (ε_p) curve of the present steel substrate has been measured in our former works [15-17, 22, 23], which is expressed by,

$$\sigma = 130+400\varepsilon_p^{0.38} \quad (1)$$

The yielding condition for the steel substrate was given by the von Mises criterion.

6.3 Results and discussion

6.3.1 Initial spalling process calculated by the finite element method

The finite element analysis was carried out for the crack spacing (L/μm, W/μm) = (20, 80), (40, 80), (60, 80) and (40, 40), (40, 60), (40, 80). As the calculation results using these crack spacing-values had similar features in the initial spalling process of the coating layer, the result for (L/μm, W/μm) = (40, 80) is representatively taken up in this part.

Figure 6.3 shows the calculated distributions of the debonding distance from the substrate to coating layer at (a) 5%, (b) 8% and (c) 10% tensile strain in the x-direction. The x-, y-and z-axes in Fig.6.3 show the coordinates indicated in the

coating layer (Fig.6.2). The distribution of the interfacial debonding distance from the substrate to coating layer in the z-direction is shown with color.

As shown in Fig.6.3, the spalling process of the present analysis could be divided into three stages. In the stage I (3-5% tensile strain), as represented in Fig.6.3 (a), interfacial debonding starts at the edge of the coating (at the position of x = L/2 and y = W/2). In the stage II (6-8% tensile strain), as represented in Fig.6.3 (b), interfacial debonding reaches the center of the coating (the position x = 0 and y = W/2). In the stage III (9-15% tensile strain), as represented by Fig.6.3 (c), the coating is largely debonded and the debonding distance increases. Figure 6.4 shows the schematic drawing of the analyzed spalling process.

Figure 6.5 shows the progress of the debonded area of coat /substrate interface with increasing applied strain. The debonded part of the coating is shown in black color in Fig.6.5. As shown in Fig.6.5, the debonded area progressively increases from the edge (x, y) = (L/2, W/2), and rapidly progresses in the y direction after the debonding at the center (x, y) = (0, W/2).

Figure 6.6 shows the change of the occupancy of the debonded area (= ratio of the debonded area (shown in block color in Fig.6.5) to the whole area of the interface) with applied tensile strain. The strains indicated with (a), (b) and (c) correspond to the strains shown in Fig.6.3 (a), (b) and (c), respectively. As shown in

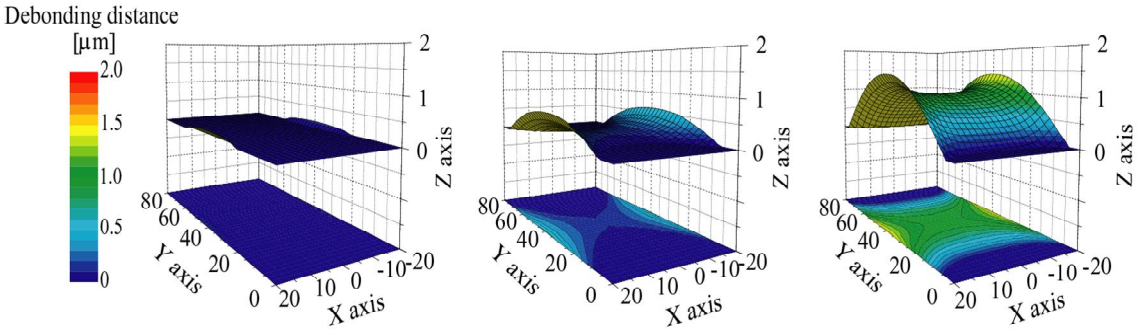

Fig.6.3 Calculated distributions of the interfacial debonding distance from the substrate to the coating layer for L=40μm and W=80μm at (a) 5%, (b) 8% and (c) 10% tensile strain.

Fig.6.6, each stage mentioned above has specific features. In the stage I, interfacial debonding starts but the occupancy of the debonded area varies only slightly. On the other hand, the occupancy of the debonded area increases largely in the stage II. In the stage III, the occupancy of the debonded area approaches unity.

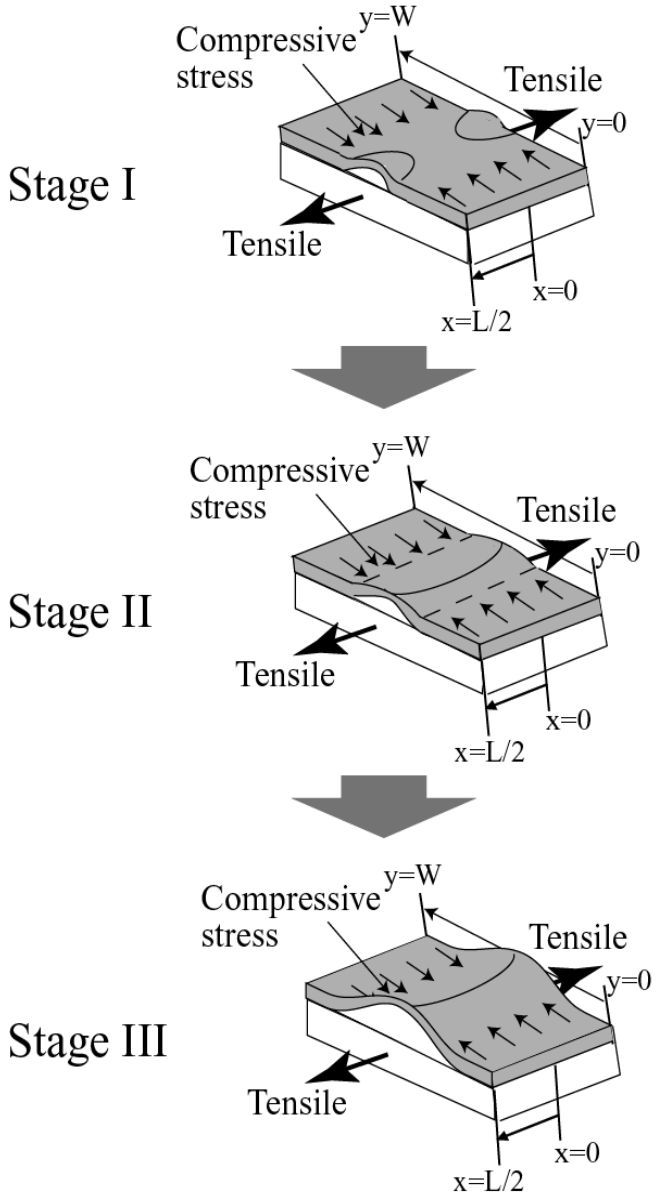

Fig.6.4 Schematic drawing of the spalling process of the coating layer.

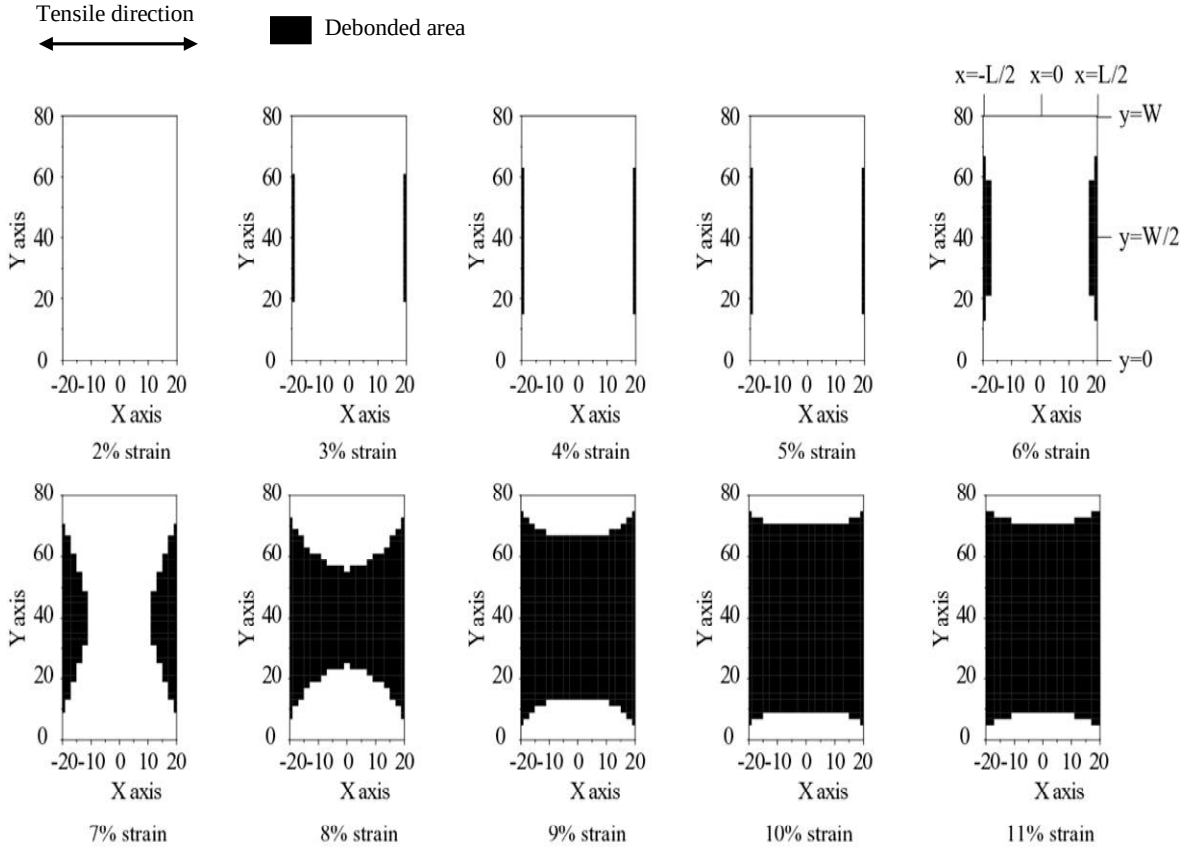

Fig.6.5 Progress of the debonded area of coat /substrate interface with increasing applied strain for the crack spacing L=40μm and W=80μm.

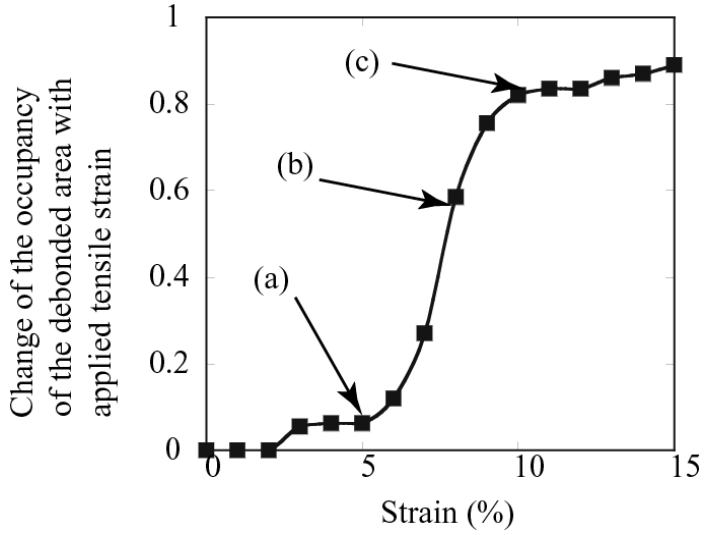

Fig.6.6 Change of the occupancy of the debonded area with applied tensile strain for the crack spacing L=40μm and W=80μm.

6.3.2 Influence of crack spacing on the spalling behavior of the coating layer

In Sec. 6.3.1, the result for (L/μm, W/μm) = (40, 80) was representatively taken up to show the feature of the spalling process qualitatively. In this part, the influence of crack spacing on the spalling behavior of the coating layer is discussed quantitatively by comparing the calculation results for the different crack spacing ((L/μm, W/μm) = (20, 80), (40, 80), (60, 80) and (40, 40), (40, 60), (40, 80)).

Figures 6.7 and 6.8 show the calculated distributions of the debonding distance from the substrate to coating layer at 10% tensile strain for the crack spacing (L/μm, W/μm) = (a) (20, 80), (b) (40, 80) and (c) (60, 80), and for the crack spacing (L/μm, W/μm) = (a) (40, 40), (b) (40, 60) and (c) (40, 80), respectively.

The following features are read from Figs. 6.7 and 6.8.

(i) The debonding distance of the coating layer decreases with decreasing crack spacing L in the tensile direction and also W in the sample width direction.

(ii) Under a given crack spacing W in the sample width direction (Fig.6.7), the debonding progresses for both small (a) and large (c) crack spacing L in the tensile direction, while the coating layer is curved more in the tensile direction for the larger crack spacing L.

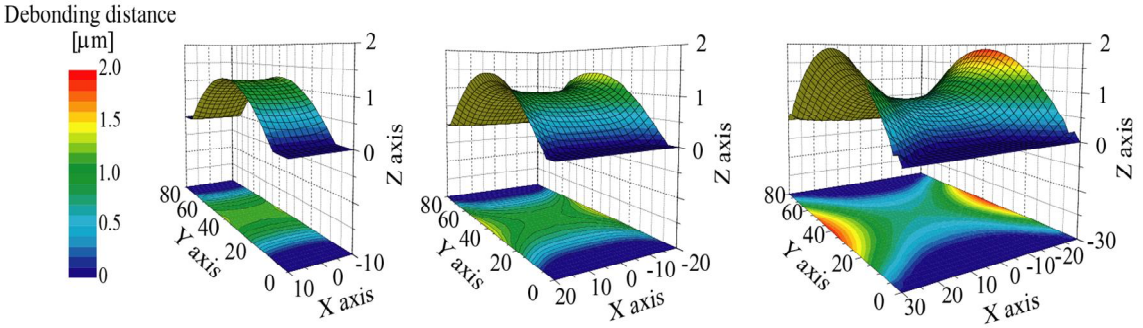

Fig.6.7 Calculated distributions of the interfacial debonding distance from the substrate to the coating layer at 10% tensile strain for the crack spacing (L/μm, W/μm) = (a) (20, 80), (b) (40,80) and (c) (60,80), respectively.

(iii) Under a given crack spacing L in the tensile direction (Fig.6.8), the debonding distance is very small for small crack spacing W but is very large for large W. The influence of the crack spacing W on the interfacial debonding is dominant in comparison with that of L under a given crack spacing W.

Figures 6.9 and 6.10 shows the progress of the debonded area of coat /substrate interface with increasing applied strain for the crack spacing (L/μm, W/μm) = (a) (20, 80), (b) (40, 80) and (c) (60, 80), and for the crack spacing (L/μm, W/μm) = (a) (40, 40), (b) (40, 60) and (c) (40, 80), respectively. Figure 6.11 shows the change of the occupancy of the debonded area with applied tensile strain (a) for the crack spacing (L/μm, W/μm) = (20, 80), (40, 80) and (60, 80) and (b) for the crack spacing (L/μm, W/μm) = (40, 40), (40, 60) and (40, 80).

As shown in Figs.6.9 and 6.11 (a), the crack spacing L in the tensile direction strongly affects on the early stage of spalling (stage I mentioned in Sec.6.3.1) but affects only slightly on the later stages II and III. In the case of (L/μm, W/μm) = (20, 80) where the crack spacing L in the tensile direction is very small, the stage I was very narrow, followed subsequently by the stage II. On the other hand, in the case (L/μm, W/μm) = (60, 80) where the crack spacing L is large, the strain at which interfacial debonding starts become low and the occupancy of the debonded area became high in the stage I.

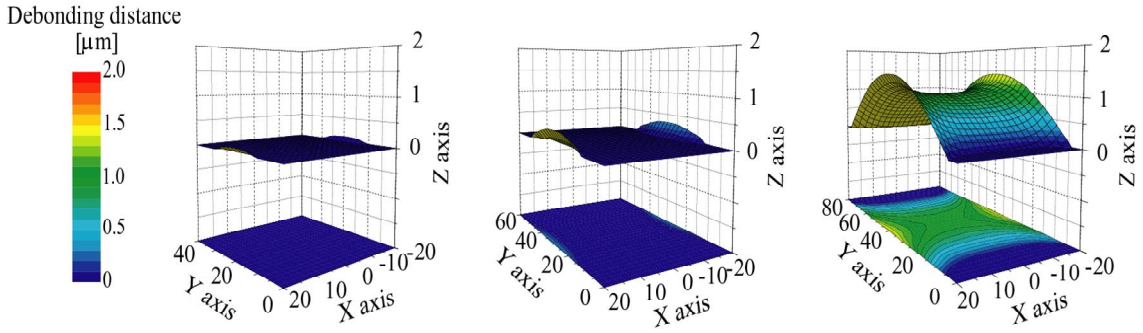

(a) (b) (c)

Fig.6.8 Calculated distributions of the interfacial debonding distance from the substrate to the coating layer at 10% tensile strain for the crack spacing (L/μm, W/μm) = (a) (40, 40), (b) (40,60) and (c) (40,80), respectively.

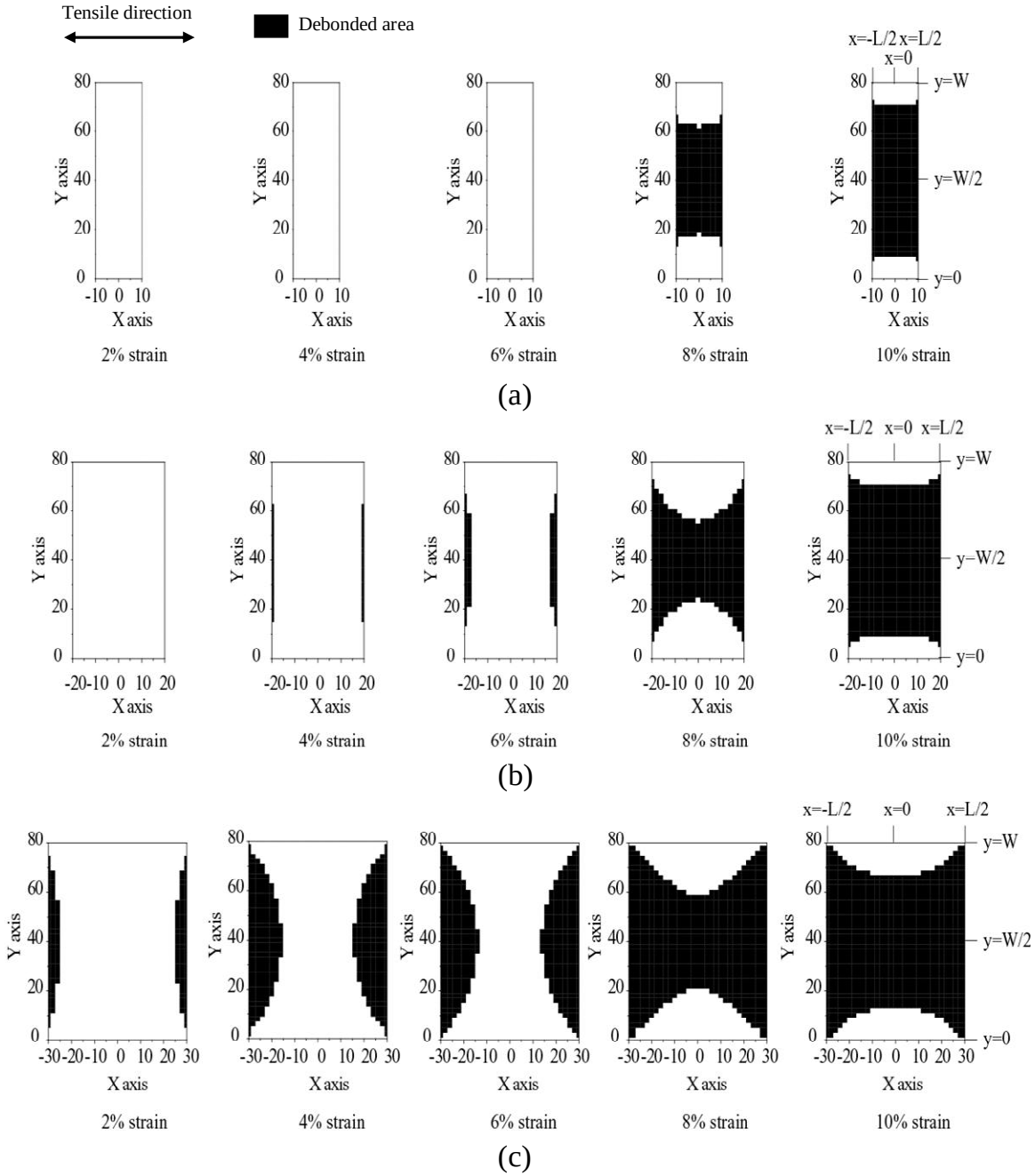

Fig.6.9 Progress of the debonded area of coat /substrate interface with increasing applied strain for the crack spacing (L/μm, W/μm) = (a) (20, 80), (b) (40, 80) and (c) (60, 80).

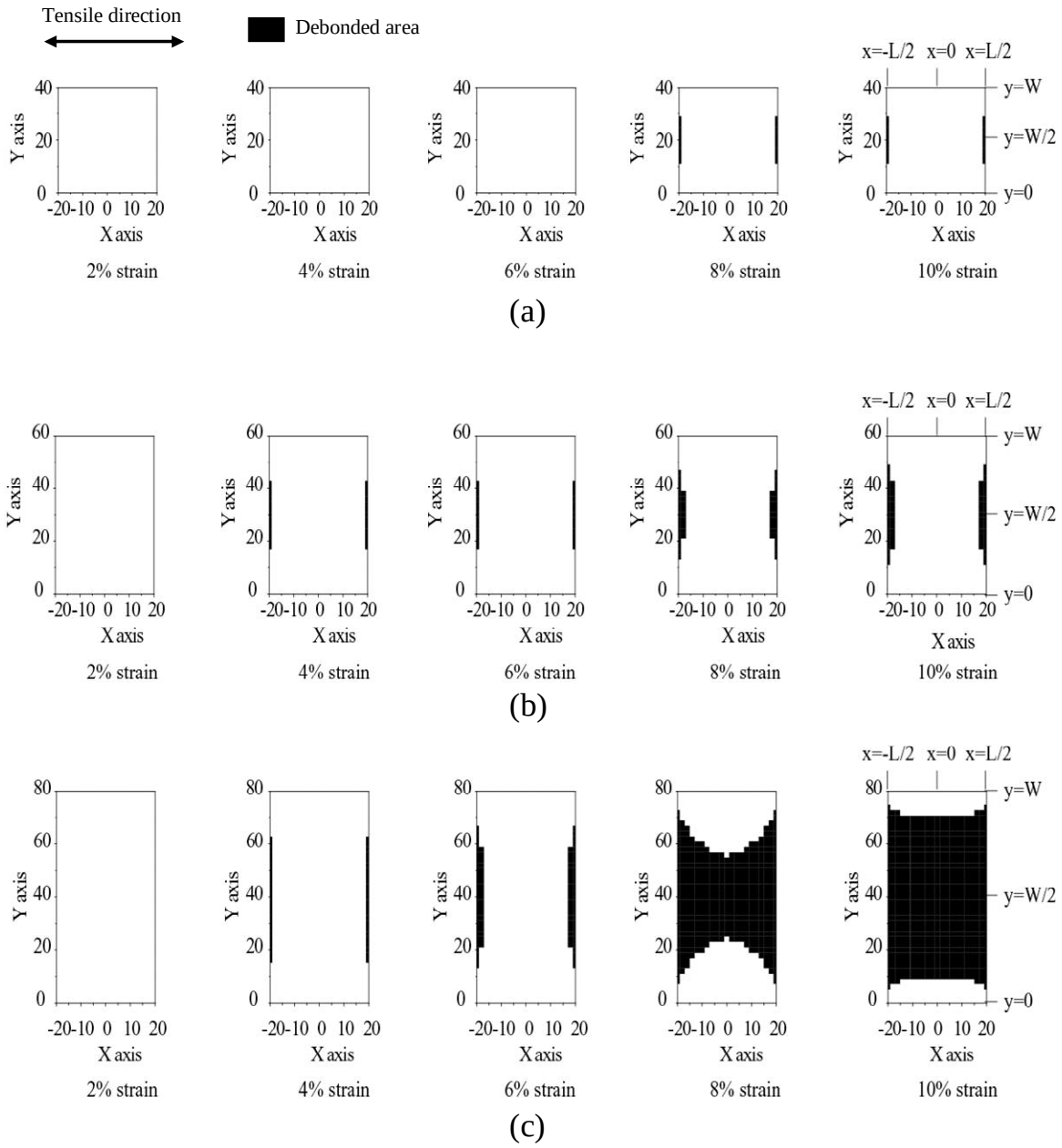

Fig.6.10 Progress of the debonded area of coat /substrate interface with increasing applied strain for the crack spacing (L/μm, W/μm) = (a) (40, 40), (b) (40, 60) and (c) (40, 80).

This means that the crack spacing L in the tensile direction affects dominantly on the initial spalling behavior.

On the other hand, as shown in Figs.6.10 and 6.11 (b), the crack spacing W in the sample width direction affects strongly on the transition from the stage I to II. In the case of (L/μm, W/μm) = (40, 40), the spalling process remained in the stage I up to the applied strain 15%. In the case of (L/μm, W/μm) = (40, 60), the occupancy of the debonded area increased slightly but the situation was the same as that in the case of (L/μm, W/μm) = (40, 40). When the crack spacing W in the sample width direction was large as in the case of (L/μm, W/μm) = (40, 80), all stages I, II and III appeared. In this way, the crack spacing W in the sample width direction gives dominant influence on the transition from the stage I to II.

Figures 6.12 and 6.13 show the changes of the debonding distance at (x, y) = (a) (L/2, W/2) and (b) (0, W/2) with applied tensile strain. The position (x, y) = (L/2, W/2) corresponds to the cracked edge of the coating, and the position (x, y) = (0, W/2) corresponds to the center of the coating, as indicated in Figs.6.12 and 6.13. At the position (x, y) = (L/2, W/2), the debonding initiates and the debonding distance is

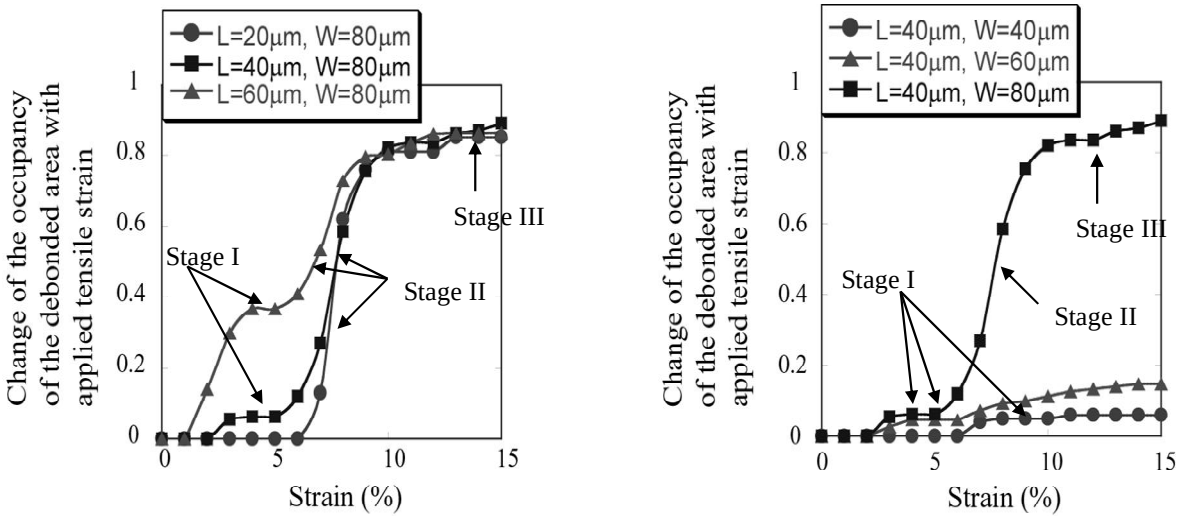

Fig.6.11 Change of the occupancy of the debonded area with applied tensile strain for the crack spacing (L/μm, W/μm) = (a) (20, 80), (40, 80) and (60, 80) and (b) (40, 40), (40, 60) and (40, 80).

maximum at any applied strain, as has been shown in Figs.6.7 and 6.8. The debonding front in the x direction (tensile direction) moves from the edge (x=L/2) to the center (x=0) with increasing applied tensile strain. The calculation results at (x, y) = (a) (L/2, W/2) and (b) (0, W/2) for the crack spacing (L/μm, W/μm) = (20, 80), (40, 80), (60, 80) in Fig.6.12 show the following features for the influence of the crack spacing L in the tensile direction on the debonding process.

As shown in Fig.6.12 (a), the larger is the crack spacing L, the larger becomes the maximum debonding distance at (x, y) =(L/2, W/2). On the other hand, as shown in Fig.6.12 (b), the debonding behavior at (x, y) = (0, W/2) in the early stage at around 7-9 % strain is almost same for all crack spacing L, and the debonding distance at (x, y) = (0, W/2) becomes slightly small with increasing crack spacing L in the later stage.

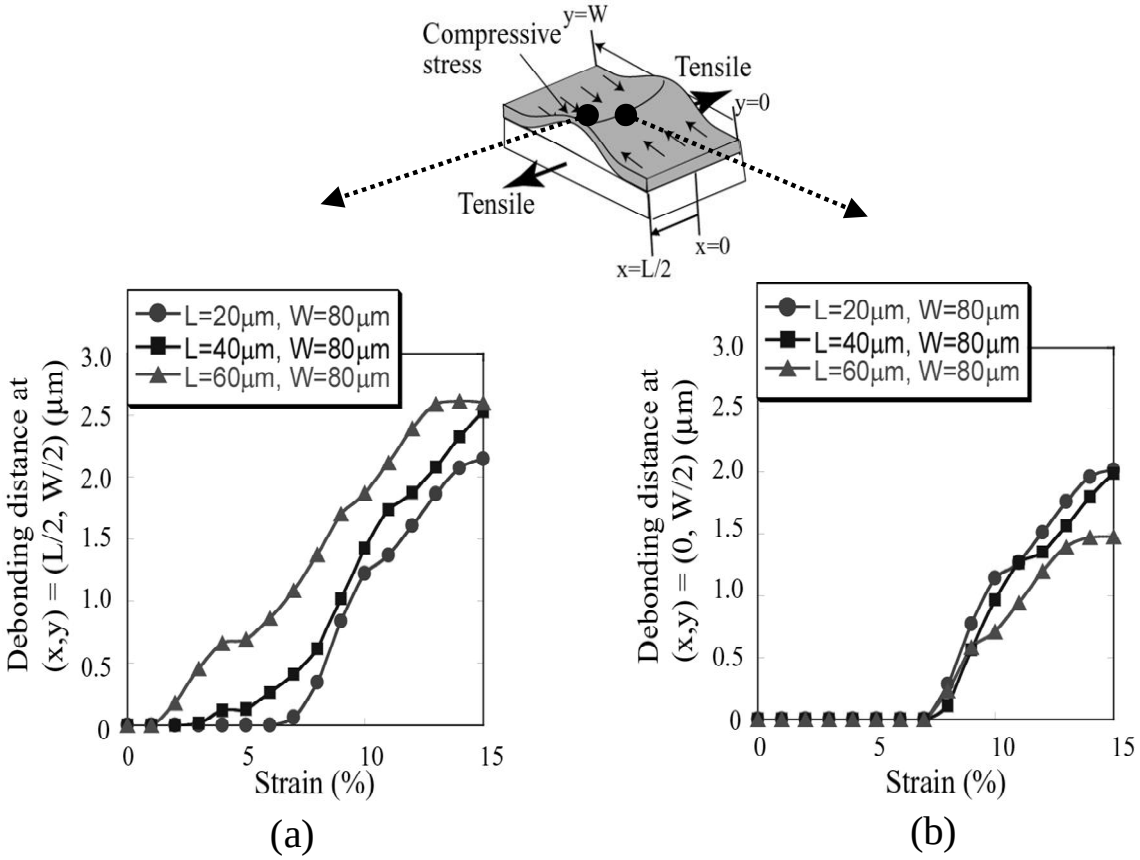

Fig.6.12 Calculated change of the debonding distance at (x, y) = (a) (L/2, W/2) and (b) (0, W/2) for the crack spacing (L/μm, W/μm) = (20, 80), (40, 80) and (60, 80).

Such a feature is accounted for as follows. The larger the crack spacing L, the higher becomes the interfacial stress to cause debonding at (x, y) = (L/2, W/2). Accordingly, in the early stage of debonding (stage I), the debonding is enhanced for large L. As shown in Fig.6.3, the curvature in the x direction (tensile direction) is small up to initiation of deboning at (x, y) = (L/2, W/2) at 5% strain. Once debonding occurs, the coating layer is curved more in the tensile direction. The curvature of the debonded region of the coating layer is large for the larger crack spacing L (Fig.6.7). This suggests that, once the debonding occurs at (x, y) = (0, W/2), the debonding does not progress further until the curvature becomes large enough to generate the critical stress to cause debonding. Accordingly, high strain is needed to cause further debonding. As a result, the debonding distance at (x, y) = (0, W/2) in stage II becomes slightly small with

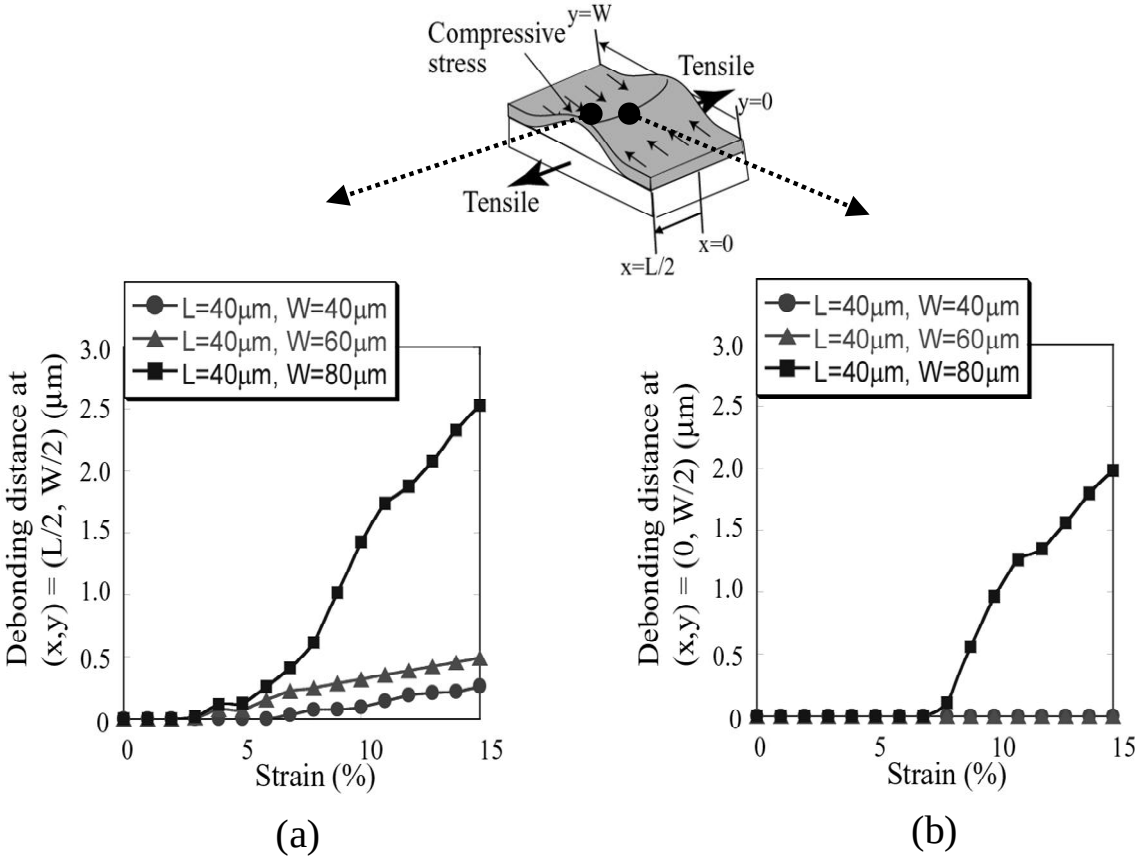

Fig.6.13 Calculated change of the debonding distance at (x, y) = (a) (L/2, W/2) and (b) (0, W/2) for the crack spacing (L/μm, W/μm) = (40, 40), (40, 60) and (40, 80).

increasing crack spacing L. In this way, it was revealed that the crack spacing in the tensile direction affects especially on the initial spalling behavior; the larger the spacing, the more the spalling is enhanced in the early stage of debonding but not in the later stage.

The calculation result of the debonding distance at (x, y) = (a) (L/2, W/2) and (b) (0, W/2) for the crack spacing (L/μm, W/μm) = (40, 40), (40, 60), (40, 80) is shown in Fig.6.13. As shown in Fig.6.13 (a), the larger the crack spacing W, the larger becomes the maximum debonding distance of the coating. As shown in Fig.6.13 (b), the debonding didn't occur at (x, y) = (0, W/2) for the crack spacing (L/μm, W/μm) = (40, 40) and (40, 60) even at 15% strain within the present calculation condition, while debonding at (x, y) = (L/2, W/2) had occurred at around 5 % strain (Fig.6.13 (a)). This means that the stage II didn't start in the case (L/μm, W/μm) = (40, 40) and (40, 60). On the contrary, for large crack pacing W, the debonding progressed extensively in the whole applied strain range investigated.

From the present work, the influence of the crack spacing on the interfacial debonding was revealed with the finite element analysis. The results suggest that, to supress the spalling of the coating layer, the crack spacing in the tensile direction should be short to retard the initiation of the debonding and the crack spacing in the sample width direction should be short, too, to retard the progress of the interfacial debonding. In our former work [15, 22], it has been shown that, when (i) the coating is thin and (ii) the substrate is hard, the crack spacing becomes small, which will supress the interfacial debonding, if the tensile strength of the coating layer and interfacial bonding strength are retained on the level of those for the low strength steel.

6.4 Conclusions

(1) The spalling process could be divided into three stages. In the stage I, interfacial debonding starts at the cracked edge of the coating (the position x = L/2 and y = W/2). In the stage II, interfacial debonding reaches the center of the coating (the position x = 0 and y = W/2). In the stage III where the debonding front has passed the center, the coating is largely debonded and the debonding distance increases.

(2) The debonding distance of the coating layer decreases with decreasing the crack spacing both in the tensile direction L and the sample width direction W. The crack spacing L in the tensile direction affects especially on the stage I behavior. The crack spacing W in the sample width direction affects especially on the transition from the stage I to the stage II.

(3) The present results suggest that, in order to supress the interfacial debonding, the crack spacing in the tensile direction should be short to retard the initial debonding, and the crack spacing in the sample width direction should be short, too, to retard the progress of the interfacial debonding.

ACKNOWLEDGEMENT

The authors wish to express their gratitude to Japan Society for the Promotion of Science for Young Scientists and to The Iron and Steel Institute of Japan for the support of the present work.

References

[1] C. E. Jordan CE, K. M. Goggins and A. R. Marder: *Metall. Mater. Trans. A*, **25** (1994), 2101.

[2] S. Lazik, C. Esling and J. Wegria: *Textures and Microstructures*, **23** (1995), 131.

[3] A. Kelly A and W. R. Tyson: *J. Mech. Phys. Solids*, **13** (1965), 329.

[4] S. Ochiai and K. Osamura: *J. Mater. Sci.*, **21** (1986), 2735.

[5] M. S. Hu and A. G. Evans: *Acta Metall.*, **37** (1989), 917.

[6] Y. Leterrier, L. Boogh, J. Andersons and J. A. E. Mason: *J. Polym. Sci., Part B: Polym. Phys.*, **35** (1997), 1449.

[7] S. Ochiai and Y. Murakami: *Metal Sci.*, **41** (1976), 401.

[8] J. Andersons, U. A. Handge, I. M. Sokolov and B. Blumen: *Eur. Phys. J.*, **B17** (2000), 261.

[9] S. Ochiai, S. Iwamoto, T. Nakamura and H. Okuda: *ISIJ Int.*, **47** (2007), 458.

[10] S. Ochiai, S. Iwamoto, T. Tomida, H. Okuda, M. Tanaka and M. Hojo: *Composite Interfaces*, **12** (2005), 655.

[11] S. Ochiai, T. Tomida, T. Nakamura, S. Iwamoto, H. Okuda, M. Tanaka and M. Hojo: *Tetsu-to-Hagane*, **91** (2005), 327.

[12] T. Nakamura, S. Ochiai, S. Iwamoto, D. Adachi and H. Okuda,: *Tetsu-to-Hagane*, **91** (2005), 342.

[13] T. Alpas, J. Inagaki: *ISIJ Int*., **40** (2000), 172.

[14] M. Sakurai, J. Inagaki, T. Alpas: *CAMP-ISIJ*, **12** (1999), 550.

[15] S. Iwamoto, S. Ochiai, T. Nakamura and H. Okuda: *Tetsu-to-Hagane,* **91** (2005), 335.

[16] S. Ochiai, S, Iwamoto, T. Tomida, T. Nakamura, H. Okuda, M. Tanaka and H. Hojo: *Metall. Mater. Trans. A*, **36A** (2005), 1807.

[17] S. Iwamoto, S. Ochiai, H. Okuda and T. Inoue: *ISIJ Int.*, **47** (2007), 930.

[18] G. Reumont, J. B. Vogt, A. Iost and J. Foct: *Surf. Coat. Tech.*, **139** (2001), 265.

[19] J. Foct: *Scripta. Metall.*, **28** (1993), 127.

[20] A. Iost and J. Foct: J. *Mat. Sci.*, **12** (1993), 1340.

[21] E. Tzimas and G. Papadrimitriou: *Surf. Coat. Tech.*, **145** (2001), 176.

[22] S. Iwamoto, S. Ochiai and H. Okuda: *ISIJ Int.*, **49** (2009), 119.

[23] S. Iwamoto, S. Ochiai and H. Okuda: *ISIJ Int.*, **49** (2009), 139.

Chapter 7

Analysis of Group-buckling and -debonding Behaviors of Galvannealed Coating Layer on Steel Substrates under Applied Tensile Strain

7.1 Introduction

The hot-dipped GA (galvannealed) steels, consisting of Fe-Zn intermetallic coating layer and substrate steel, are widely used as architectural and car-body materials due to their high corrosion resistance and weldability [1, 2]. As these materials are composed of brittle coating layer with low failure strain and ductile substrate with far higher failure strain, the coating layer exhibits multiple cracking perpendicular to the tensile direction [3-8], and then spalled when tensile stress is applied externally. The spalling of the coating layer is caused by the compressive stress-induced buckling in the sample width direction [7], followed by interfacial debonding. The SEM image and schematic representation of the buckling behavior of the GA coating layer in the sample used in this work under applied tensile strain are shown in Fig.7.1. The details of the sample specification and the procedure for tensile test and fracture morphology observation will be shown later in Sec.7.2.1.

In the buckling behavior, series of cracked-coating layers arraying along the tensile direction exhibit group-buckling as will be shown later in Fig.7.4. However, the mechanism of such a group-buckling has not been revealed yet. In the present work, the group-buckling behavior was observed in detail with the scanning electron microscope and analyzed with 3-dimentional finite element models.

For analysis of the group-buckling behavior, the following cases, shown schematically in Fig.7.2, were taken up. The coatings named coats (i), (ii) and (iii) are lined up in the tensile direction. When the bonding strength in the coating / substrate interfaces of each coating is equal (Case I in Fig.7.2), the debonding of the coating layer

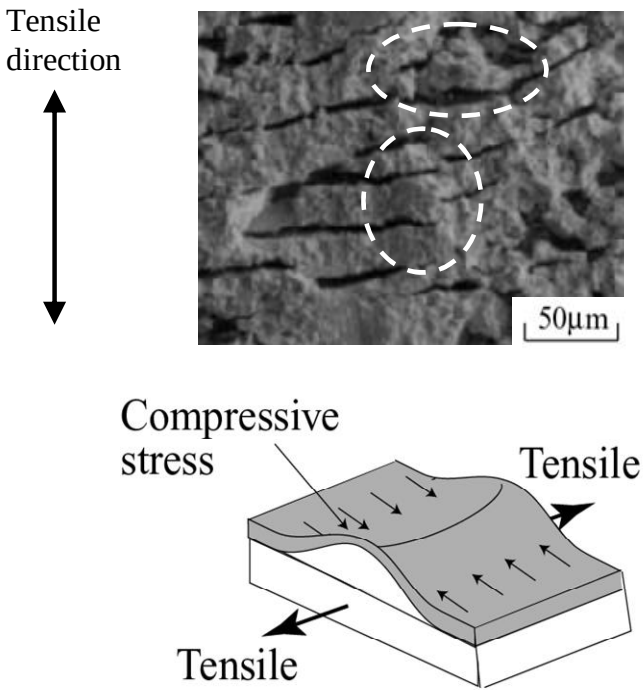

Fig.7.1 SEM image and schematic representation of the buckling behavior of the coating layer.

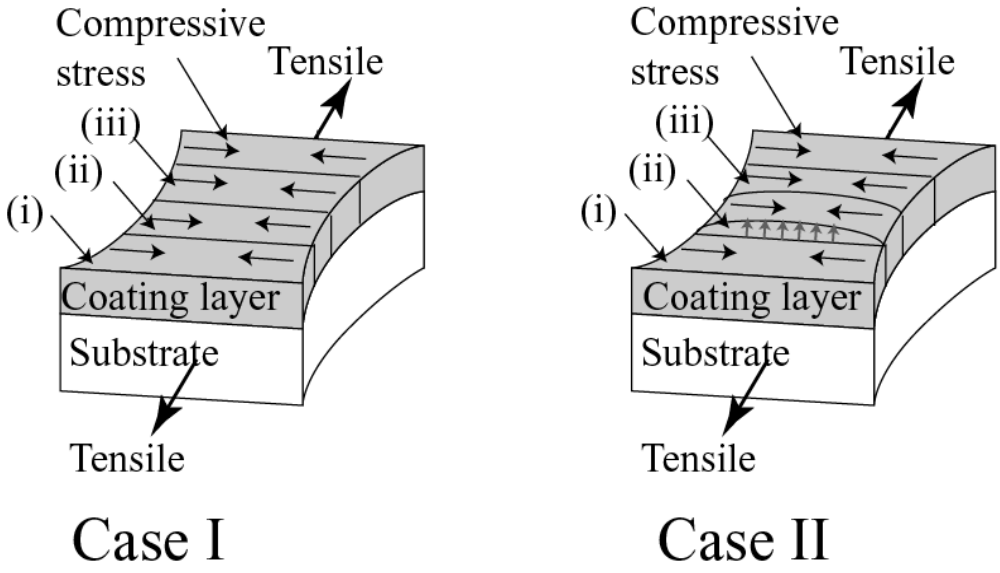

Fig.7.2 Schematic representation of the cases employed for analysis of the group-buckling behavior.

occurs at the same time. On the other hand, when the bonding strength in the coating / substrate interface of coat (ii) is weaker than those of coat (i) and (iii) (Case II in Fig.7.2), the interfacial debonding of the coat (ii) occurs first. Under the condition that the coats (i) and (iii) have a common bonding strength in both Cases I and II, whether the group-bucking/debonding occurs or not can be judged by comparing the behavior of coat (i) and (iii) in Case I to those in Case II; when the debonding of coat (i) and (iii) for Case II are larger than those for Case I, the group-buckling should take place.

7.2 Experimental procedure

7.2.1 The group-buckling observation of the coating layer

The used samples were the hot-dipped Fe-Zn intermetallic compound-coated IF (Interstitial Free) steels. These samples were supplied as the common samples for the research group on structure and property of the coating on GA (galvannealed) steels, organized in the Iron and Steel Institute of Japan. The overall thickness of the coating layer was 10 μm.

For tensile test, the samples with a length 100 mm, width 10 mm and thickness 0.8 mm were prepared. Tensile test was carried out at room temperature at a crosshead speed of 8.3×10^{-6} m/s. The strain for a gage length 50 mm was measured by the non-contact laser extensometer (Shimadzu DVE-200).

The measurement of the change of the crack spacing in the coating layer has been presented in our former work [9]. In the present work, compressive fracture and spalling behavior, especially the group-buckling, of the tensile-tested samples were carefully observed with the scanning electron microscope (Joel, JSM-5410LS).

7.2.2 Finite element analysis

3-dimentional models for analysis of interfacial debonding of the coating layer were prepared as follows. The morphology of the specimen with multiple-cracked

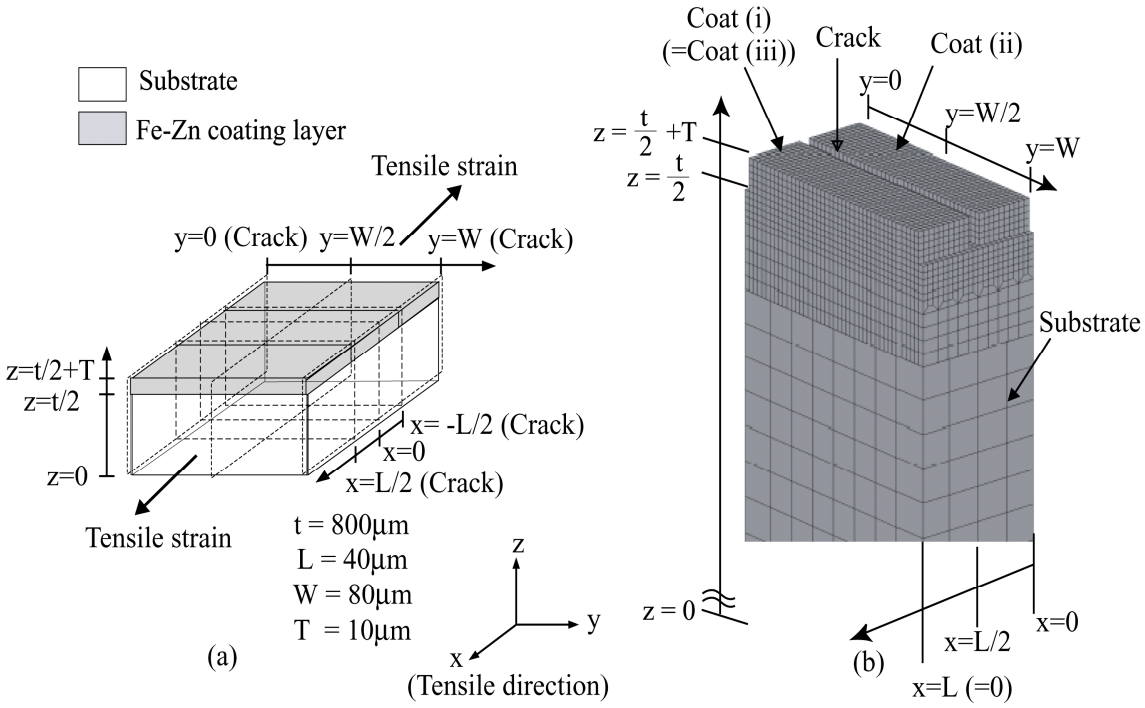

Fig.7.3 FEM-mesh of the GA steel for the group-buckling analysis.

Fe-Zn intermetallic compound coating layer is schematically shown in Fig.7.3 (a) where L is the crack spacing in the tensile direction, W is the crack spacing in the width direction, t is the thickness of the substrate steel and T is the thickness of the coating layer. As indicated in Fig.7.3 (a), the longitudinal distance x was taken to be zero at the middle, and to be L/2 at the broken end. The distance y in the width direction was taken to be zero at the broken end, to be W/2 at the middle, and to be W at the other broken end. The vertical distance z was taken to be zero at the middle of substrate in the thickness direction. As the thickness of the substrate was 800μm, the distance z of the coating layer / substrate interface was taken to be 400μm, and the distance z was taken to be 400μm +T (= 10μm in the present sample) at the surface of the coating layer. For this analysis, the crack spacing in the x-direction L = 40μm, and that in the y-direction W = 80μm were used, where W = 80μm corresponds to the thermally induced critical crack spacing in the coating layer [9, 10], and L = 40μm corresponds to the critical

length at which buckling behavior of the coating layer were observed.

To describe the interfacial debonding of the brittle material with finite element method, spring elements were commonly used. In the present work, we used spring elements which are fractured at certain stress and don't work after their fracture. The critical stress to cause the fracture of the spring elements was regarded as the interfacial bonding strength. In the present analysis, it was taken to be 100MPa for all coats in Case I and for coat (i) in Case II, as in our preceding work [11].

The finite element mesh for the present analysis is shown in Fig.7.3 (b). In Case I, the bonding strength 100MPa was used for coat (i) (=coat (iii)) and coat (ii), respectively. In Case II, the bonding strength 100MPa was commonly used for coat (i) (=coat (iii)) and the bonding strength 60 and 80MPa were used for coat (ii). In the calculation, the group-buckling process was assumed to occur in the sequence in which (i) a piece of cracked-coating exhibits buckling first and (ii) such a preceding buckling enhance the bucking of the neighboring coating in the tensile direction, as mentioned above.

The present specimens had been heated at 773K for formation of the intermetallic compounds and cooled down to room temperature. Therefore the temperature change $\Delta T = -475$ K was input in order to incorporate the residual stress. In the calculation, the tensile strain was applied from 0 to 10% in the x-direction.

The analysis was carried out with the commercial finite element code MARC/Mentat2003. The Young's modulus, shear modulus, Poisson's ratio and coefficient of thermal expansion of the steel substrate were taken to be 210GPa [12], 81GPa, 0.30 [12] and 2.2×10^{-5}/K [13, 14] respectively [15]. Those of the coating layer were taken to be 140GPa [12], 54GPa, 0.30 [12] and 1.1×10^{-5}/K [13, 14], respectively, as similarly as in our preceding works [9-11]. It has been known that the coating layer is composed mainly of the ζ, δ_1, Γ_1 and Γ phases and δ_1 phase is the thickest under the usual fabrication route [12, 15]. In the present samples, the volume fraction of the δ_1 phase was estimated to be 70-80% from the composition image of the polished side surface. Concerning the elastic constants (E, ν and G), no data have been reported for the ζ, Γ_1 and Γ phases. Only the values for the δ_1 phase [13] are available. Due to these reasons, the elastic constants of the δ_1 phase, which occupies 70-80% of the coating layer and therefore practically governs the deformation of the coating layer, were used

as an approximation. With these values, the multiple cracking behavior of the GA coating layer, observed experimentally, has been described well [9, 10].

The true stress (σ) - true plastic strain (ε_p) curve of the present steel substrate has been measured in our former work [9, 10], which is expressed by,

$$\sigma = 130+400\varepsilon_p^{0.38} \quad (1)$$

The yielding condition for the steel substrate was given by the von Mises criterion.

7.3 Results and discussion

7.3.1 Morphology observation result

SEM image and schematic representation of the group-buckling behavior of the coating layer are shown in Fig.7.4. The coatings surround by circles refer to the group buckling.

The possible process of the group-buckling inferred from the present observation is twofold; (a) the buckling of all coatings occurs at one time and (b) the buckling of coatings occurs consecutively along the tensile direction. Based on these observation results, the finite element models mentioned in Sec.7.2.2 were prepared.

In our recent research, the grain sizes of the substrate steel were measured experimentally. The grain size of the present sample was 10.3μm in on average [16], and its standard deviation was 5.3μm [16]. As shown in Fig.7.4, the group-buckling reached more than 100μm long in the tensile direction. This suggests that the group-buckling is not caused by the mismatch of the slip system of the substrate grain.

This group-buckling phenomenon doesn't apply only to GA steels. Similar group-buckling of the coatings in the brittle coating-ductile substrate composite systems was also observed in Al_2O_3-coated aluminum wire, as shown in Fig.7.5.

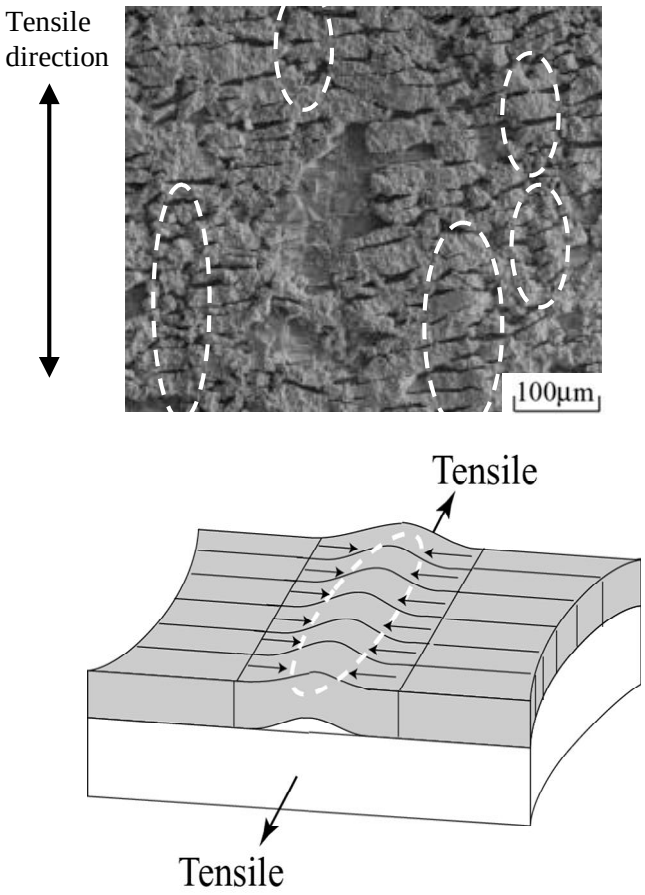

Fig.7.4 SEM image and schematic representation of the group-buckling behavior of the coatings.

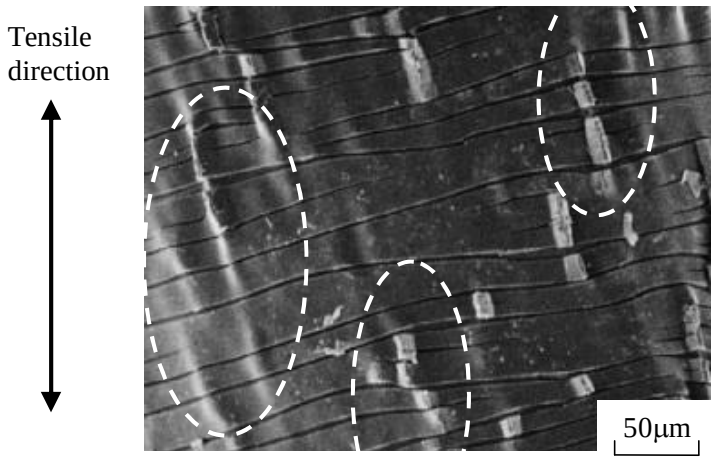

Fig.7.5 SEM image of the group-buckling behavior observed in Al_2O_3-coated aluminum wire.

7.3.2 Results of the finite element analysis

Figures 7.6 and 7.7 show the calculated distribution of the interfacial debonding distance from the substrate to coats (i) and (ii), respectively, under the condition of the bonding strength of coat (i) $\sigma_{(i),\ int.}$ =100MPa and that of coat (ii) $\sigma_{(ii),\ int.}$ = (a) 60MPa, (b) 80MPa and (c) 100MPa. The x-, y-and z-axes in Figs.7.6 and 7.7 show

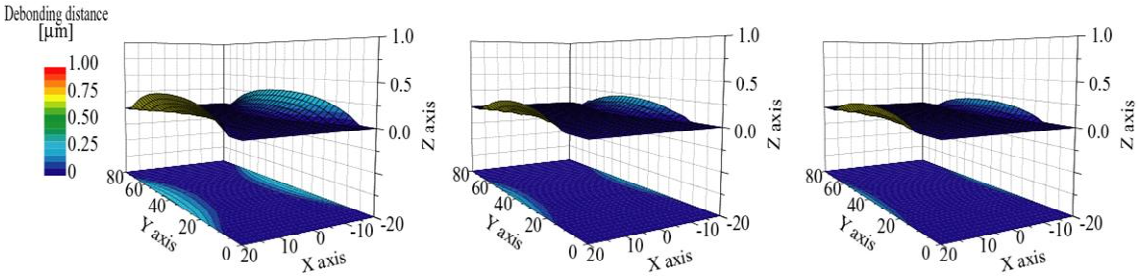

(a) (b) (c)

Fig.7.6 Calculated distributions of the interfacial debonding distance from the substrate to coat (i) at 5% tensile strain in the x-direction under the condition of $\sigma_{(i),\ int.}$ =100MPa and $\sigma_{(ii),\ int.}$ = (a) 60MPa, (b) 80MPa and (c) 100MPa.

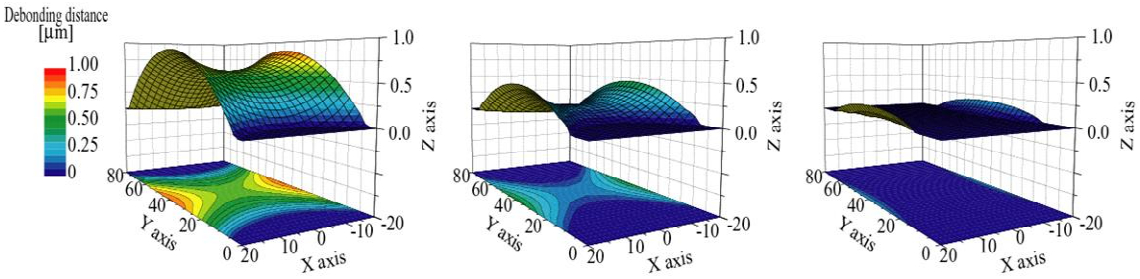

(a) (b) (c)

Fig.7.7 Calculated distributions of the interfacial debonding distance from the substrate to coat (ii) at 5% tensile strain in the x-direction under the condition of $\sigma_{(i),\ int.}$ =100MPa and $\sigma_{(ii),\ int.}$ = (a) 60MPa, (b) 80MPa and (c) 100MPa.

the coordinates indicated in the coating layer (Fig.7.3). The distribution of the interfacial debonding distance from the substrate to coatings in the z-direction is shown with color.

The debonding distance from substrate to coating was maximum at x = L/2 and y = W/2 for all calculation results. The interfacial stress is highest at x = L/2 and y = W/2 since the difference in amount of deformation between the coat and substrate is largest. Accordingly, the debonding occurs first at x = L/2 and y = W/2 and then extends into the middle. The debonded part moves upward rapidly since the constraint from the substrate has vanished. As the result, the shape of the coat becomes like a horse saddle. Details of the numerical results will be shown in Figs. 7.8 and 7.9.

As shown in Fig.7.7, the lower the bonding strength $\sigma_{(ii),\ int.}$, the larger became the interfacial debonding distance of coat (ii). Meanwhile, the results shown in Fig.7.6 revealed that the debonding distance of coat (i) became larger for low bonding strength of coat (ii)-substrate interface $\sigma_{(ii),\ int.}$, although the bonding strength in coat (i) $\sigma_{(i),\ int.}$ was same ($\sigma_{(i),\ int.}$=100MPa). That is, the group-buckling occurs, originating from the buckling of the coating with weak interface, coat (ii) in the present analysis.

Figure 7.8 and 7.9 shows the change of the debonding distance at (x, y) = (L/2, W/2) and (0, W/2) with applied tensile strain for coat (i) and coat (ii). The position (x, y) = (L/2, W/2) corresponded to the position getting the maximum value of the debonding distance. The position (x, y) = (0, W/2) corresponded to the center of the coating which is important to evaluate the progression of interfacial debonding.

As shown in Fig.7.9, the lower the bonding strength of the coat (ii)-substrate interface $\sigma_{(ii),\ int.}$, the larger became the debonding distance of coat (ii) at both (x, y) = (L/2, W/2) and (0, W/2).

As shown in Fig.7.8, the debonding distance at both (x, y) = (L/2, W/2) and (0, W/2) in coat (i) also became larger with low bonding strength of the coat (ii)-substrate interface $\sigma_{(ii),\ int.}$. In addition, the applied strain at which the interfacial debonding started became lower with low bonding strength of coat (ii) $\sigma_{(ii),\ int.}$ at (x, y) = (0, W/2) in coat (i), as shown in Fig.7.8 (b). From this result, it is expected that the debonding of coat (ii) affected not only on the maximum debonding distance of coat (i) but also the progression of interfacial debonding of coat (i).

From the comparison of the Fig.7.8 and Fig.7.9, it was found that the

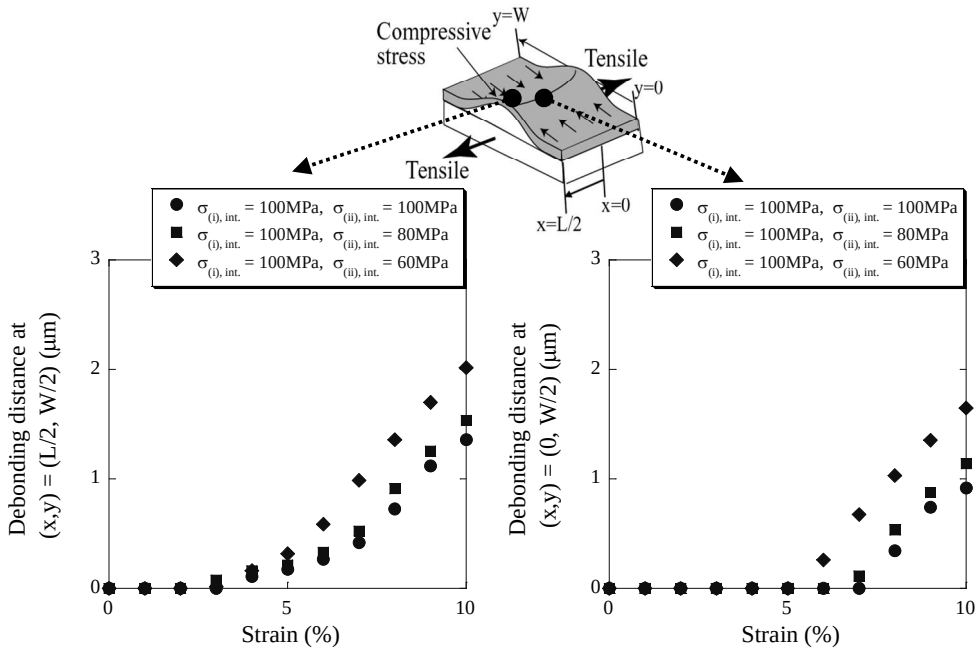

(a) (b)

Fig.7.8 Calculated change of the debonding distance at (x, y) = (L/2, W/2) (a) and (0, W/2) (b) for coat (i) under the condition of $\sigma_{(i),\ int.}$ =100MPa and $\sigma_{(ii),\ int.}$ = 60MPa, 80MPa and 100MPa.

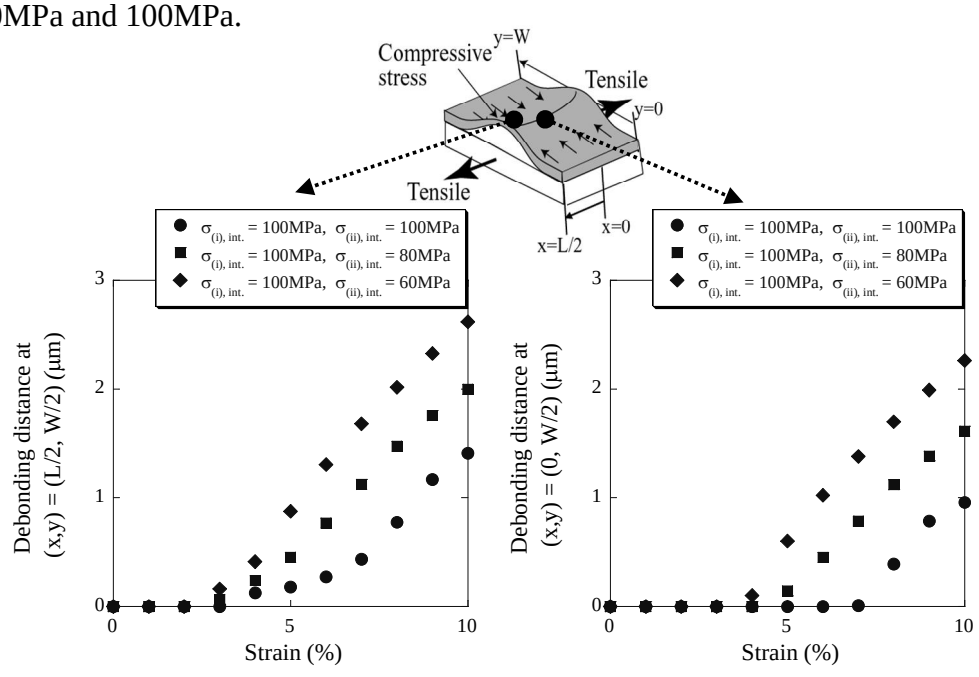

(a) (b)

Fig.7.9 Calculated change of the debonding distance at (x, y) = (L/2, W/2) (a) and (0, W/2) (b) for coat (ii) under the condition of $\sigma_{(i),\ int.}$ =100MPa and $\sigma_{(ii),\ int.}$ = 60MPa, 80MPa and 100MPa.

debonding distance of coat (ii) was not directly reflected in that of coat (i). As shown in Fig.7.8, the debonding distance of the coat (i) under the condition of $\sigma_{(ii),\ int.}$ = 100MPa was only slightly smaller than that under the condition of $\sigma_{(ii),\ int.}$ = 80MPa, in contrast to the debonding distance of the coat (ii) which was much larger under the condition of $\sigma_{(ii),\ int.}$ = 80MPa.

The progress of the debonded area of the coat (i)-substrate interface and coat (ii)-substrate interface with increasing applied strain, under the condition of $\sigma_{(i),\ int.}$ =100MPa and $\sigma_{(ii),\ int.}$ = (a) 100MPa, (b) 80MPa and (c) 60MPa, are shown in Figs.7.10 and 7.11, respectively. The debonded part of the coating is shown in black color in Figs.7.10 and 7.11. As shown in Fig.7.10 (a), the debonded area progressively increases from the edge (x, y) = (L/2, W/2), and rapidly progresses in the y direction after the debonding at the center (x, y) = (0, W/2).

Figure 7.12 shows the change of the occupancy of the debonded area (= ratio of the debonded area (shown in block color in Figs.7.10 and 7.11) to the whole area of the interface) with applied tensile strain for coat (i) (a) and (ii) (b). The lower the bonding strength, the larger became the occupancy of the debonded area of the coat (ii)-substrate interface, as shown in Fig.7.12 (b). For the coat (i)-substrate interface, as shown in Fig.7.12 (a), the occupancy of the debonded area also became larger for low bonding strength of the coat (ii)-substrate interface $\sigma_{(ii),\ int.}$.

As indicated in Figs.7.8 and 7.12 (a), the preceding debonding of the coating with low interfacial bonding strength enhances the interfacial debonding of the neighboring coating. In this way, the group-buckling phenomenon in the galvannealed coatings was accounted for by the mechanical viewpoint under the scattered interfacial bonding strength. This is the first approach to make clear the mechanism of group-buckling using numerical analysis.

As mentioned above, similar group-buckling behaviors were also observed in Al_2O_3-coated aluminum wire. It is possible that the mechanism of group-buckling is universally applied for all brittle coating composite, not only galvannealed steel, by the present mechanical approach.

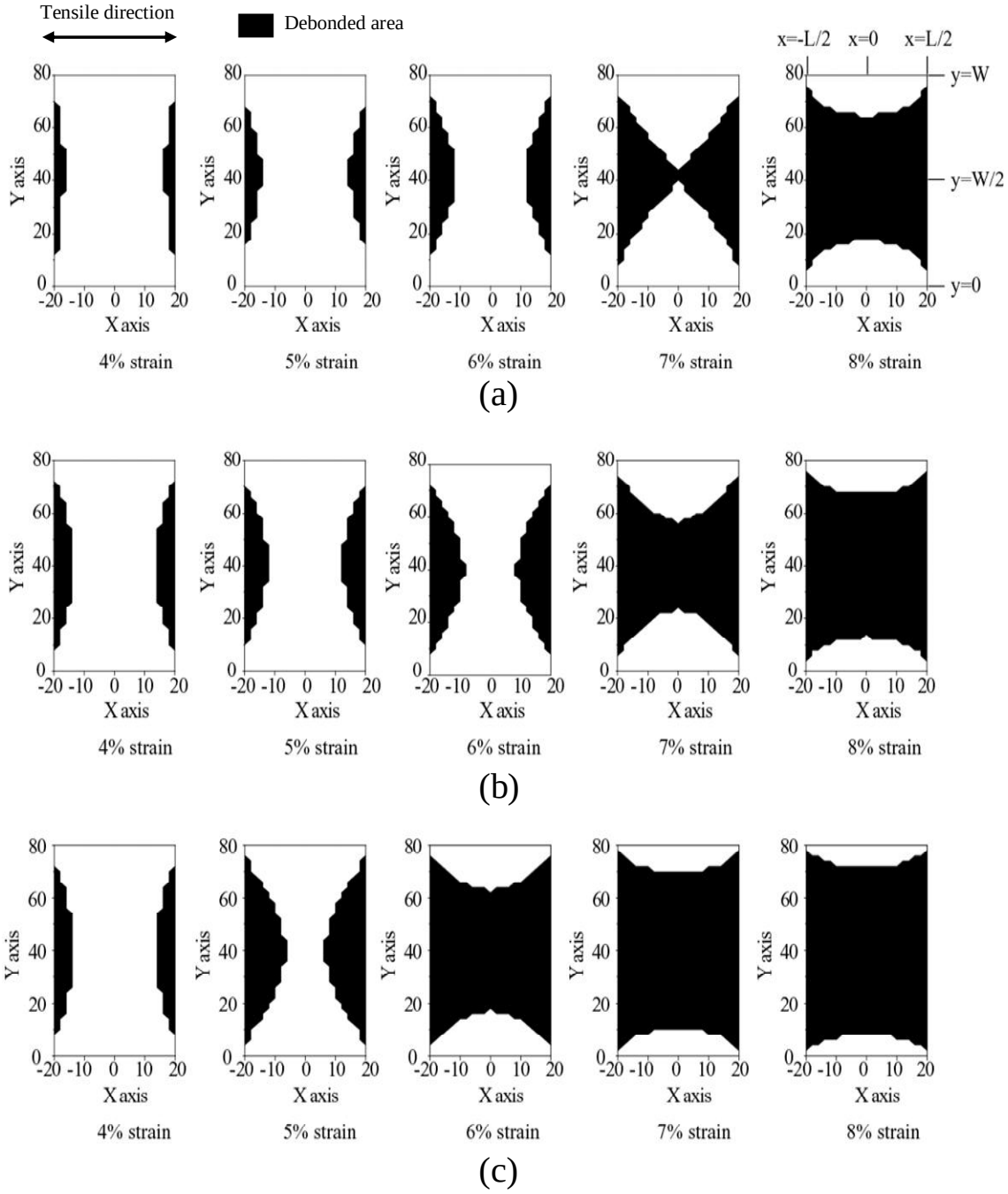

Fig.7.10 Progress of the debonded area of the coat (i)-substrate interface with increasing applied strain, under the condition of $\sigma_{(i),\ int.}$ =100MPa and $\sigma_{(ii),\ int.}$ = 60MPa, 80MPa and 100MPa.

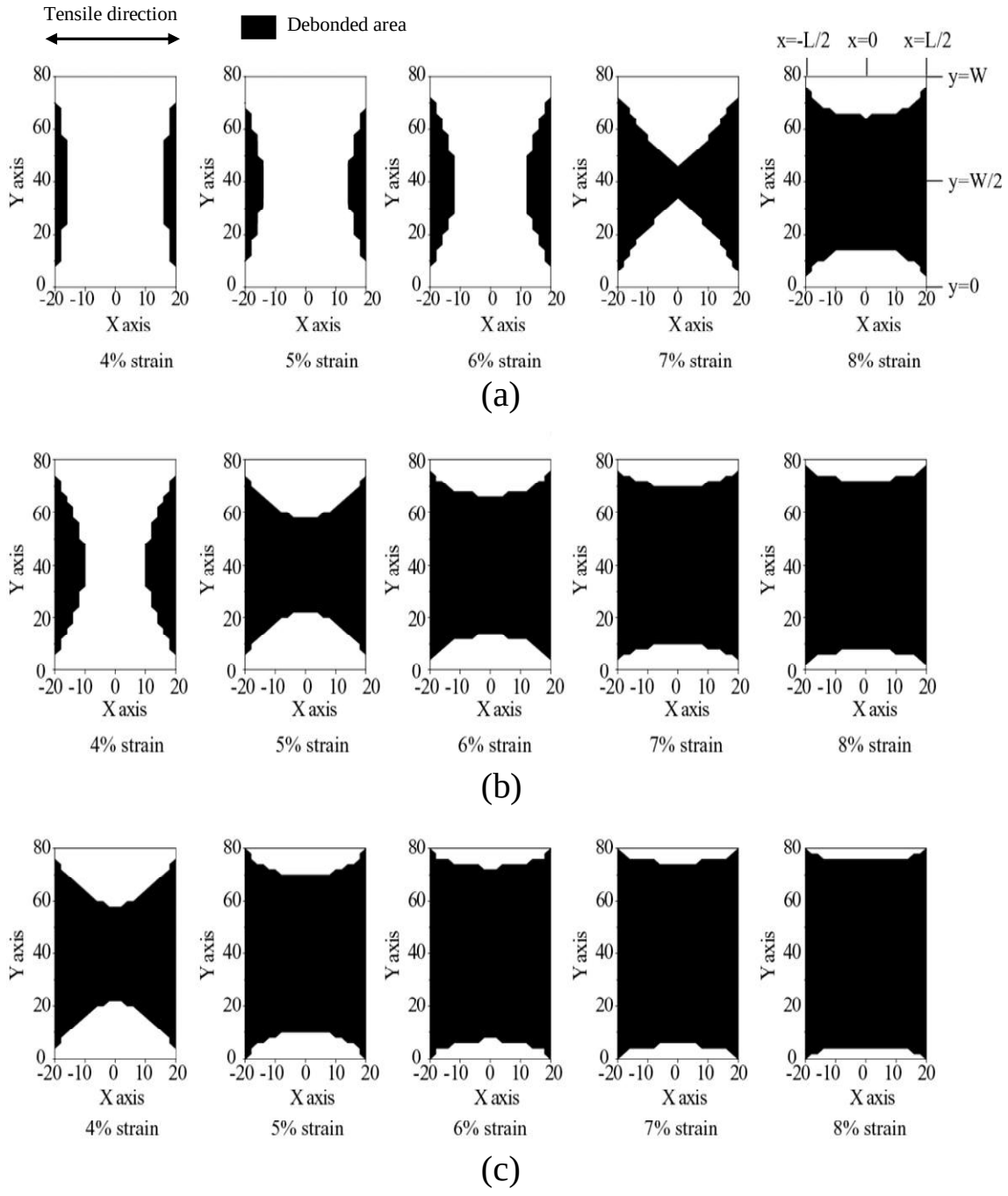

Fig.7.11 Progress of the debonded area of the coat (ii)-substrate interface with increasing applied strain, under the condition of $\sigma_{(i),\ int.}$ =100MPa and $\sigma_{(ii),\ int.}$ = 60MPa, 80MPa and 100MPa.

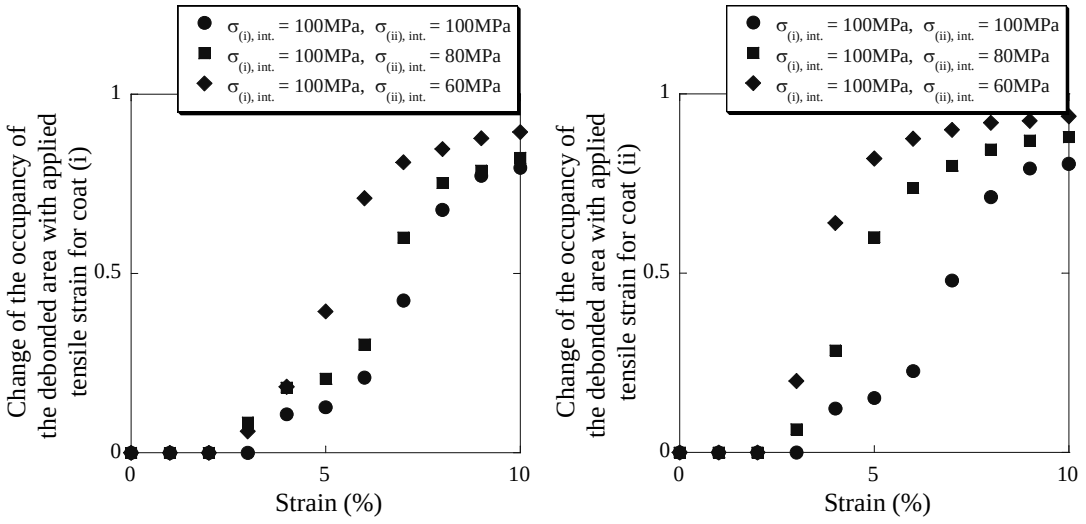

Fig.7.12 Change of the occupancy of the debonded area with applied tensile strain for coat (i) (a) and coat (ii) (b).

7.4 Conclusions

(1) The observation of the specimens revealed that the galvannealed coating layer on steel substrate exhibits the group buckling/interfacial debonding under applied tensile strain, and the group-buckling is not caused by the buckling at one time upon the mismatch of the slip system of the substrate grain from the comparison between the grain size of substrate steel and the length of the group-buckled coatings.

(2) The finite element stress analysis revealed that the debonding distance of coat (i) became larger for low interfacial bonding strength between coat (ii) and substrate. This means that the group-buckling occurs, originating from the buckling of the coating with weak interfacial bonding.

(3) At the center of the coating, the applied strain at the onset of the interfacial debonding becomes lower for low interfacial bonding strength of the corresponding and neighboring coatings. The occupancy of the debonded area also becomes larger

for low interfacial bonding strength of the corresponding and neighboring coatings.

(4) Similar group-buckling behavior was also observed in Al_2O_3-coated aluminum wire. The mechanical approach developed in this work is applicable not only to galvannealed steel but also to brittle coating composites for analysis of the group-buckling.

ACKNOWLEDGEMENT

The authors wish to express their gratitude to Japan Society for the Promotion of Science for Young Scientists and to The Iron and Steel Institute of Japan for the support of the present work.

References

[1] C. E. Jordan CE, K. M. Goggins and A. R. Marder: *Metall. Mater. Trans. A*, **25A** (1994), 2101.

[2] S. Lazik, C. Esling and J. Wegria: *Textures Microstruct.*, **23** (1995), 131.

[3] A. Kelly A and W. R. Tyson: *J. Mech. Phys. Solids*, **13** (1965) 329.

[4] S. Ochiai and K. Osamura: *J. Mater. Sci.*, **21** (1986), 2735.

[5] M. S. Hu and A. G. Evans: *Acta Metall.*, **37** (1989), 917.

[6] Y. Leterrier, L. Boogh, J. Andersons and J. A. E. Mason: *J. Polym. Sci. B. Polym. Phys.*, **35** (1997), 1449.

[7] S. Ochiai and Y. Murakami: *Met. Sci.*, **41** (1976), 401.

[8] J. Andersons, U. A. Handge, I. M. Sokolov and B. Blumen: *Eur. Phys. J.*, **B17** (2000), 261.

[9] S. Iwamoto, S. Ochiai, T. Nakamura and H. Okuda: *Tetsu-to-Hagane*, **91** (2005), 335.

[10] S. Ochiai, S, Iwamoto, T. Tomida, T. Nakamura, H. Okuda, M. Tanaka and H. Hojo: *Metall. Mater. Trans. A*, **36A** (2005), 1807.

[11] S. Iwamoto, S. Ochiai, H. Okuda and T. Inoue: *ISIJ Int.*, **47** (2007), 930.

[12] G. Reumont, J. B. Vogt, A. Iost and J. Foct: *Surf. Coat. Technol.*, **139** (2001), 265.

[13]J. Foct: *Scr. Metall.,* **28** (1993), 127.

[14] A. Iost and J. Foct: *J. Mater. Sci.*, **12** (1993), 1340.

[15] E. Tzimas and G. Papadrimitriou: *Surf. Coat. Technol.*, **145** (2001), 176.

[16] T. Nakamura, S. Ochiai, S. Iwamoto, D. Adachi and H. Okuda: *Tetsu-to-Hagane*, **91**(2005), 342.

Chapter 8

Conclusions

To describe the fracture and spalling process of galvannealed coating and to find the way of the fracture control, the modeling based on the observation and the mechanical stress analysis using finite element method were carried out.

In Chapter 2, tensile fracture and spalling behavior of the Fe-Zn intermetallic coating of galvannealed steel, together with that of the alumina coating on anodic-oxidized aluminum as a reference were studied. The main results are summarized as follows.

(1) The coating showed multiple cracking in the as-supplied condition. When tensile strain was applied, the multiple cracking progressed more.

(2) After the progress of the multiple cracking, the coating was fractured two times compressively in the width direction of the sheet samples. In the first compressive fracture process, buckling, wedging and wearing of coating occurred, causing flaking and powdering of the coating and mode II type fracture in the δ_1 and Γ_1 layers. Thus the upper thick $\zeta+\delta_1$ and $\zeta+\delta_1+\Gamma_1$ layers were spallled off, and, the $\delta_1+\Gamma_1+\Gamma$ and $\Gamma_1+\Gamma$ layers remained on the substrate. Then, in the second compressive fracture process, the layers that remained after the first compressive fracture were fractured also compressively under further increased applied strain due to the increased compressive stress in the width direction. The second compressive fracture caused the mode II type fracture of the Γ-substrate interface and spalling of the remaining layers.

(3) When the Al_2O_3 coatings were thin ($t < 30\mu m$), the coatings exhibited compressive fracture in the circumferential direction. When the Al_2O_3 coatings were thick ($t > 30\mu m$), the coatings exhibited interfacial debonding. In the specimens with thin Al_2O_3 coatings, buckling and wedging patterns were observed.

In Chapter 3, multiple cracking of the galvannealed coating layer was

studied. To estimate the strength of the coating layer and to predict the change of the critical and average crack spacing of the coating layer, finite element analysis was carried out. The main results are summarized as follows.

(1) Based on the finite element analysis and Kelly – Tyson equation, the following equation was derived,

$$\frac{\sigma_{x,\max}}{\sigma_s} = C\frac{L}{T} \qquad C \approx 0.18$$

(2) Application of equation in (1) to the experimental results revealed that the average strength of coating layer $\sigma_{c,\ UTS}$ on IF and SPCC substrate steels was around 260MPa.

(3) The critical length of the coating layer L_c and the average crack spacing of the coating layer L_{ave} at the strain were expressed as,

$$L_c = \frac{T}{C}\left(\frac{\sigma_{c,\ UTS}}{\sigma_s}\right), \qquad L_{ave} = \frac{3T}{4C}\left(\frac{\sigma_{c,\ UTS}}{\sigma_s}\right)$$

With this equation, as the $\sigma_{c,\ UTS}$-value is now known (260MPa), the change of the critical length and the average crack spacing of the coating layer and with applied strain could be predicted to a first approximation for any species of the substrate steel only by substituting the flow stress after corresponding strain of the substrate and thickness of the coating layer.

In Chapter 4, stress analysis of the buckled- and interfacial debonded-coating layer was carried out. The main results are summarized as follows.

(1) The observation of the specimens revealed that (i) the galvannealed coating layer on steel substrate exhibited interfacial debonding under applied tensile strain, following the multiple cracking of the coating layer, (ii) in the debonding process, the coating layer is first bent by the compressive stress in the width direction, then the tensile side of the bent coating layer is cracked, and finally the coating layer is spalled from the substrate steel due to the buckling induced interfacial debonding.

(2) The analytical results of the 3-dimentional finite element models revealed the following features for the interfacial debonding. (a) At zero tensile strain, the stress of the coating layer in the width direction is tensile due to the residual strain arising

from the mismatch of the coefficient of thermal expansion between the coating layer and substrate. (b) With increasing applied tensile strain, the compressive strain is exerted in the width direction due to the larger plastic deformation of the substrate. Also, due to the same reason, the coating layer is bent and the tensile stress is generated at the coating layer / substrate interface. (c) Then the stress on the tensile side of the bent coating layer becomes high enough to cause tensile fracture of the coating layer. Accordingly, the coating layer exhibited flex crack, and then interfacial debonding is enhanced more with increasing tensile strain, due to the enhanced interfacial tensile stress. These analytical results accounted for well the experimentally observed features of spalling process.

In Chapter 5, influences of the high tensile strength steel substrate on the multiple cracking and spalling was studied by the finite element stress analysis. The main results are summarized as follows.

The influences of the high tensile strength steel substrate on the multiple cracking and spalling was studied by the finite element stress analysis. It was revealed that the replacement of the high strength substrate for the low one acts to enhance the multiple cracking and to reduce the interfacial debonding through the enhancement of multiple cracking, if the tensile strength of the coating layer and interfacial bonding strength are retained on the level of those for the low strength steel (IF and SPCC).

In Chapter 6, influences of the crack spacing in the tensile direction and that in the sample width direction on the interfacial debonding were studied. The main results are summarized as follows.

(1) The spalling process could be divided into three stages. In the stage I, interfacial debonding starts at the cracked edge of the coating (the position $x = L/2$ and $y = W/2$). In the stage II, interfacial debonding reaches the center of the coating (the position $x = 0$ and $y = W/2$). In the stage III where the debonding front has passed the center, the coating is largely debonded and the debonding distance increases.

(2) The debonding distance of the coating layer decreases with decreasing the crack spacing both in the tensile direction L and the sample width direction W. The crack spacing L in the tensile direction affects especially on the stage I behavior. The

crack spacing W in the sample width direction affects especially on the transition from the stage I to the stage II.

(3) The present results suggest that, in order to supress the interfacial debonding, the crack spacing in the tensile direction should be short to retard the initial debonding, and the crack spacing in the sample width direction should be short, too, to retard the progress of the interfacial debonding.

In Chapter 7, group-buckling behavior was observed and analyzed. It was observed that the preceding buckling of the coating enhances the buckling of the neighboring coating. The main results are summarized as follows.

(1) The observation of the specimens revealed that the galvannealed coating layer on steel substrate exhibits the group buckling/interfacial debonding under applied tensile strain, and the group-buckling is not caused by the buckling at one time upon the mismatch of the slip system of the substrate grain from the comparison between the grain size of substrate steel and the length of the group-buckled coatings.

(2) The finite element stress analysis revealed that the debonding distance of coat (i) became larger for low interfacial bonding strength between coat (ii) and substrate. This means that the group-buckling occurs, originating from the buckling of the coating with weak interfacial bonding.

(3) At the center of the coating, the applied strain at the onset of the interfacial debonding becomes lower for low interfacial bonding strength of the corresponding and neighboring coatings. The occupancy of the debonded area also becomes larger for low interfacial bonding strength of the corresponding and neighboring coatings.

(4) Similar group-buckling behavior was also observed in Al_2O_3-coated aluminum wire. The mechanical approach developed in this work is applicable not only to galvannealed steel but also to brittle coating composites for analysis of the group-buckling.

In conclusion, the present work revealed comprehensively the cracking and spalling behavior of the galvanized coating layer by experiment and modeling analysis.

be utilized in practical application as a tool for description and prediction of the behavior not only of galvannealed steel but also of various brittle coating layer-ductile substrate systems.

Acknowledgement

The present thesis contains the results of the researches in Professor Ochiai's laboratory, Department of Materials Science and Engineering, Kyoto University. Many people who deserve my gratitude my gratitude have contributed to the success of this work.

First of all, I would like to express my deep gratitude to Professor Shojiro Ochiai, for his help and appropriate guidance. I owe all my works to his continuous support and the long –term discussions with him. I think he is one of the best leaders and researchers in the world. I am very pressed with and proud of being one of his students.

I would like to thank Associate Professor Hiroshi Okuda for his helpful suggestions, guidance and discussions of my research. I also would like to thank Professor Yasuhiro Awakura for helpful suggestions during reviewing this thesis.

I am grateful to Tadanobu Inoue (National Institute for Materials Science) for his helpful advices about numerical analysis. I used his suggestions as a trigger to find a solution of problems.

I wish to express my gratitude to Japan Society for the Promotion of Science for Young Scientists and the Iron and Steel Institute of Japan and JFE 21st Century Foundation for the support of this work.

Finally, I would like to thank to my parents for their countless love and continuous support to have opportunity to study. And I would like to thank to all Ochiai's laboratory members, they are my friends for life.